Title

Quantitative Assessment of the Response to Changing Sediment Supply, North Fork, American River, California

Authors

Rutten, Luke Thomas
Mount, Jeffrey F
Larsen, Eric W

Publication Date

1999-07-01

Quantitative Assessment of the Response to Changing Sediment Supply, North Fork, American River, California

By

Luke Thomas Rutten, Jeffrey F. Mount, and Eric W. Larsen
Department of Geology
University of California, Davis
Davis, CA 95616

TECHNICAL COMPLETION REPORT

Project Number: W-894
Start: July 1997
Duration: Two years

July, 1999

University of California Water Resources Center

The research leading to this report was supported by the University of California Water Resources Center, as part of Water Resources Center Project UCAL-WRC-W-788.

TABLE OF CONTENTS

ABSTRACT

Changes in sediment supply relative to transport capacity in gravel-bed streams lead to adjustments in stream geomorphology. Dietrich et al. (1989) propose that when sediment supply is low relative to transport capacity, bed surface coarsening develops due to selective erosion of fines. They developed a dimensionless bedload transport rate (q*), which is the ratio between the sediment transport rate of the surface layer and the transport rate of material as fine as the sub-surface or bedload. Flume experiments show that q* approaches unity when supply meets or exceeds capacity, and decreases in value when supply decreases. Longitudinal profiles and cross-section surveys on 7 km of the North Fork American River, CA show a downstream increase in supply relative to transport capacity. Q* values calculated from 15 sediment samples show corresponding increases downstream, indicating that the q* method may be useful for detecting trends in the supply-capacity relationship. Strong trends, however, were only seen when looking at the entire 7-km reach. On short reaches with limited data, absolute values of q* cannot be used for an accurate assessment of the supply-capacity relationship.

KEY WORDS

Geomorphology (1075), mines and mining (1505), rivers and river beds (2000), sediment generation, movement, and accumulation (2080), sedimentation (2085), streams and stream dynamics (2300), watersheds and watershed management (2690).

PROBLEM AND RESEARCH OBJECTIVES

The relationship between sediment supply and transport capacity in gravel-bed rivers exerts a fundamental control on channel morphology and dynamics. Changes in sediment supply or transport capacity in a given reach may result in local alteration of morphological and hydraulic characteristics. Additionally, systematic downstream changes in channel morphology throughout a watershed appear to be tied to changes in the supply:capacity relationship (Montgomery and Buffington, 1997). Studies have shown that changes in this relationship may be detectable through analysis of the texture of the bedload and bed surface and the relative transport rates of the bedload and bed surface material (Dietrich et al., 1989, Kinerson, 1990, and Lisle et al., 1993).

In a series of flume experiments, Dietrich et al. (1989) demonstrated that changes in sediment supply and transport capacity were reflected in changes in the transport rate of the bed surface layer material versus the total bedload. Dietrich et al. (1989) developed a dimensionless sediment transport ratio (q^*) that expresses the relationship between transport rates of the bed surface material and the total bedload. Later flume studies by Lisle et al. (1993) confirmed the utility of this approach in assessing changes in sediment supply versus transport capacity. However, to date, there have been no published field tests of the methods developed by Dietrich et al. (1989).

This study evaluates q^* as a measure of the supply:capacity relationship on a 7-km reach of the North Fork American River (NFAR), CA. The NFAR is a gravel-bedded river that has a bedrock controlled pool-riffle morphology. The study reach exhibits areas of degradation and aggradation in response to a large sediment slug that was introduced to the river by hydraulic gold mining in

the late 19th and early 20th centuries (Laddish, 1996 and James, 1997). The results of this study indicate that while q* may not accurately record the supply:capacity relationship in short (one to two channel widths) reaches, it may reveal trends over longer reaches.

BACKGROUND

Much work has been done on the response of channels to changes in sediment supply and transport capacity. Numerous studies have focused on channel adjustments due to river regulation (Petts, 1979, Williams and Wolman, 1984, and Everitt, 1993, among others) and episodic inputs of sediment (Gilbert, 1917, Benda, 1990, James, 1994, and Cenderelli and Kite, 1998, among others). However, few studies have attempted to develop tools to measure the supply:capacity relationship in a given reach without relying on long-term survey records. The work of Dietrich et al. (1989), Kinerson (1990), and Lisle et al. (1993), show that q* may be such a tool. Lisle and Hilton (1992), demonstrate that V*, which is the fraction of total pool volume filled with fine sediment deposits, may also be useful for measuring the supply:capacity relationship. Therefore, the approach developed by Dietrich et al. (1989), and tested here on the NFAR in this study, has the potential to be an indicator of the supply:capacity relationship in the absence of long-term survey records.

Theory

Sediment transport occurs when the bed shear stress (τ_b) exerted on the sediment by the flow exceeds the critical bed shear stress (τ_c) required to initiate motion. Stress has units of force per unit area. The bed shear stress is approximately proportional to the depth of water (H) and the energy slope (S) of the water (Henderson, 1966):

$$\tau_b = \rho_w g H S. \qquad 1)$$

The critical bed shear stress can be related to the median grain size (D_{50}, that size of 50% of the grains are less than) of the sediment:

$$\tau_c = 0.045 g(\rho_s - \rho_w) D_{50} \qquad 2)$$

where: g is the acceleration due to gravity, ρ_s is the density of the sediment, and ρ_w is the density of water. The coefficient 0.045 is equal to the dimensionless critical bed shear stress (τ_c^*) (Dietrich et al., 1989). The bedload sediment transport rate (q), expressed in units of mass per unit time, can be calculated using the Meyer-Peter and Mueller (1948) equation:

$$q = k(\tau_b - \tau_c)^{3/2} \qquad 3)$$

where k is a constant.

Dietrich et al. (1989) noted that bed surface coarsening results when sediment supply is low relative to transport capacity. The coarsening is presumed to be a product of selective erosion of fine sediment from the bed surface. Thus, in a channel with low sediment supply relative to transport capacity, the bedload transport rate of the coarse bed surface layer material would be less than that of the finer overall bedload. They developed a dimensionless bedload transport rate:

$$q^* = \frac{q_s}{q_l} = \left(\frac{\tau_b - \tau_{cs}}{\tau_b - \tau_{cl}}\right)^{1.5} \qquad 4)$$

where q_s is the transport rate of the bed surface layer material, q_l is the transport rate of the bedload material, τ_b is the bed shear stress, and τ_{cs} and τ_{cl} are the critical bed shear stresses of the bed surface material and the bedload respectively.

If a stream is at equilibrium, sediment supply is balanced by the streams transport capacity. Also, all sizes of material are moved on the bed. This results in the bedload having approximately the same grain size distribution and transport rate as the bed surface material. In this case, q* would equal unity. However, when sediment supply is decreased, fine sediment is progressively removed from the bed due to selective transport. These fines are not replenished due to low supply from upstream, and the bedload becomes progressively finer than the bed surface. In this case, the transport rate of the fine bedload is greater than that of the coarse bed surface, and q* is less than unity.

In order to test the utility of q*, Dietrich et al., (1989) and Lisle et al., (1993) conducted laboratory flume experiments. Their results show that when supply meets or exceeds capacity, the coarse bed surface layer is absent, and q* values are approximately equal to 1. When the supply decreases relative to capacity, bed surface coarsening increases, the zone of active bedload transport is constricted to a narrow portion of the flume, and q* decreases.

Field Studies of Morphological Response to Changing Supply and Capacity

Field studies of the response to relative changes in supply and capacity show results similar to those seen in the flume studies. Work on the Raba River, Poland demonstrated that decreased sediment supply and increased transport capacity due to river regulation resulted in channel degradation and bed surface coarsening (Wyzga, 1993). In Redwood Creek, CA, which is responding to increased sediment supply, Lisle and Madej (1992) found that the spatial distribution of the degree of paving, which is the ratio of the bed surface grain size to the subsurface grain size, a measure of bed surface coarsening, was related to variations in bed shear stress, or transport capacity. Zones of high shear stress possessed a high degree of paving while sheets of fine sediment covered the bed in low shear stress zones (Lisle and Madej, 1992), showing that local changes in transport capacity lead to changes in surface texture and paving.

Both of these studies show that bed surface texture changes as a result of changes in supply or capacity. Presumably, corresponding changes in q* could also be measured in these sites. Low values of q* would be expected in the Raba River and in the high shear stress zones of Redwood Creek. The low stress zones in Redwood Creek should show higher q* values.

Kinerson (1990) found that calculated q* values, bed surface coarseness, and the degree of paving correlated well with qualitative assessments of sediment supply on six streams in Northern California. However, coarse patches were seen in high supply streams due to local trapping of sediment upstream by debris dams. Also, fine patches were present in low supply streams, possibly due to migrating sediment waves. On individual streams, the ratio of bed shear stress to critical bed shear stress (shear stress ratio) showed results similar to q*. This is

especially clear on Jacoby Creek, and suggests that other measures such as the shear stress ratio may be used in conjunction with q* to quantify the supply:capacity relationship.

Lisle and Hilton (1992) used an alternative measure, V*, which is the fraction of total pool volume filled by fine sediment, to assess the supply:capacity relationship. They found that V* correlated well with a qualitative ranking of sediment supply on eight tributaries of the Trinity River, CA. On one particular site, a sharp increase in V* values revealed the presence of an illegal mining operation that was contributing sediment to the creek.

These studies show that response to changes in supply or capacity may be detected in streams using grain size and sediment transport characteristics. The responses that were seen in the flume studies were also present in the field. Therefore, measuring q* in a reach may result in a quantitative assessment of the supply:capacity relationship.

Site Descriptions

North Fork American River Watershed The watershed of the North Fork American River (NFAR) is located on the western slope of the northern Sierra Nevada range (Figure 1). From it's headwaters at an elevation of 2413 m to the confluence with the Middle Fork American River at 162 m, the river is 104 km in length with an average gradient of 0.022, encompassing a drainage area of 886 km^2. Throughout the basin, the river is incised into a steep-walled canyon with ridges 300-600 m above the channel. The canyon walls have gradients of 0.50 to 0.75.

The bedrock geology of the upper watershed consists of primarily Cretaceous-Jurassic aged granodiorite, Jurassic metavolcanics, and Paleozoic sandstones. The lower-most watershed (containing the study reach) is comprised of Jurassic aged metasediments and Paleozoic metasedimentary melange (Wagner et al., 1981 and Saucedo and Wagner, 1982). Auriferous gravels of Eocene age are found in various locations throughout the middle watershed (Figure 1). The ridge tops in the watershed contain Tertiary volcaniclastics and basalt flows.

The North Fork American River watershed receives most of its average annual precipitation of 1,430 mm between October and April with January generally being the wettest month. The majority of the precipitation above 1,700 m elevation falls as snow. Average daily discharge on the NFAR is 22.2 cms and the major runoff period occurs during spring snowmelt between April and May. Large flood events occur during the winter months after considerable snowpack has accumulated and warm sub-tropical storms produce rain at high elevations. This leads to rain-on-snow conditions that cause rapid melting of the snowpack. A series of such storms occurred during New Year's 1997, leading to a record discharge of 1,840 cms in the North Fork. The watershed contains no significant flood retention structures.

Hydraulic Gold Mining Sediment The North Fork American River was a bedrock lined channel with a low sediment supply when it received approximately 163 million cubic meters of hydraulic gold-mining sediment in the late 1800s (Laddish, 1996). James (1991, 1994) found that Sierran streams impacted by hydraulic mining sediment initially responded by aggrading in the tributaries near the sediment source. The floods of 1862 scoured the tributaries and transported much of this sediment down into the main stems and into the Central Valley where it caused

widespread aggradation, and channel avulsion. At one time, the channel bed elevation of the levied lower American River was higher than the floodplain outside the levees (James 1994).

The continuing response of the Sierran streams to this sediment input makes them especially appealing for q* studies. Studies on the lower Bear River, CA, which is the next watershed north of the NFAR, show response characteristics that are similar to those seen in the q* studies reported above. In response to increased supply, the channel of the Bear River initially underwent aggradation and avulsion. The aggraded channel had bed material that was considerably finer than the pre-mining channel sediment. After mining was enjoined in 1884 and the supply was reduced, channel incision began. By 1983, the channel was once again coarse-bedded with bed elevations near pre-mining levels (James 1991). Measurements of q* on the fine-bedded Bear River during high supply driven aggradation would presumably have been near unity. Once supply was reduced and incision was occurring, measured q* values would be expected to be less than one. Laddish (1996) reports that the NFAR is still recovering from hydraulic mining sediment, suggesting that reaches of high and/or low supply may be mapped and tested with q* measurements.

Study Site The study site is a 7-km reach of the NFAR from Ponderosa Bridge to Lake Clementine near Auburn, CA (Figure 2). This reach has a lower gradient than the upstream canyon and forms the first significant storage site of hydraulic mining sediment downstream from the source. In 1995, approximately 10.5 million cubic meters of sediment remained in the reach, (Laddish, 1996). This sediment blankets the canyon floor to an average width of approximately 90 m between steep canyon walls composed of bedrock and a Pleistocene-aged

glacial outwash terrace. Due to a steeper gradient, the elevation of the Pleistocene terrace relative to the channel decreases downstream (from approximately 30 m at the upstream end) and eventually disappears roughly 4,000 m down the reach. The reach has a pool-riffle morphology that is controlled by bedrock bends and obstructions. Lake Clementine is created by the North Fork Dam, which was built in 1939 by the U.S. Army Corps of Engineers to capture mining debris. The dam has no water supply, flood control, or hydroelectric capacity.

METHODOLOGY

The q* equation requires inputs of bedload and bed surface grain size, as well as local water surface slope, and local depth of water. Thus, measurements of these parameters along the study reach are required in order to plot q* versus distance downstream. In order to test if q* correlates with the supply:capacity relationship on the NFAR, an independent measure of the supply:capacity relationship is needed. This was done by identifying areas of long-term degradation and aggradation. Degrading reaches were considered low supply or supply-limited reaches; aggrading reaches were considered relatively high supply or transport-limited reaches (after Dietrich et al. 1989, Lane et al. 1996, and Montgomery and Buffington 1997). Values of q* are expected to correlate with the independent assessment of the supply:capacity relationship.

Channel Change Over Time

In order to identify areas of degradation and aggradation along the reach, longitudinal profiles from 1936 and 1995 (Laddish, 1996), and 15 cross-section profiles from 1996 and 1997 were compared. The surveying method used for the 1936 longitudinal survey is not available but is

assumed to have been done with a surveyors level, rod and chain, while the 1996 survey used a digital level and stadia rod.

Fifteen cross-sections were established and surveyed in the summer and fall of 1996 and resurveyed during the summer of 1997. Each cross-section was surveyed using an electronic distance meter (EDM) total station. They were oriented perpendicular to the low flow channel. At some sites, the perpendicular orientation to the low flow channel is oblique to the flood channel.

Seven cross-sections were located at or near those surveyed by Laddish (1996). Others were evenly spaced throughout the reach and located on straight reaches with symmetrical cross-sections as often as possible. The 1996 cross-sections extended across the entire valley floor and up both canyon walls, while the 1997 surveys included the 1997 high-water mark on each canyon wall. On average, the spacing of survey shots along each cross-section was less than 2 meters.

The cross-sectional area beneath the 1997 high-water mark was calculated for each cross-section. Average cross-section depth was found by dividing the area by the total top width of the water surface at flood stage.

Grain Size Sampling

Subsurface grain size data was used to represent the bedload grain size. Lisle (1995) reports that in locations with a drainage area greater 100 km^2, the subsurface material approximates the bedload. Flume studies by Parker et al. (1982a) also showed that the subsurface and bedload grain size are similar. Due to the large size of the NFAR, bedload sampling was not possible. Therefore, the subsurface material was assumed to approximate the bedload.

Throughout the study reach, surface and subsurface sediment samples were taken on the tops of each alternate bar. All samples were located near the geographic center of the bar, which was determined by pacing out the length and width of each bar. This bar center location is assumed to experience average conditions of flow and shear stress exerted on the entire bar.

Surface sediment samples were tabulated into 1/2 ϕ (phi) sizes by performing Wolman (1954) counts. Once the surface count was completed, the surface layer was removed to a depth equal to the surface D_{84} and the subsurface was mixed using a shovel and/or pick ax. The subsurface sediment was then sampled on a ten by ten taped grid that had grid spacing equal to half the surface D_{100}, after the methods of Buffington (1996), and Wohl et al. (1996). The subsurface sediment was also tabulated into 1/2 ϕ sizes. On all counts, material finer than 8 mm was lumped together.

Energy Slope

Calculation of q* requires an estimation of energy slope and local depth as well as grain size. The slope of the 1997 high water was chosen as the energy slope for this study because it could

be most easily surveyed and calculated. The 1997 high-water mark was surveyed in the summer and fall of 1997 along both banks throughout the study reach using the EDM. Survey points were collected on average every 50 meters down both the left and right banks.

The local slope for each sediment sample site (at the center of the bar) was calculated from the bar head to the bar tail. When possible, these locations also corresponded to upstream and downstream riffle crests. However, due to the bedrock controls on the location of bars, pools and riffles, the bar head did not always have a corresponding riffle. When this was the case, the crossover point between bars was used. This slope is thought to encompass one entire bar-pool unit and is similar to the method used by Andrews (1994) to calculate bedload transport in Sagehen Creek, CA. Once the endpoints of the slope were determined, the longitudinal profiles of the right and left bank high-water marks were plotted and slopes were calculated by linear regression. The slope and the local depth of water over each sediment sample site was determined by interpolation between the right and left bank water surface profiles.

PRINCIPAL FINDINGS AND SIGNIFICANCE

Results of this study (summarized in tabular form in Appendix 1) show that values of q* generally correlate with degrading and aggrading reaches in the study area. This illustrates the potential utility of q* measurements to identify the character of the relationship between sediment supply and transport capacity in gravel-bedded rivers. However, there are several issues pertaining to the reliability of q* measurements that must be considered. These issues include the sensitivity of the q* equation to errors in the input variables, local hydraulic variations caused by canyon morphology, and the origin of bed coarsening in transport-limited reaches.

Sensitivity of q*

Small variations in any of the inputs lead to considerable change in q* values. Sensitivity analysis of the q* equation conducted for this study shows that a -25% change in local slope results in q* values equal to 0.35-0.86 times the original value. Changing the local slope by +25% results in q* values equal to 1.06-1.33 times the original value. A -25% change in subsurface grain size results in q* values equal to 0.66-0.89 times the original. When the subsurface grain size is off by +25%, q* is 1.13-1.77 times the original. Looking at the local depth, a –25% change leads to q* equaling 0.35-0.94 times the original. A +25% change in local depth results in q* values equal to 1.03-1.33 times the original. This sensitivity of the q* equation requires that all inputs are carefully measured. Errors in the measured inputs may lead to unrealistic results.

Given the sensitivity of the q* calculations, the choice of the local water surface slope is critical. The choice of the local slope in this study was guided by the method of Andrews (1994). However, in his original study, Andrews' (1994) choice of slope was tested by comparing calculated to measured bedload transport rates. No such comparison was possible in this study, due to the difficulty of measuring bedload during the 1997 flood.

The local water surface slope, which determines the hydraulic forces, is strongly controlled by local variations in the NFAR canyon morphology. The effect of these variations can be seen by examining the outliers on the q* and shear stress ratio plots. There are three q* values shown in Figure 7 that fall outside of the overall trend (stations 1,610, 2,475, and 5,835 m). The point at 1610 m (SS 4) has a degree of paving equal to one, which results in q*=1. Based on field

observations, the lack of paving here is interpreted to be due to the deposition of fines in slack water upstream of the confluence of the NFAR and Codfish Creek (see Figure 2). The low slope over this point (Figure 6a) supports this interpretation.

The high q* value at this point suggests that, in some cases, local variations in the supply:capacity relationship over a long reach may be detected by q*. The backwater area of the Codfish Creek confluence would have had a low transport capacity relative to supply and therefore, this site can be thought of as transport-limited. Considering this scenario, a high q* value would be expected here.

This situation is analogous to the spatial variations found by Kinerson (1990). In his study, coarse patches, which would have low q* values, were seen in high supply streams due to local trapping of sediment upstream by debris dams. He also found fine patches, which would have high q* values, in low supply streams, possibly due to migrating sediment waves. However, downstream, in the transport-limited reach, q* values are not as high at that seen at 1610 m. Therefore, the absolute value of q* may be misleading. It is best to look at the variation of q* values relative to upstream and downstream samples.

The second outlier is located at 2,475 m (SS 6). At this point, calculated bed shear stress did not exceed the calculated critical shear stress, resulting in an undefined q* and a shear stress ratio of less than one. This low bed shear stress is the result of a low local slope. The low slope is interpreted to be due to superelevation of the water surface caused by a bedrock bend. The superelevation is caused by water backing up behind the bend, thus lowering the slope

immediately upstream of the bend. Due to this low slope, the calculated shear stress for this point is not large enough to initiate motion. Given this local deviation, this point may be disregarded.

The last outlier, at 5,835 m (SS 13), also has a low q* value as the result of a low-water surface slope. In this case, the low slope is due to the backwater caused by Lake Clementine. This point may also be disregarded.

Examination of the outliers reveals that local variations in canyon morphology has a strong control on local slope and ultimately hydraulics. Such variation must be considered when interpreting q* results.

Bed Coarsening in the Transport-limited Reach

As previously mentioned, bed surface coarsening is theoretically not expected to be present in reaches that are at equilibrium. This is due to the balance between the sediment supply and transport capacity in such reaches. In transport-limited reaches, an over abundance of fine sediment may actually result in bed surface fining (Kinerson, 1990). However, the data from the NFAR show bed surface coarsening present in the transport-limited reach (Figure 5b). This coarsening prevents q* from approaching unity in this reach. Therefore, q* values of 1 may not necessarily occur in areas of aggradation.

Bed surface coarsening in the transport-limited reach may be explained by the concept of equal mobility (Parker and Klingeman, 1982, Andrews, 1983 and Andrews and Erman, 1986). This concept suggests that the coarse surface layer is always present, in order to render all grain size

fractions equally mobile due to higher exposure and protrusion into the flow of coarse grains and hiding of fine grains. Thus, when flows reach the threshold of movement, all grain sizes move under similar flow magnitudes. In this sense, the coarse surface layer regulates the movement of bedload by making all grain sizes equally mobile. The coarse surface layer is intact at all times, even during active bedload movement. Therefore, on the NFAR equal mobility may cause paving in the transport-limited reach.

Winnowing of fines by waning flows may also cause the coarse surface layer in the aggrading portion of the reach. At the peak of aggradation during the 1997 flood, the bed may have indeed been unpaved. At this point, measurements of q* would have been near unity. However, as the flow decreased and aggradation stopped, fine material may have been winnowed from the bed surface, leaving the surface more coarse. Values of q* after this winnowing occurred would be lower than those measured at the peak of aggradation. Therefore, this winnowing of fines may cause lower than expected q* values in the transport-limited reach. Smaller flows that occurred after the 1997 flood but before the bed was sampled may have also winnowed fines from the bed.

The above discussion reveals that bed coarsening, whether through equal mobility of bed surface material, or winnowing of fines by smaller flows, will lead to lowered q* values in transport-limited reaches. For this reason, single values of q* in single reaches are unlikely to be useful for interpreting the supply:capacity relationships. However, as noted, analysis of q* values over multiple reaches and in conjunction with shear stress ratios may indicate significant trends in the supply:capacity relationship.

Limited Data Set

Another potential problem with the current analysis is the limited data set. The limited number of data points is due to the sampling scheme used. Each alternate bar in the reach was sampled for surface and subsurface grain size. Given the scheme of sampling only the center of each alternate bar, a limited number of sampling sites were available. All available sites were measured for this study. A more detailed sampling scheme on the bars and in the channel, may yield a clearer correlation.

Future work on the NFAR should include an increased number of grain size samples throughout the reach. In addition, areal mapping and sampling of grain size patchiness in a number of short reaches may allow analysis of local variations of shear stress and q*, similar to that done on Redwood Creek by Lisle and Madej (1992).

FINDINGS, CONCLUSIONS, AND RECOMMENDATIONS

Supply- and Transport-limited Reaches

In order to test whether q* correlates with changes in the supply:capacity relationship, long-term survey data was used to define supply-limited and transport-limited reaches. The supply:capacity relationship was then compared with the calculated q* values. Supply-limited and transport-limited reaches can be defined by delineating areas of degradation and aggradation. Theoretically, q* should be less than one in supply-limited reaches and equal to one in transport-limited reaches.

Supply-limited and transport-limited reaches on the NFAR were determined by observing long-term changes in bed elevation shown by comparison of the 1936 and 1995 longitudinal profiles (Figure 3). This plot shows the channel degrading as much as 5 m in the upstream, supply-limited reach (0-4,500 m). Aggradation of up to 8 m has occurred in the downstream, transport-limited reach (4,500-7,600 m). Therefore, the supply:capacity relationship changes longitudinally from supply-limited upstream to transport-limited downstream.

This pattern is supported by comparison of the cross-section areas and depths from 1996 and 1997 (Figure 4a and b). The cross-section area and average cross-section depth increased as much as 28 m^2 and 0.24 m respectively, in the upstream, supply-limited reach (0-3,000 m) and decreased as much as 38 m^2 and 0.21 m respectively, in the downstream, transport-limited reach (3,000-6,300). The difference in the reach lengths between Figures 3 and 4a and b is due to differences in survey methods. The distance downstream on the longitudinal survey plot was determined by the length of the thalweg while the distance downstream of the cross-section plots was determined by the length of the shorter 1997 flood channel axis. All remaining plots use this shorter flood channel axis distance downstream. The cross-section survey data are included in Appendix 2.

The work of Dietrich et al., (1989) and Lisle et al., (1993) suggests that q* is less than one in supply-limited reaches and equal to or greater than one in transport-limited reaches. The survey data from the NFAR show that the upstream reach (0-3,000 m) is supply-limited while the downstream reach (3,000-6,300 m) is transport-limited. These reach lengths are based on Figures

4a and b. Given this longitudinal change in the supply:capacity relationship, q* can be expected to increase downstream.

Grain Size Distributions and Degree of Paving

Since subsurface textures are used to represent bedload texture, values of q* vary inversely with the degree of paving. In supply-limited reaches, selective erosion of fines will presumably create a surface layer that is more coarse than the subsurface material or bedload. In transport-limited reaches, surface coarsening does not occur and the size of the surface and subsurface or bedload are similar. Therefore, the degree of paving should be greater than one in supply-limited reaches and near one in transport-limited reaches. Also, due to selective erosion, the surface D_{50} in supply-limited reaches should be greater than that of transport-limited reaches, given that both reaches have equal subsurface D_{50}. Based on the survey data presented above, the degree of paving and the surface D_{50} should decrease longitudinally downstream in response to declining transport capacity and/or increased sediment supply.

The surface grain size data (Figure 5a) follow the expected trend. There is downstream fining of both the surface D_{50} and subsurface D_{50}. The surface D_{50} decreases from 128 mm to 52 mm while the subsurface D_{50} decreases from 90 mm to 38 mm. There is also downstream fining within both the supply-limited and transport-limited reaches. In the supply-limited reach, surface D_{50} decreases from 128 mm to 97 mm and the subsurface D_{50} decreases from 90 mm to 44 mm. The average surface D_{50} is 104 mm, while the average subsurface D_{50} is 68 mm. In the transport-limited reach, surface D_{50} decreases from 108 mm to 52 mm and the subsurface D_{50} decreases

from 66 mm to 38 mm. The average surface D_{50} is 71 mm, while the average subsurface D_{50} is 50 mm. The complete sediment sample data set can be found in Appendix 3.

Although the downstream fining is expected, this trend may also be influenced by local sources of coarse bed material. Erosion of the Pleistocene terrace in the upstream portion of the reach appears to be supplying coarse material to the bed (Laddish, 1996). Downstream, this terrace is not exposed and is therefore not supplying coarse material directly to the channel. While most of the coarse sediment that is being supplied is likely being moved by the river in the upstream reach, the coarsest material (boulder-sized) is apparently not being transported to the downstream reach. Therefore the local source of large material from the Pleistocene terrace may be one cause of the overall downstream fining.

While the downstream fining of the surface follows the expected trends, the subsurface also fines downstream, thus causing the degree of paving (Figure 5b) to lack a distinct downstream trend. The degree of paving varies from 1 to 2.2 throughout the entire reach with most values between 1.17 and 1.8. The average degree of paving for the entire study reach is 1.49. The supply-limited reach displays more scatter than the transport-limited reach and has a reach averaged degree of paving of 1.59. The transport-limited reach has an average degree of paving of 1.44. Although this shows a downstream decrease in average degree of paving, it is not as pronounced as expected.

Values of q* increase with decreasing degree of paving. When the degree of paving is greater than one, q* is less than one. When the degree of paving approaches one, q* does as well. The

data reveal that the degree of paving is greater than one throughout the reach and does not follow a distinct trend. This suggests that the longitudinal plot of q* may also lack a definite trend. Also, the paving data show that q* will not equal one in the transport-limited reach, contrary to what is expected. However, q* is also a function of the local slope and depth of water, a study of which may shed light on what can be expected in the q* results.

Local Slope and Depth of Water

The local water surface slope and depth of water are used to determine shear stress in calculating q*. Based on the decreasing bed surface slope in the longitudinal profile (Figure 3), and considering that Lake Clementine is a local base level for the reach, local water surface slope can be expected to decrease downstream. Also, the long-term pattern of degradation upstream and aggradation downstream supports an expected downstream decrease in slope.

Longitudinal changes in local depth of water are harder to predict. Local depths may be effected by the elevation of the bar top relative to the high-water mark, as well as superelevation caused by bedrock bends and constrictions. However, average depths should increase downstream overall given the decreased slope and the possible back water effect from Lake Clementine.

Figures 6a and b show that neither the slope or depth follow the expected trends. The local water surface slope decreases from 0.0057 to 0.0019 in the first 2,500 m but then remains scattered between 0.002 and 0.004. Slopes in the supply-limited reach range from 0.0057 to 0.0019 and average 0.0037. The transport-limited reach has slopes from 0.0035 to 0.0014 with an average of 0.0019. Local depth varies from 2.1 m to 4.4 m with most values between 2.6 m and 4.0 m. The

average local depth of water in the supply-limited reach is 3.2 m. The transport-limited reach has an average local depth of 3.3 m. Although there is considerable scatter in the data, the averages show an overall decrease in local slope between the supply-limited and transport-limited reaches. There is no observable change in reach-averaged local depth.

Most of the variation in slope and depth appears to be due to local characteristics instead of reach-scale changes. These variations may have a significant impact on the values of q*. These local controls include bedrock bends and obstructions, variations in cross-section area, and the elevations of the bars relative to the high-water mark, as well as backwater effects at the confluence of Codfish Creek with the NFAR (see Figure 2). Local water surface profiles can be found in Appendix 4, and the high-water survey data are included in Appendix 5.

Changes in q* and Shear Stress

Considering the progressive downstream change of the study reach from supply-limited to transport-limited reaches, it is expected that q* will increase longitudinally. Figure 7 shows that overall, calculated q* values increase in the downstream direction, mirroring the inferred increase in the supply relative to capacity. The three outliers, at 1,610, 2,475, and 5,835 m are evaluated in the Discussion of Results. The remaining points show a trend of increasing q* ranging from 0.38 to 0.81. The values in the supply-limited reach range from 0.45 to 0.63 and have an average of 0.52. In the transport-limited reach, the data ranges from 0.38 to 0.81 and has an average of 0.64. Although q* increases downstream as expected, it does not approach or exceed one in the transport-limited reach as expected. This is due to the fact that the degree of paving is greater than one throughout the entire reach, except at 1,610 m.

The results of Kinerson (1990) suggest that the shear stress ratio (τ_b/τ_c) may also be used to measure the supply:capacity relationship. His data from Jacoby Creek, CA show that the shear stress ratio shows results similar to q*. Shear stress ratios in this study were calculated and compared with q*. A plot of the shear stress ratio should increase downstream.

With the exception of the points at 2,475 and 5,835 m, the plot of the shear stress ratio shows an increasing trend longitudinally (Figure 8). This trend is clearer in the transport-limited reach. In the supply-limited reach the ratio is relatively constant. The shear stress ratio ranges from 1.30 to 2.68, and the average ratio in the supply-limited reach is 1.65 while the transport-limited reach averages 1.92. Although the average values are considerably different between the two reaches, the overall trend has a lower slope than the q* plot.

The data show that q* correlates with the supply:capacity relationship in the NFAR. Longitudinally, q* changes from low values in the degrading, supply-limited reach to high values in the aggrading, transport-limited reach. In addition, the shear stress ratio also showed differences between the two reaches. Average values of this ratio are lower in the supply-limited reach than in the transport-limited reach. Therefore, these two measurements may be used in conjunction to identify variations of the supply:capacity relationship over extended reaches in a gravel-bedded river.

SUMMARY

Measuring q* may prove to be an effective method of assessing the supply:capacity relationship in gravel-bedded rivers. Flume studies by Dietrich et al. (1989) and Lisle et al. (1993) show that

q* corresponds positively with sediment supply relative to capacity. Field work by Kinerson (1990) showed that q* correlated well with qualitative assessments of sediment supply on six streams in Northern California. He also found that the shear stress ratio may be another measure of the supply:capacity relationship by showing that it revealed similar results as q* on Jacoby Creek.

This paper presents a study of the correlation between values of q* and the supply/capacity relationship on a 7-km reach of the North Fork American River, CA. Long- and short-term survey data reveal a degrading, supply-limited reach upstream and an aggrading, transport-limited reach downstream, thus showing a downstream increase in supply relative to capacity. Using the 1997 high-water mark as an energy slope, and surface and subsurface grain size distributions from thirteen alternate bars, q* values show an increasing trend downstream that correlates with the increasing supply. Shear stress ratios for each sample site also increased downstream, thus showing that both q* and the shear stress ratio may be correlated with the supply:capacity relationship on the NFAR. Sensitivity of the q* equation to input variables, local variations of hydraulic conditions due to channel morphology, and the occurrence of paving in transport-limited reaches must be considered when conducting and analyzing studies using q*. The use of the absolute value of one q* measurement on a short reach will not give an accurate assessment of the supply/capacity relationship. Comparison of relative q* values on long reaches may reveal useful trends. Further refinement of the trends found in this study may be accomplished by more thorough sampling and areal mapping of grain size patchiness and bed shear stress.

FIGURES

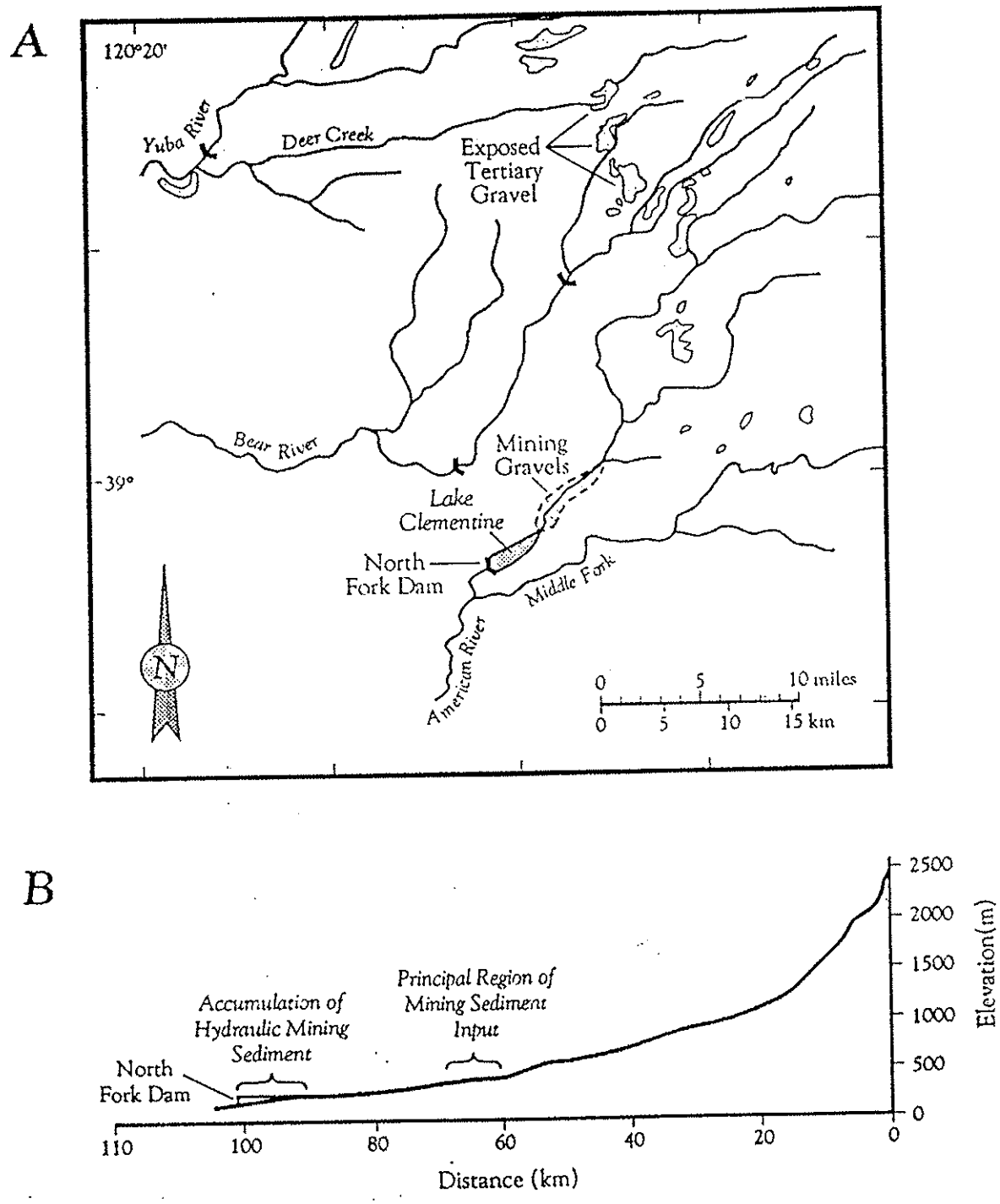

Figure 1. A) Generalized map of North Fork American River drainage. The field site for this study extends for 7 km upstream from Lake Clementine. B) Longitudinal profile of North Fork watershed from summit to confluence with Middle Fork (from Laddish, 1996).

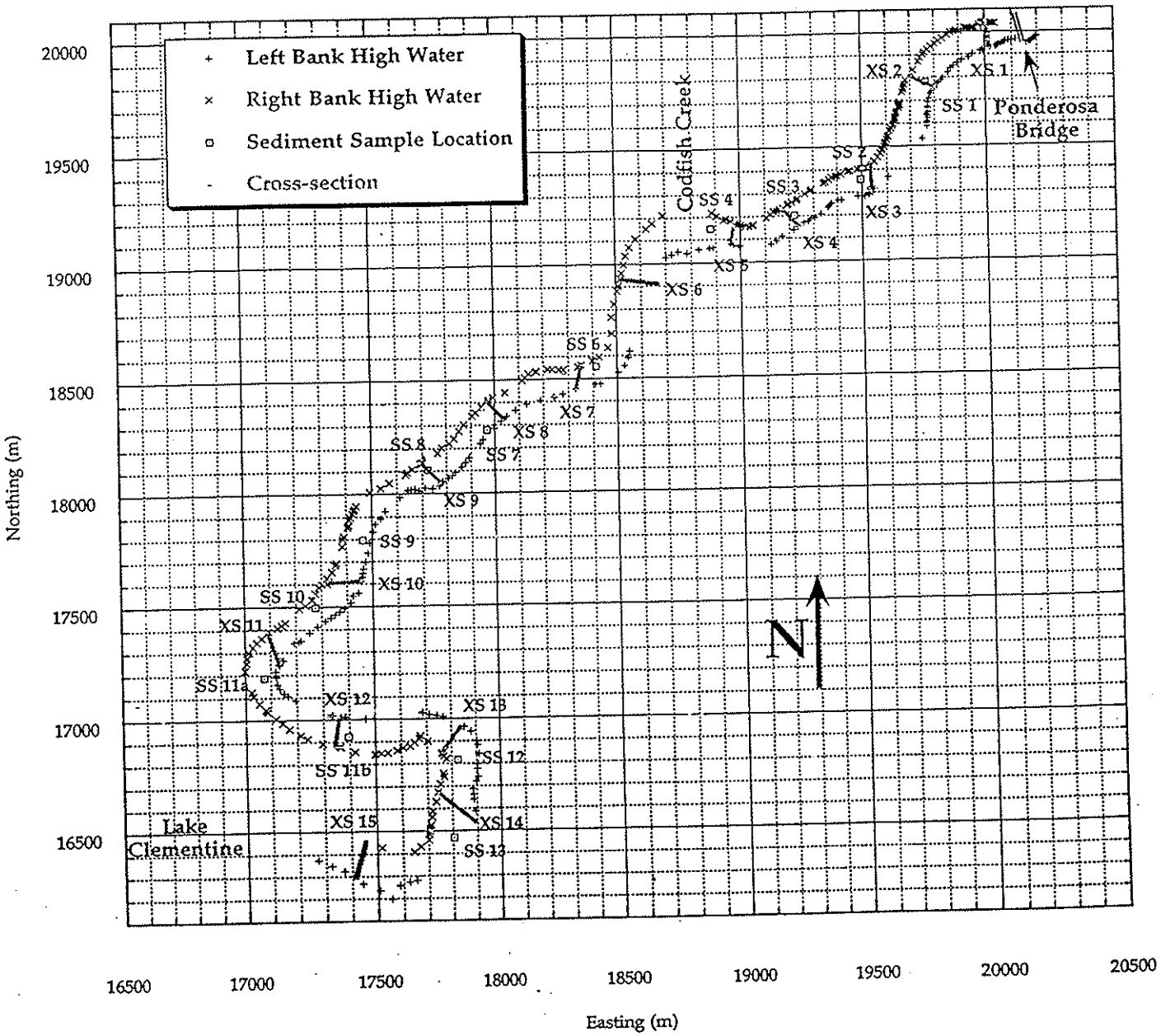

Figure 2. Study Site showing 1997 high water survey points, cross-section survey, and sediment sample locations.

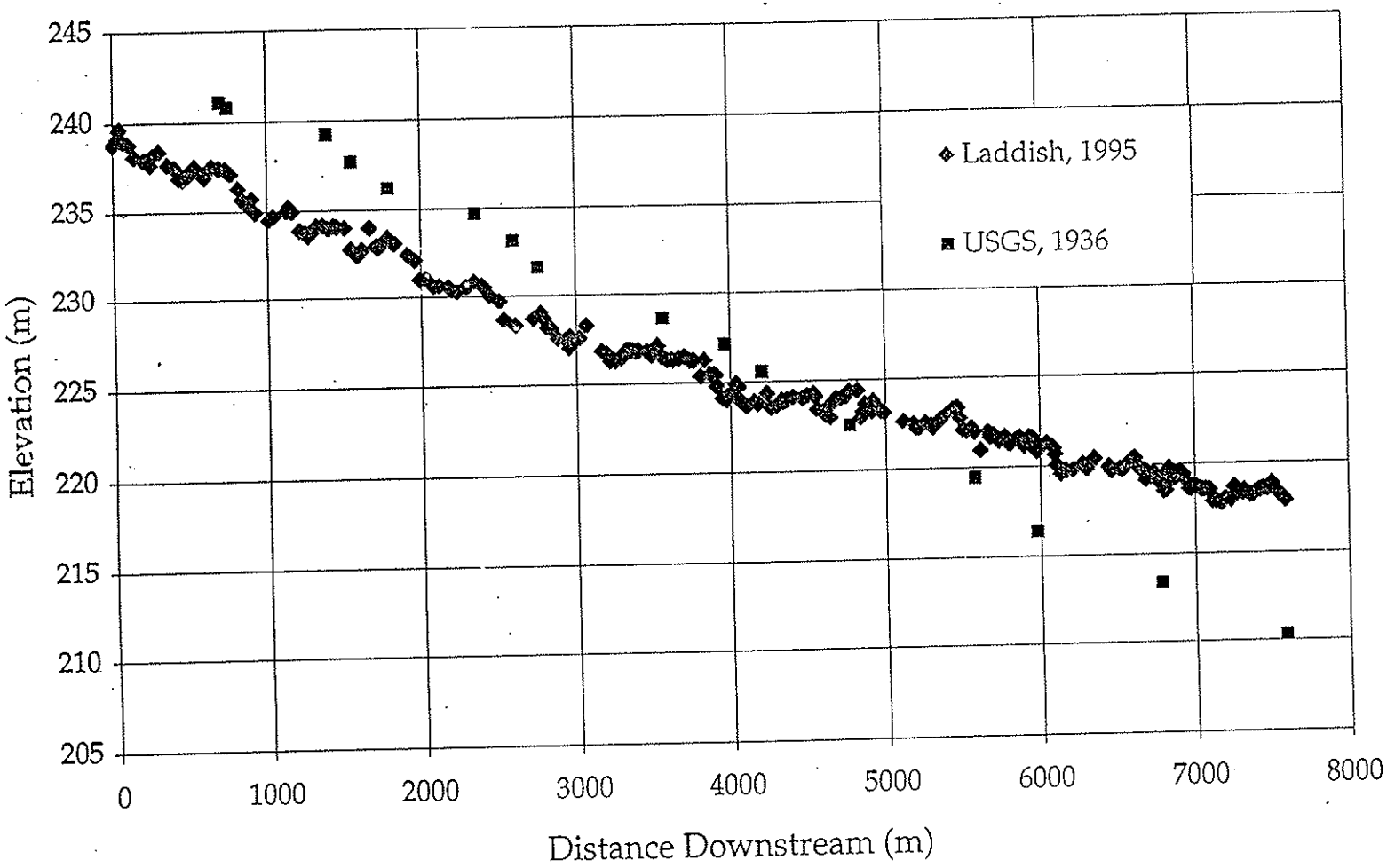

Figure 3. Longitudinal Profile, North Fork American River, Ponderosa Bridge to Lake Clementine (USGS, 1936 and Laddish, 1995).

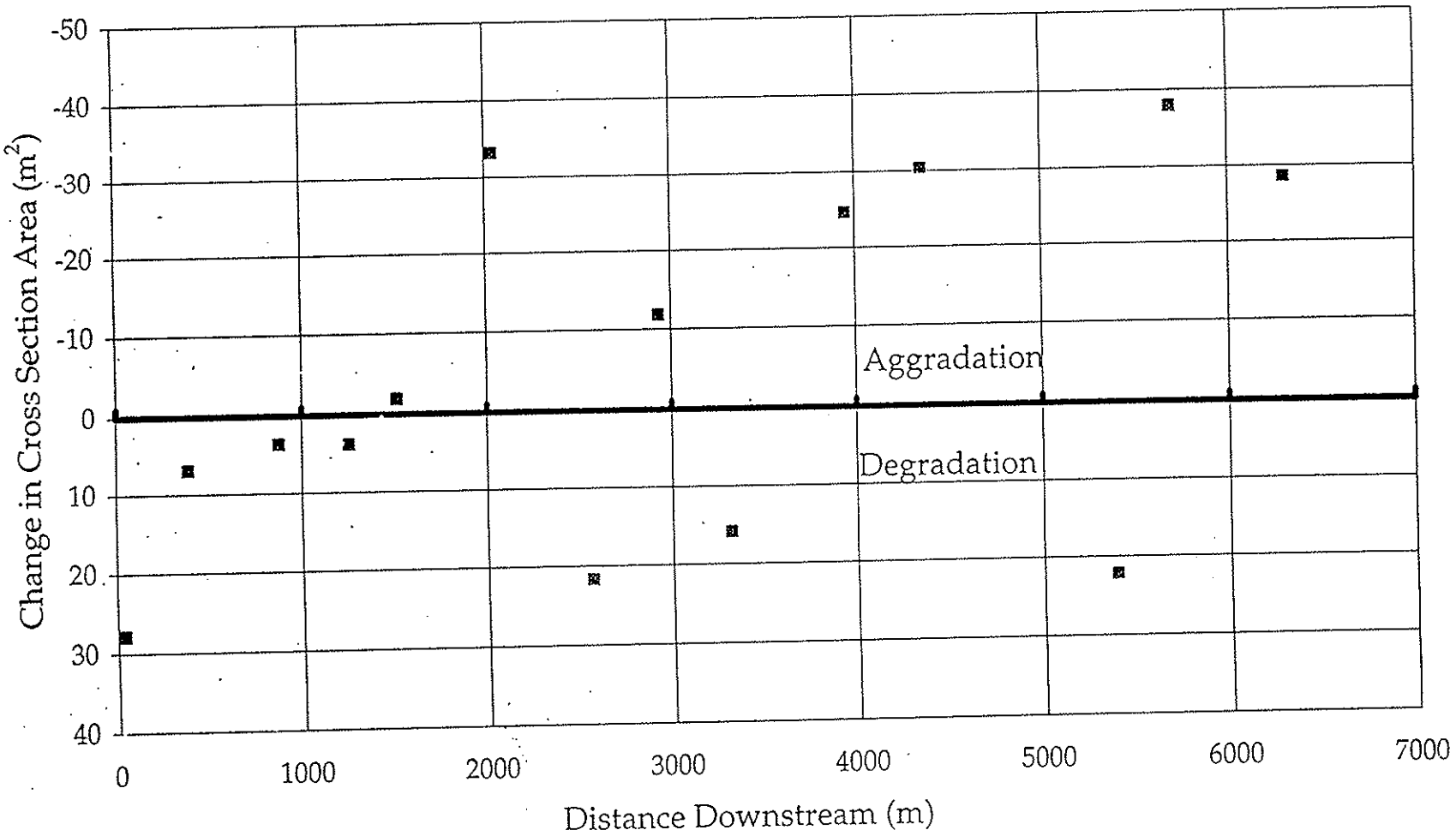

Figure 4a. Change in Cross-Section Area between 1996 and 1997.

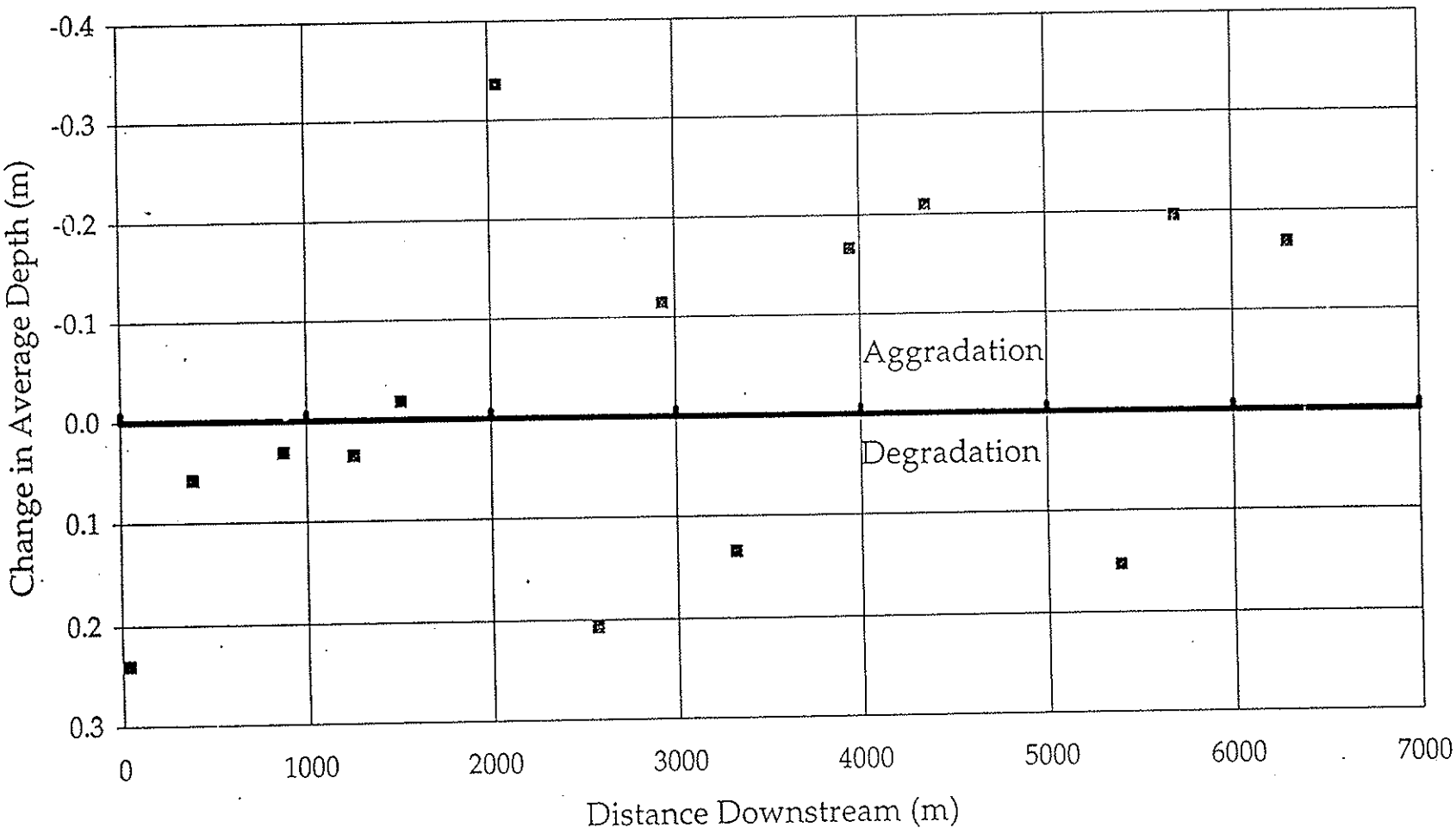

Figure 4b. Change in Average Cross-Section Depth between 1996 and 1997.

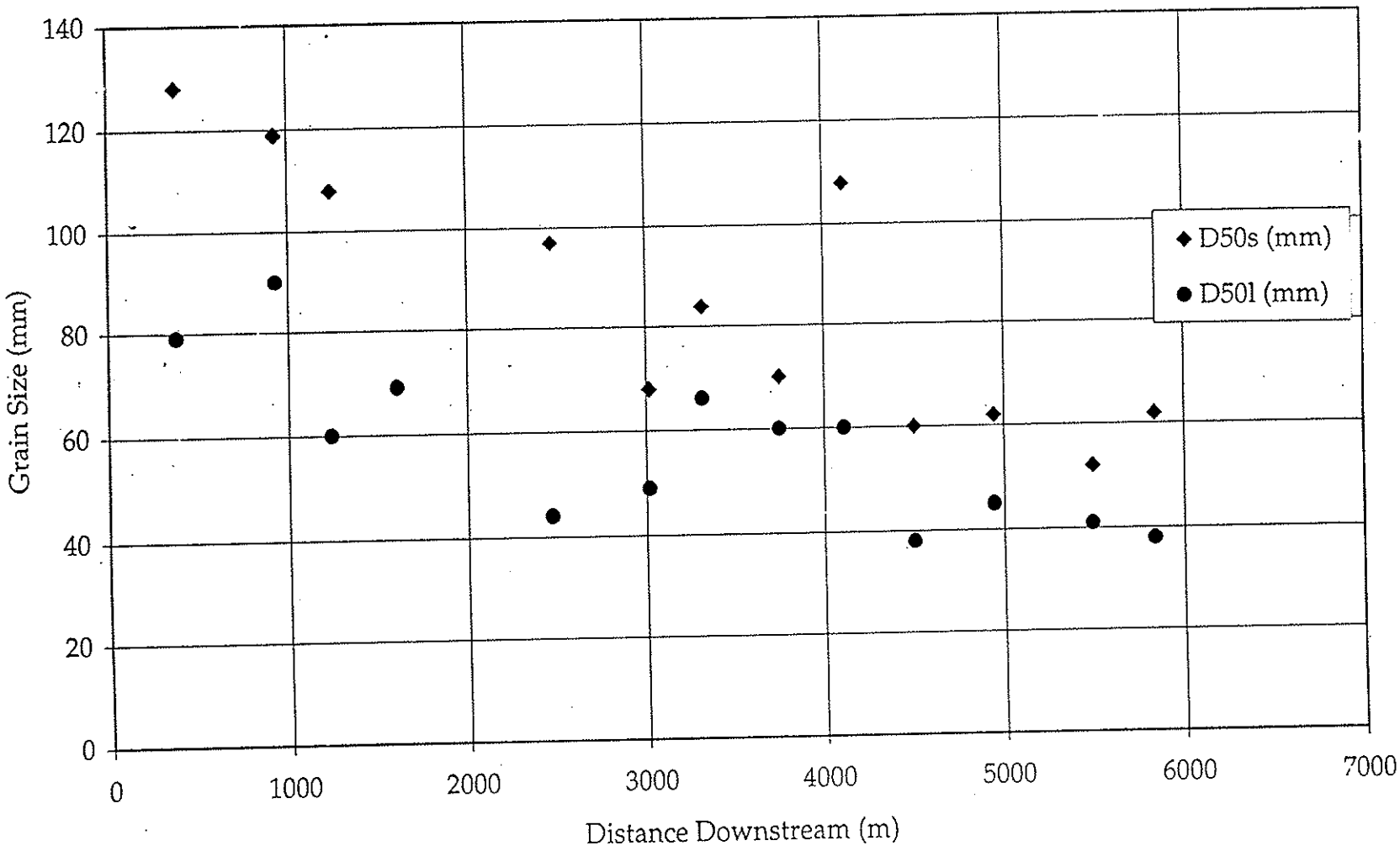

Figure 5a. Surface and Subsurface Grain Size Data

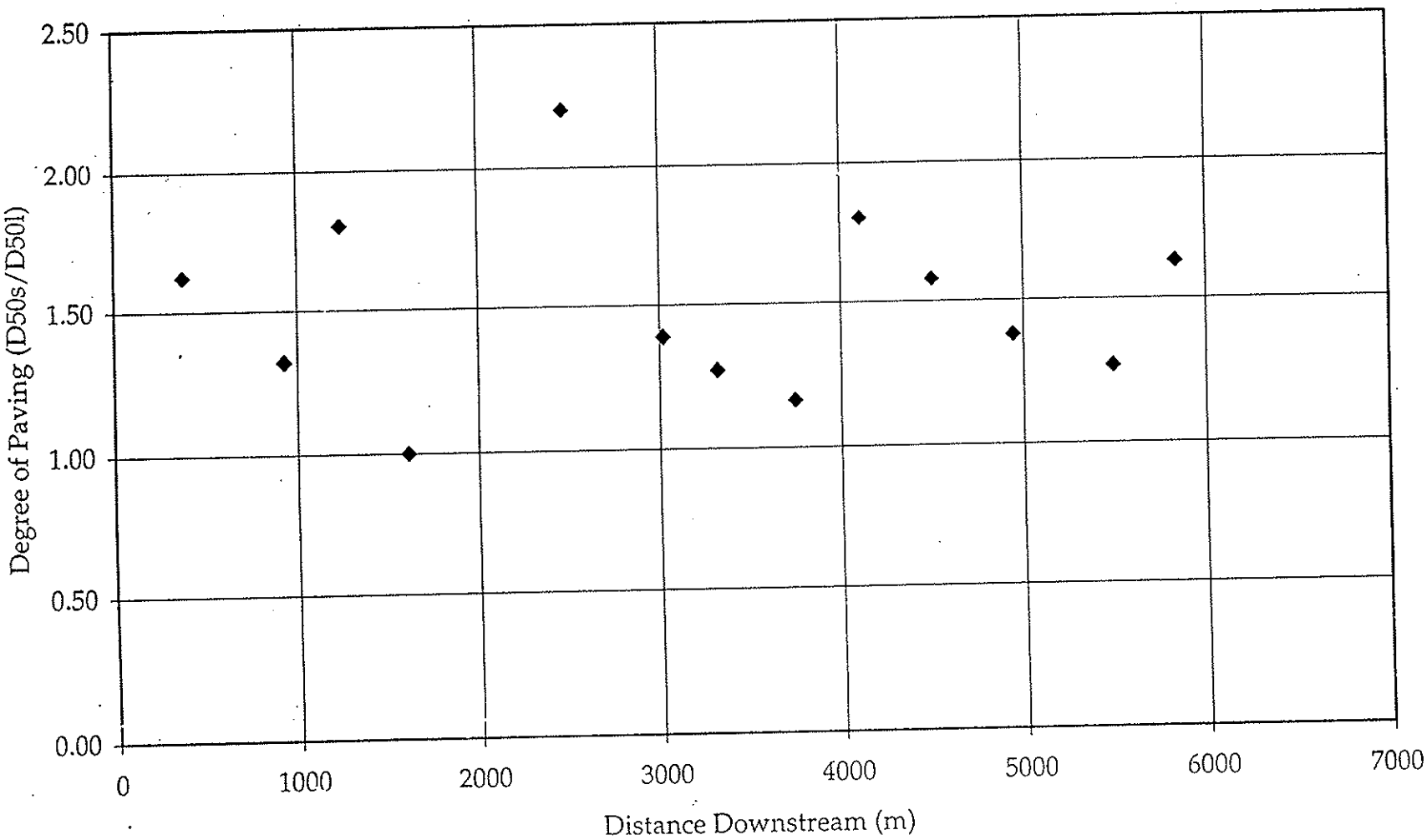

Figure 5b. Degree of Paving

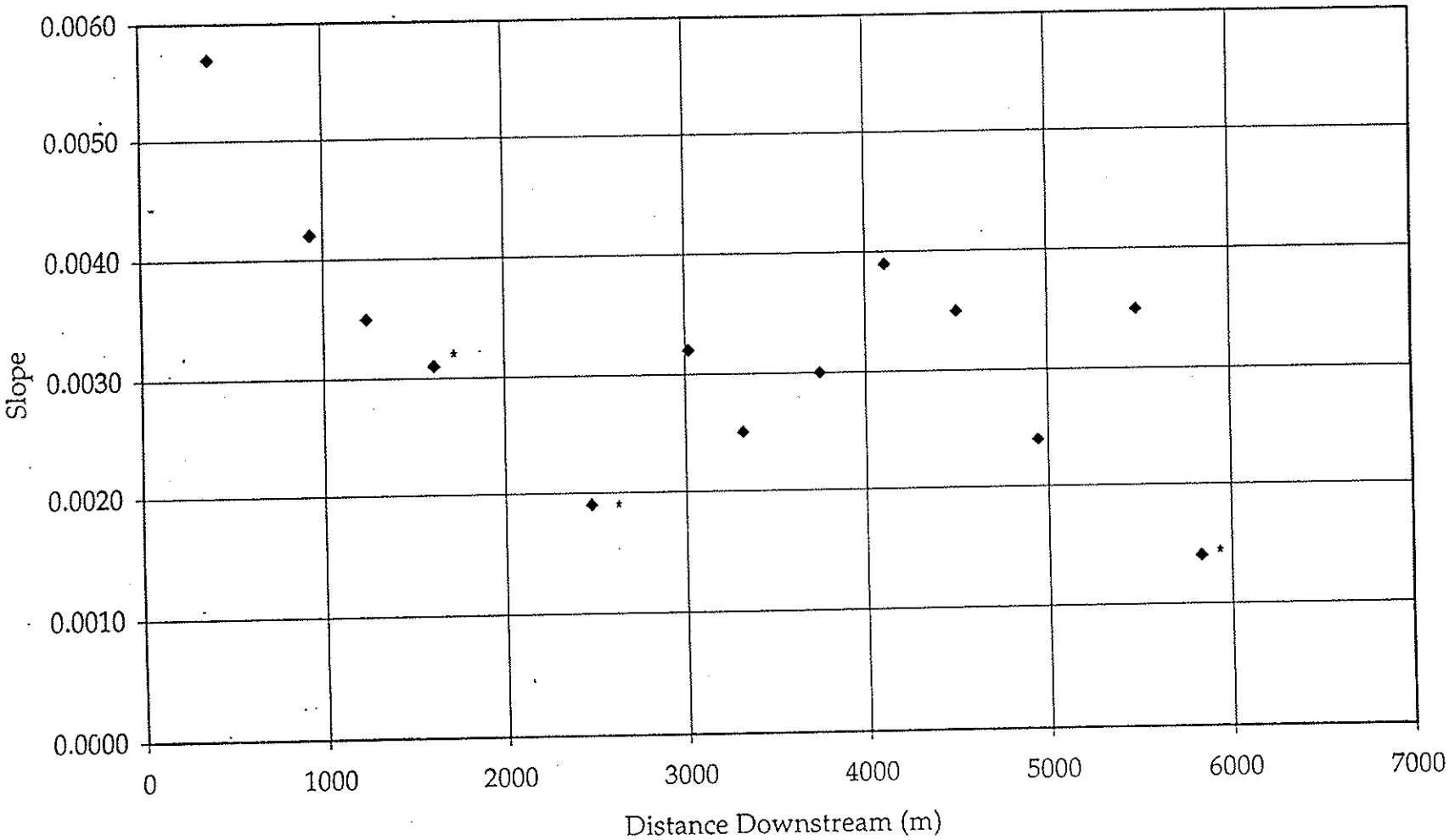

Figure 6a. Local Water Surface Slope (* point influenced by local hydraulic conditions, see discussion in text).

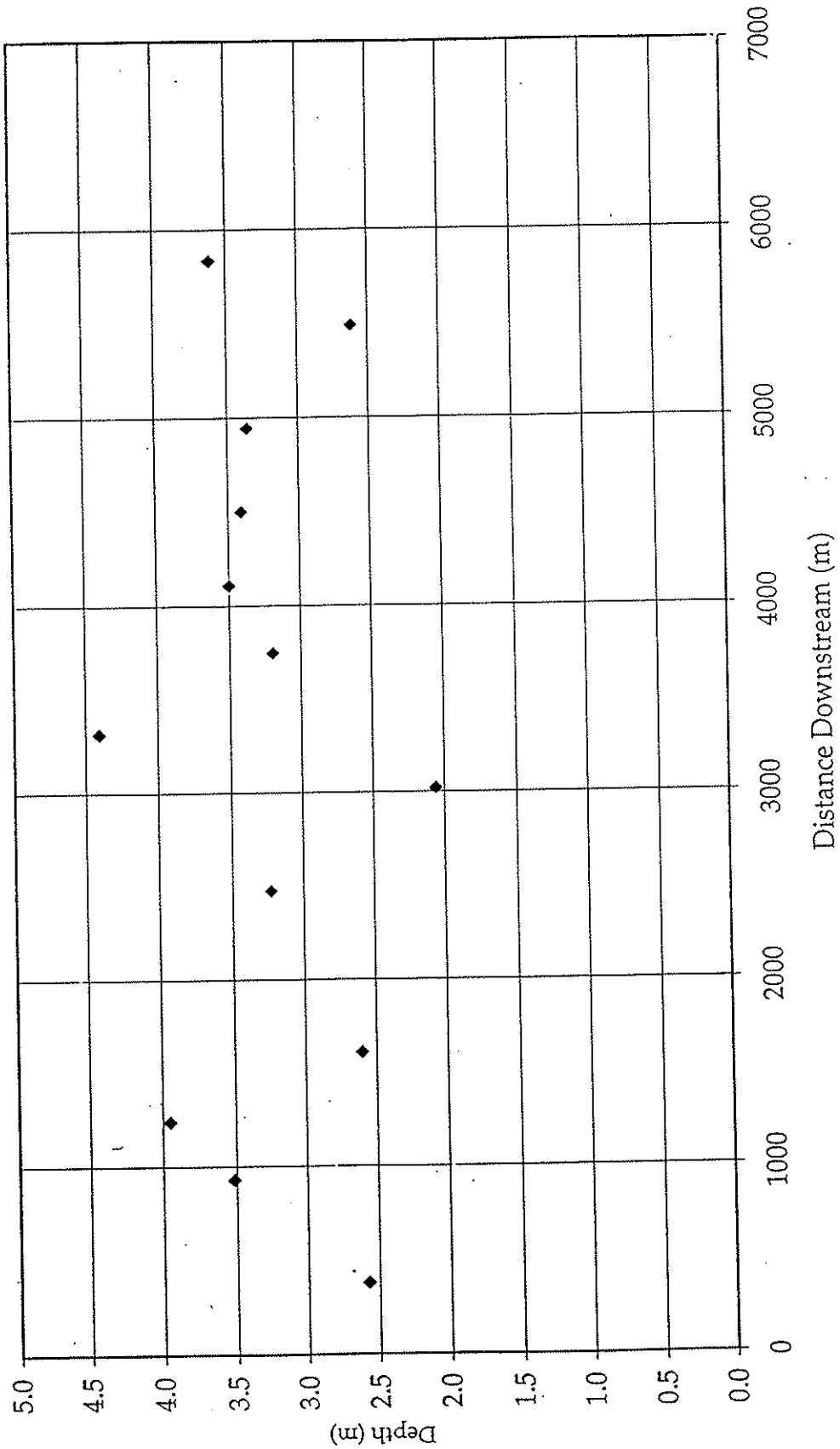

Figure 6b. Local Depth of Water.

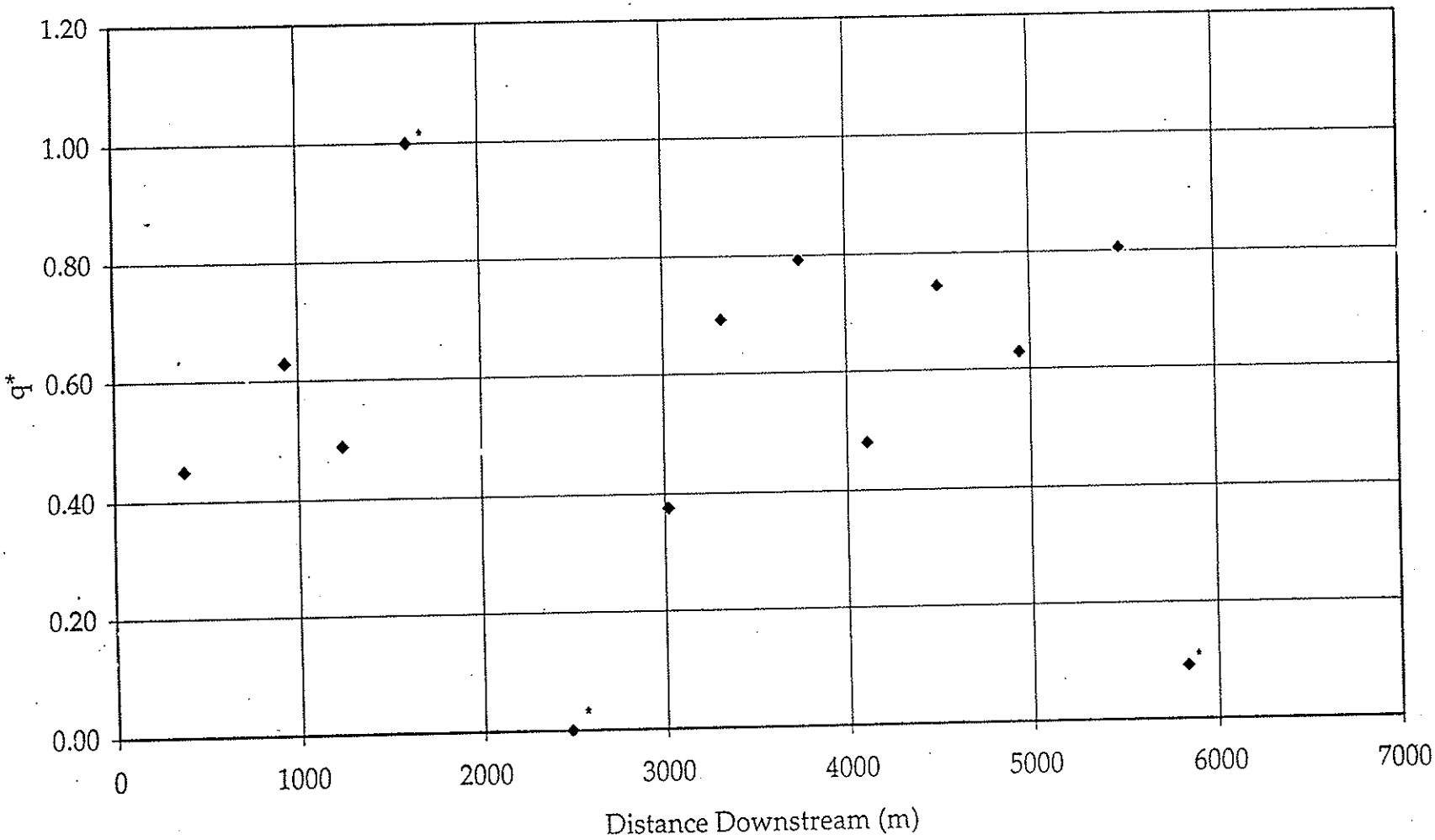

Figure 7. Calculated q* values (* point influenced by local hydraulic conditions, see discussion in text).

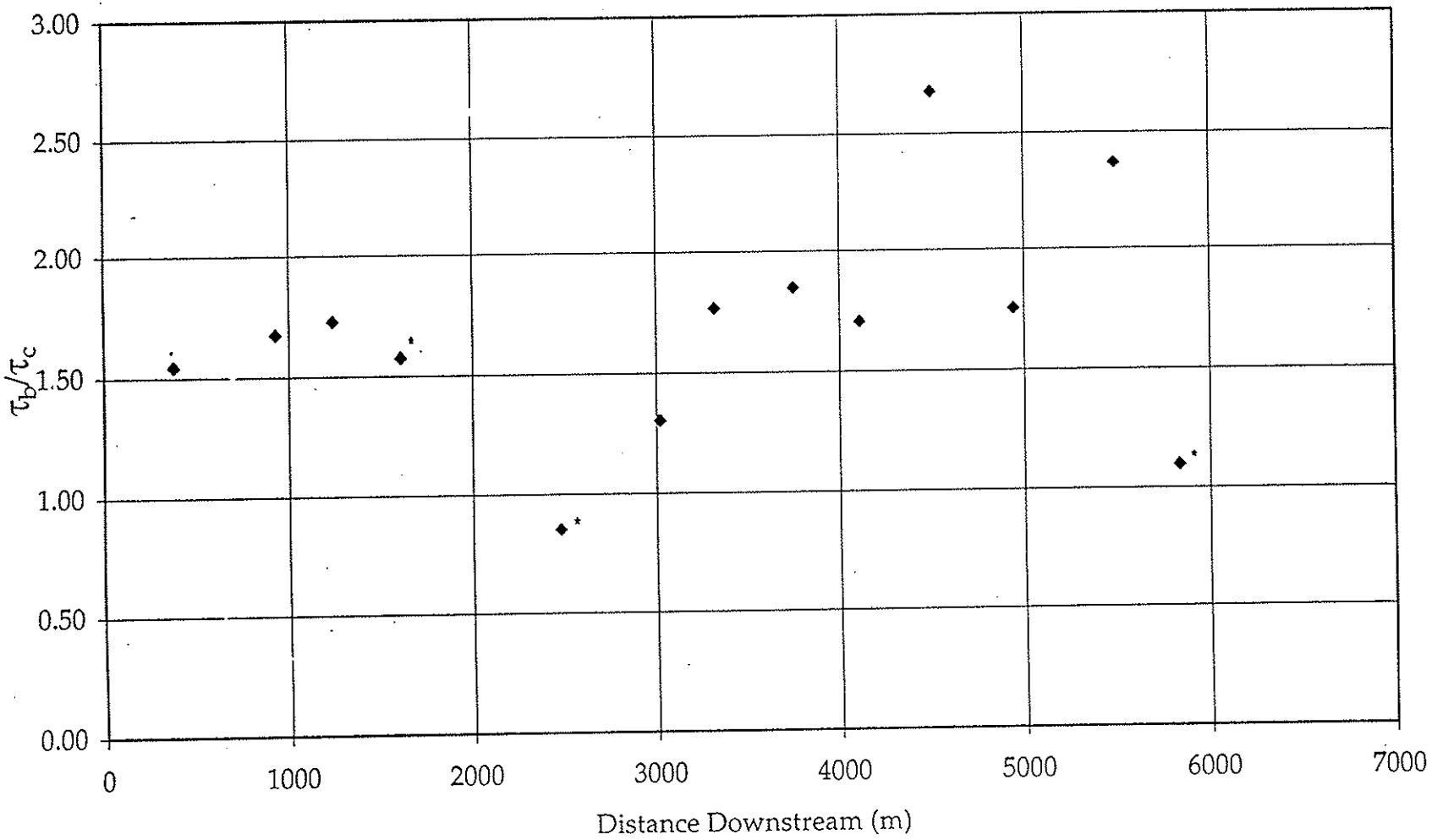

Figure 8. Shear Stress Ratio. Bed shear stress over critical bed shear stress (* point influenced by local hydraulic conditions, see discussion in text).

SOURCES

Andrews, E.D. 1994. Marginal bed load transport in a gravel bed stream, Sagehen Creek, California. *Water Resources Research* 30(7): 2241-2250.

_____. and Erman, D.C. 1986. Resistance in the size distribution of surficial bed material during an extreme snowmelt flood. *Water Resources Research* 22(2): 191-197.

_____. 1983. Entrainment of gravel from naturally sorted riverbed material. *Geological Society of America Bulletin* 82: 1225-1231.

_____. 1980. Effective and bankfull discharges of streams in the Yampa river basin, Colorado and Wyoming. *Journal of Hydrology,* 46: 311-330.

Ashworth, P.J., and Ferguson, R.I. 1989. Size-selective entrainment of bed load in gravel bed streams. *Water Resources Research* 25(4): 627-634.

Benda, L. 1990. The influence of debris flows on channels and valley floors in the Oregon coast range, USA. *Earth Surface Processes and Landforms* 15: 457-466.

Buffington, J.M. 1996. An alternative method for determining subsurface grain size distributions of gravel-bedded rivers. *Eos, Transactions, American Geophysical Union* 77(46): F250.

Cenderelli, D.A., and Kite, J.S. 1998. Geomorphic effects of large debris flows on channel morphology at North Fork Mountain eastern West Virginia, USA. *Earth Surface Processes and Landforms* 23(1): 1-19.

Church, M.A., McLean, D.G., and Wolcott, J.F. 1987. River Bed Gravels: Sampling and Analysis. (3): 43-88. In: Thorne, C. R., Bathurst, J. C., and Hey, R. D. *Sediment Transport in Gravel-bed Rivers.* John Wiley & Sons Ltd.: London.

Dietrich, W., Kirchner, J., Ikeda, H., and Iseya, F. 1989. Sediment supply and the development of the coarse surface layer in gravel-bedded rivers. *Nature* 340: 215-218.

Everitt, B., 1993. Channel responses to declining flow on the Rio Grande between Ft. Quitman and Presidio, Texas. *Geomorphology* 6: 225-242.

Gilbert, G.K. 1917. Hydraulic mining debris in the Sierra Nevada. United States Geological Survey Professional Paper 105: 154 pp.

Henderson, F.M. 1966. *Open Channel Flow.* MacMillan Series in Civil Engineering, MacMillan Publishing Co., Inc., New York: 522 pp.

James, L.A. 1997. Time and the Persistence of Alluvium: River Engineering, Fluvial Geomorphology, and Mining Sediment in California. In: Giardino, J.R., and Marstou, R. (eds), *Engineering Geomorphology,* Proceedings Binghamton Geomorphology Symposium, Italy.

_____. 1994. Channel changes wrought by gold mining: northern Sierra Nevada, California: Effects of Human-Induced Changes on Hydrologic Systems, *American Water Resources Association* June: 629-638.

_____. 1991. Incision and morphologic evolution of an alluvial channel recovering from hydraulic mining sediment. *Geological Society of America Bulletin* 103: 723-736.

_____. 1989. Sustained storage and transport of hydraulic gold mining sediment in the Bear River, California. *Annals of the Association of American Geographers* 79: 570-592.

Keller, E.A. 1971. Areal sorting of bed-load material: The hypothesis of velocity reversal. *Geological Society of America Bulletin* 82: 753-756.

Kinerson, D. 1990. Bed surface response to sediment supply. M.S. thesis, University of California, Berkeley, California.

Laddish, K.M. 1996. Response of the North Fork of the American River, California, to Hydraulic Mining. M.S. thesis, University of California, Davis, California.

Lane, S.N., Richards, K.S., and Chandler, J.H. 1996. Discharge and sediment supply controls on erosion and deposition in a dynamic alluvial channel. *Geomorphology* 15: 1-15.

Lisle, T.E. 1986. Stabilization of a gravel channel by large streamside obstructions and bedrock bends, Jacoby Creek, northwestern California. *Geological Society of America Bulletin,* 97: 999-1011.

_____. 1995. Particle size variations between bed load and bed material in natural gravel bed channels. *Water Resources Research* 31(4): 1107-1118.

Lisle, T.E., Iseya, F., and Ikeda, H. 1993. Response of a channel with alternate bars to a decrease in supply of mixed-size bed load: a flume experiment: Water Resources Research, 29(11): 3623-3629.

Lisle, T.E., and Madej, M.A. 1992. Spatial Variation in Armouring in a Channel with High Sediment Supply. In: Billi, P., Hey, R. D., Thorne, C. R., and Tacconi, P., *Dynamics of Gravel-bed Rivers.* (13): 277-293.

Lisle, T.E., and Hilton, S. 1992. The volume of fine sediment in pools: an index of sediment supply in gravel-bed streams. *Water Resources Bulletin* 28(2): 371-383.

Meyer-Peter, E., and Mueller, R. 1948. Formulas for bed-load transport. International Association of Hydraulic Research, 2nd Meeting Proceedings, Stockholm: 39-64.

Montgomery, D.R., and Buffington, J.M. 1997. Channel-reach morphology in mountain drainage basins. *Geological Society of America Bulletin* 109(5): 596-611.

Parker, G., Dhamotharan, S., and Stefan, H. 1982a. Model experiments on mobile, paved gravel bed streams: Water Resources Research, 18, p. 1395-1408.

Parker, G., Klingeman, P.C., and McLean, D.G. 1982b. Bedload and size distribution in paved gravel-bed streams. Journal of Hydraulics Division, American Society of Civil Engineers, 108(HY4): 544-571.

Parker, G., and Klingeman, P.C. 1982. On why gravel bed streams are paved. *Water Resources Bulletin,* 18(2): 1409-1423.

Petts, G.E.. 1979. Complex response of river channel morphology subsequent to reservoir construction. *Progress in Physical Geography* 3: 329-362.

Saucedo, G.L., and Wagner, D.L. 1992. Geologic Map of the Chico Quadrangle, CA, California Department of Mines and Geology.

United States Geological Survey. 1942. 1936 plan and profile, American River California. Unpublished file report, Map Library, University of California, Berkeley.

Wagner, D.L., et al. 1992. Geologic map of the Sacramento Quadrangle, CA, California Department of Mines and Geology.

Wilcock, P.R., and McArdell, B.R. 1993. Surface-based fractional transport rates: Mobilization thresholds and partial transport of a sand-gravel sediment. *Water Resources Research* 29(4): 1297-1312.

Wilcock, P.R., and Southard, J.B. 1989. Bed load transport of mixed size sediment: fractional transport rates, bed forms, and the development of a course bed surface layer. *Water Resources Research* 25(7): 1629-1641.

Williams, G.P., and Wolman, M.G. 1984. Downstream effects of dams on alluvial rivers. United States Geological Survey Professional Paper 1286: 83 pp.

Wohl, E.E., et al. 1996. A comparison of surface sampling methods for coarse fluvial sediments. *Water Resources Research* 32: 3219-3226.

Wolman, M.G. 1954. A method of sampling coarse river-bed material. *EOS Transactions, American Geophysical Union* 35: 951-956.

Wyzga, B. 1993. River response to channel regulation: case study of the Raba River, Carpathians, Poland. *Earth Surface Processes and Landforms* 18: 541-556.

APPENDICES

Appendix 1

Summary Table

SUMMARY TABLE OF DATA, NORTH FORK AMERICAN RIVER

Bar #	Sediment Sample # ss#	Nearby XS#	Sample Location Dist. Downstream (m)	Surface Samples			Subsurface Samples			Degree of paving D50s/D50l	Local Depth of Water (m)	Local Slope	q*	Shear Stress Ratio
				D50s (mm)	D84s (mm)	% quartz	D50l (mm)	D84l (mm)	% quartz					
1	1	1,2,3	380	128	239	2	79	180	6	1.62	2.6	0.0057	0.45	1.54
2	2	3	930	119	294	3	90	304	8	1.32	3.5	0.0042	0.63	1.67
3	3	4	1240	108	175	3	60	152	14	1.80	4.0	0.0035	0.49	1.72
4	4	5	1610	69	175	7	69	158	8	1.00	2.6	0.0031	1.00	1.57
6	6	7	2475	97	231	5	44	100	8	2.20	3.2	0.0019	null	0.85
7	7	8	3020	68	108	6	49	104	9	1.39	2.1	0.0032	0.38	1.30
8	8	9	3320	84	158	8	66	137	4	1.27	4.4	0.0025	0.69	1.76
9	9	10	3750	70	137	5	60	128	5	1.17	3.2	0.0030	0.79	1.85
10	10	10,11	4110	108	175	2	60	115	2	1.80	3.5	0.0039	0.48	1.70
11a	11a	11	4500	60	115	5	38	90	8	1.58	3.4	0.0035	0.74	2.68
11b	11b	12	4945	62	119	10	45	100	8	1.38	3.4	0.0024	0.63	1.75
12	12	13,14	5490	52	90	10	41	97	12	1.27	2.6	0.0035	0.81	2.37
13	13	14	5835	62	119	17	38	100	18	1.63	3.6	0.0014	0.09	1.10

Appendix 2

1996 and 1997 Cross-section Survey Data

Fifteen cross-sections were established and surveyed in the summer and fall of 1996 and resurveyed during the summer of 1997. Each cross-section was surveyed using a Leica TC800 electronic distance meter (EDM) total station, and was permanently monumented by setting at least three 3/8 inch by 4 inch stainless steel rods into bedrock with epoxy or by pounding 3/8 inch by 3 feet rebar into the gravel bars. These monuments allowed for the exact re-establishment of the original cross-section orientation.

Locations of the cross-sections were chosen such that seven were located near those surveyed by Laddish (1996), they were evenly spaced throughout the reach on straight reaches with symmetrical cross-sections as often as possible. The data is presented in x, y, z coordinates (Easting, Northing, Elevation). The surveys were set up such that North was set perpendicular to the channel at each cross-section, facing the right bank. Therefore, the cross-sections could be easily plotted by changing the Northing data to Distance. In this way, the distance values increase toward the right bank. The monuments are labeled with both the cross-section number and monument number in the data (i.e. x10m2). The station monuments (survey origin) are labeled with just the cross-section number (i.e. x10sta). Other notes include, Pleist Trc (Pleistocene Terrace), LEW/REW (left and right edge of water), 97 L/RHW (1997 left and right bank high water mark).

The cross-sectional area beneath the 1997 high water mark was calculated for each cross-section by splitting the cross-section into rectangular cells and summing the area of each cell. Average cross-section depth was found by dividing the area by the total width and changes in area and depth between 1996 and 1997 were calculated.

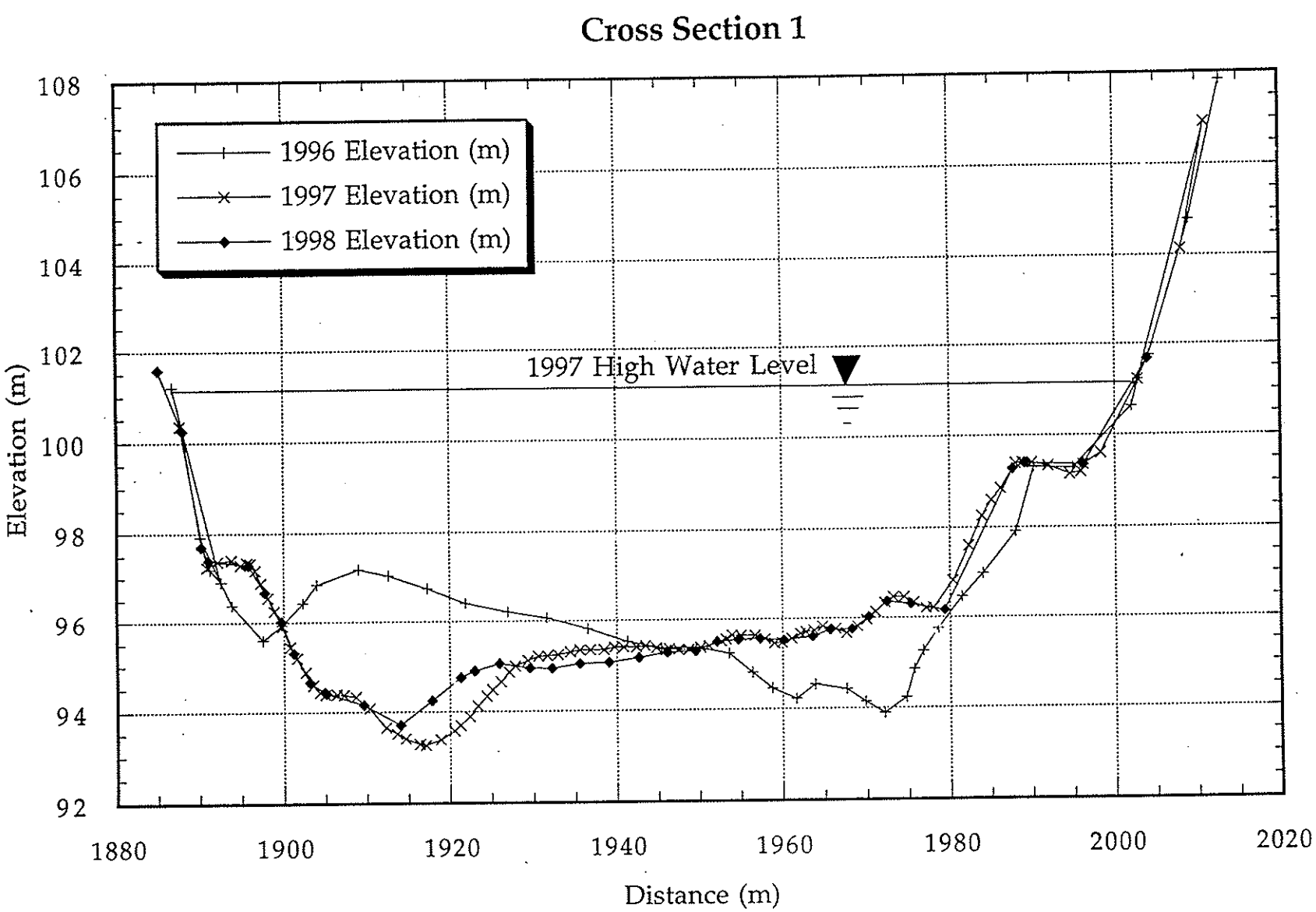
Cross Section 1
1996 Elevation (m)
1997 Elevation (m)
1998 Elevation (m)
1997 High Water Level
Elevation (m)
Distance (m)
108
106
104
102
100
98
96
94
92
1880
1900
1920
1940
1960
1980
2000
2020

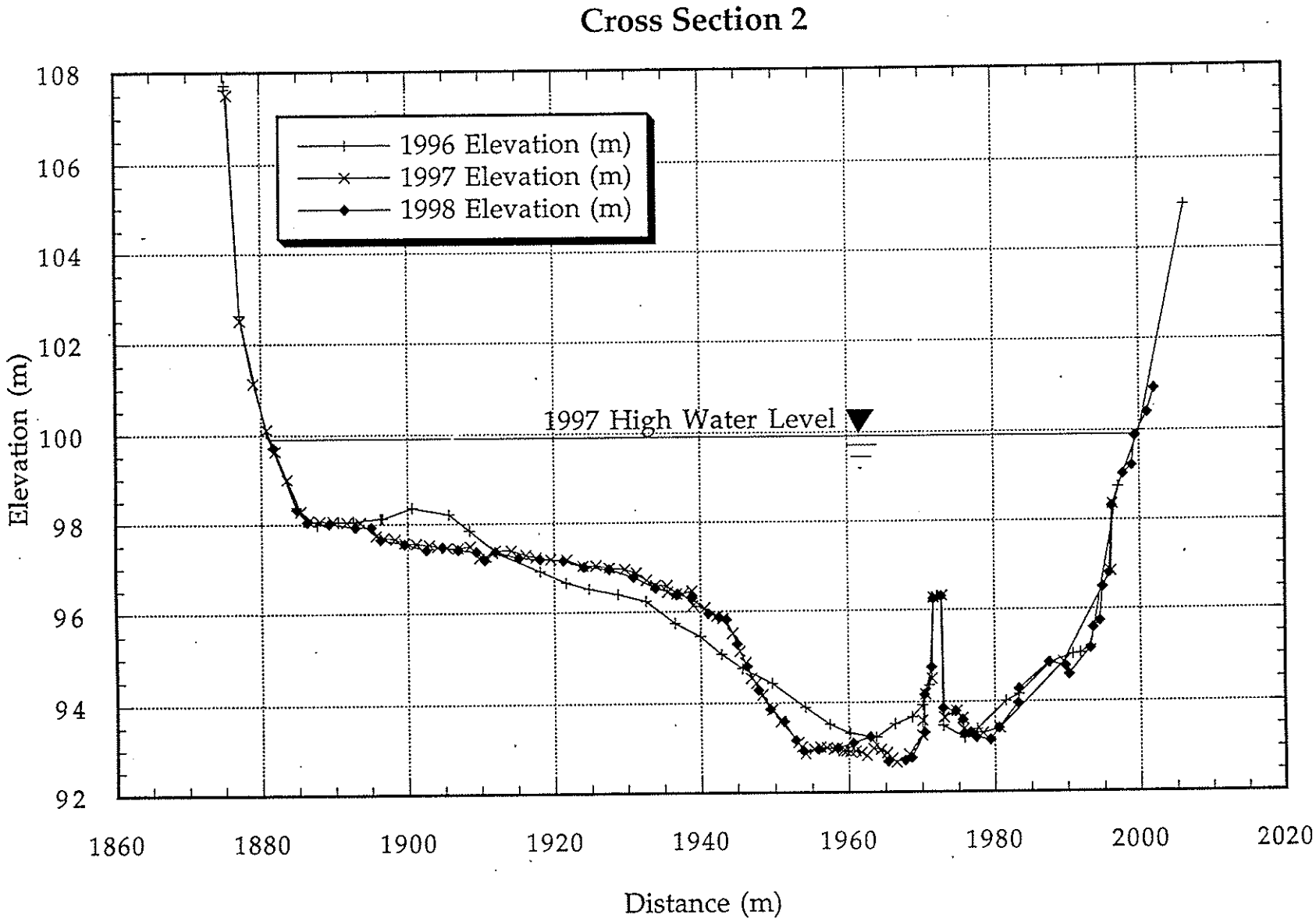
Cross Section 2
1996 Elevation (m)
1997 Elevation (m)
1998 Elevation (m)
1997 High Water Level
Elevation (m)
Distance (m)
108
106
104
102
100
98
96
94
92
1860
1880
1900
1920
1940
1960
1980
2000
2020

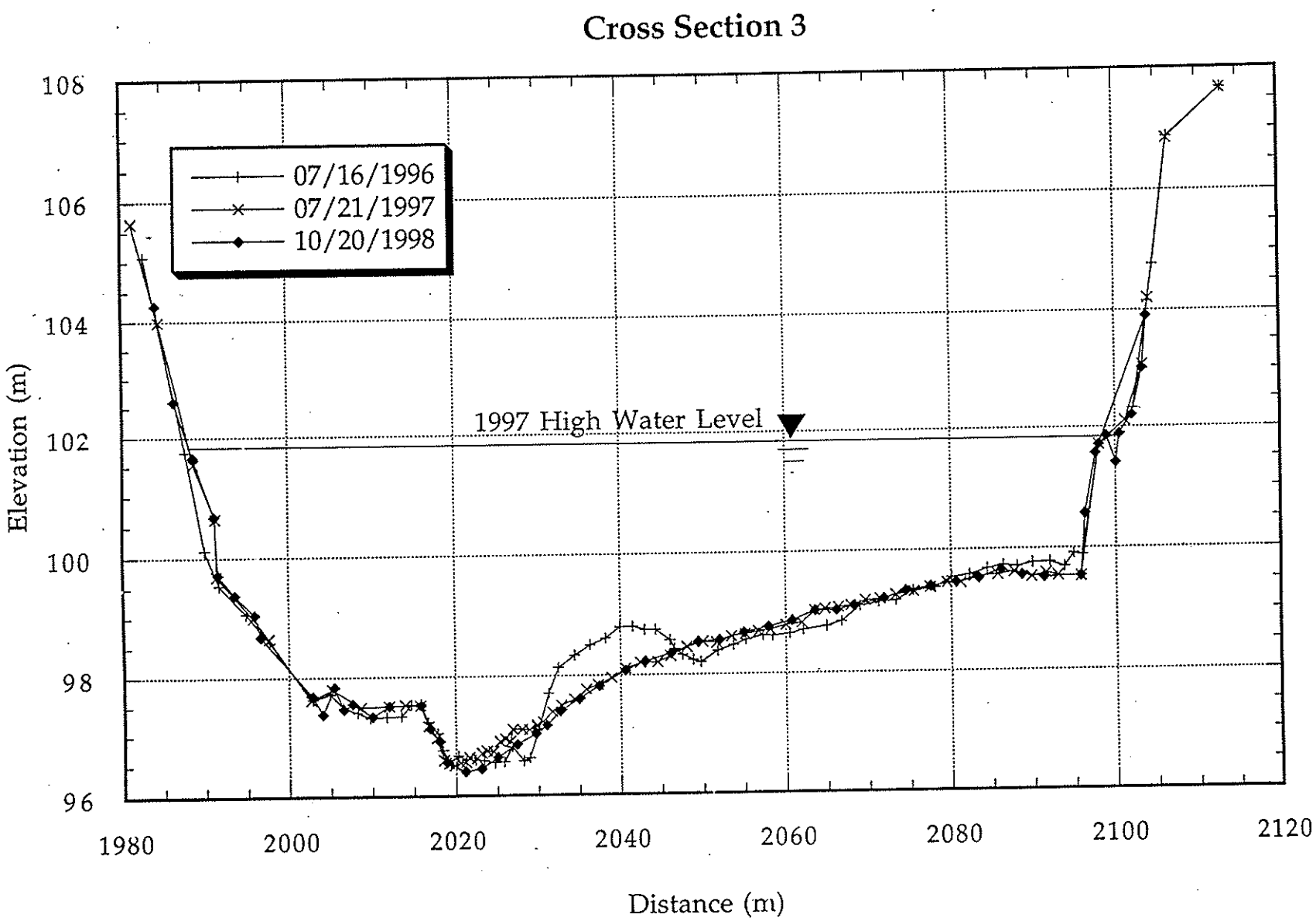
Cross Section 3
07/16/1996
07/21/1997
10/20/1998
1997 High Water Level
Elevation (m)
Distance (m)
108
106
104
102
100
98
96
1980
2000
2020
2040
2060
2080
2100
2120

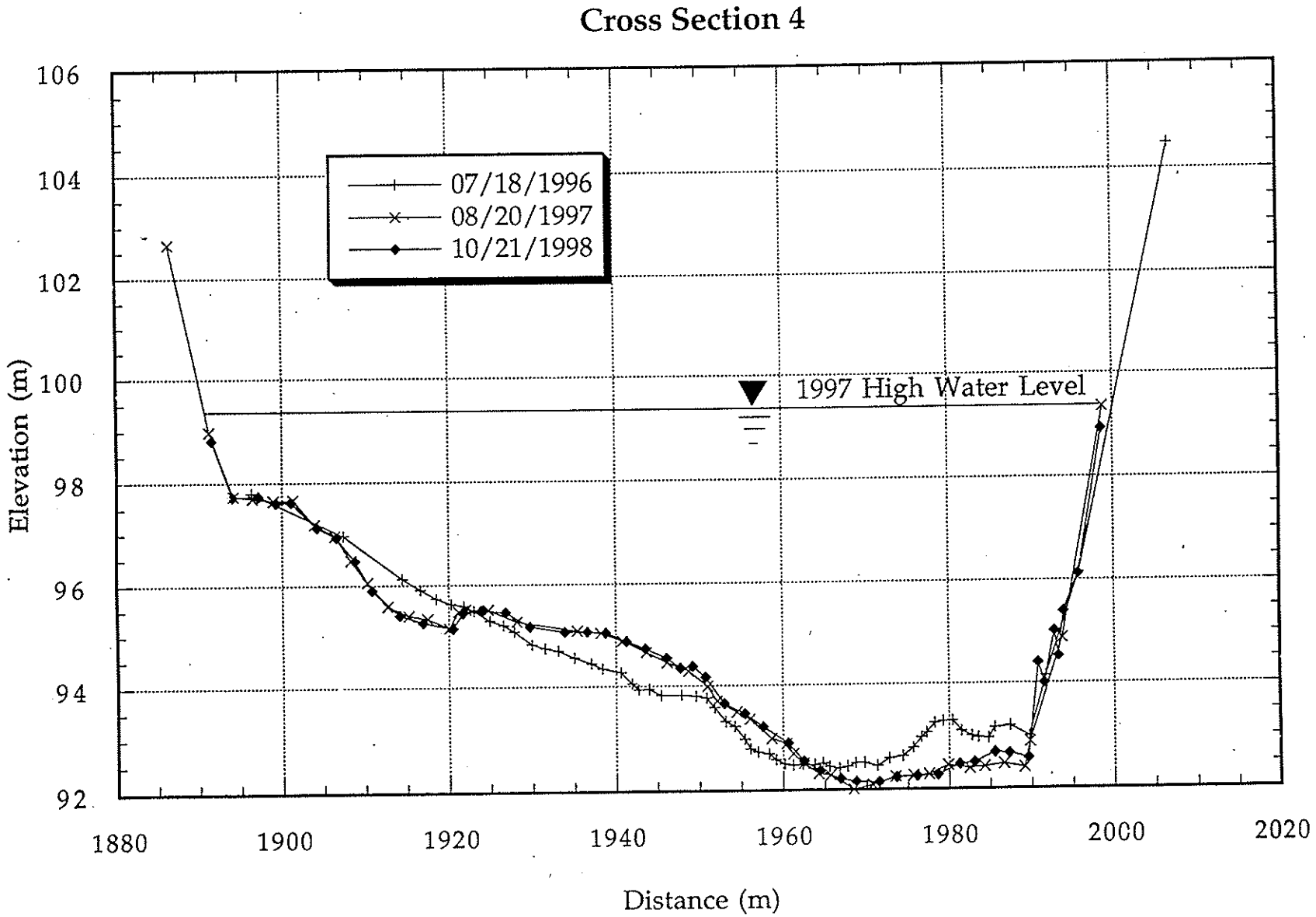
Cross Section 4
106
104
102
100
98
96
94
92
Elevation (m)
07/18/1996
08/20/1997
10/21/1998
1997 High Water Level
1880
1900
1920
1940
1960
1980
2000
2020
Distance (m)

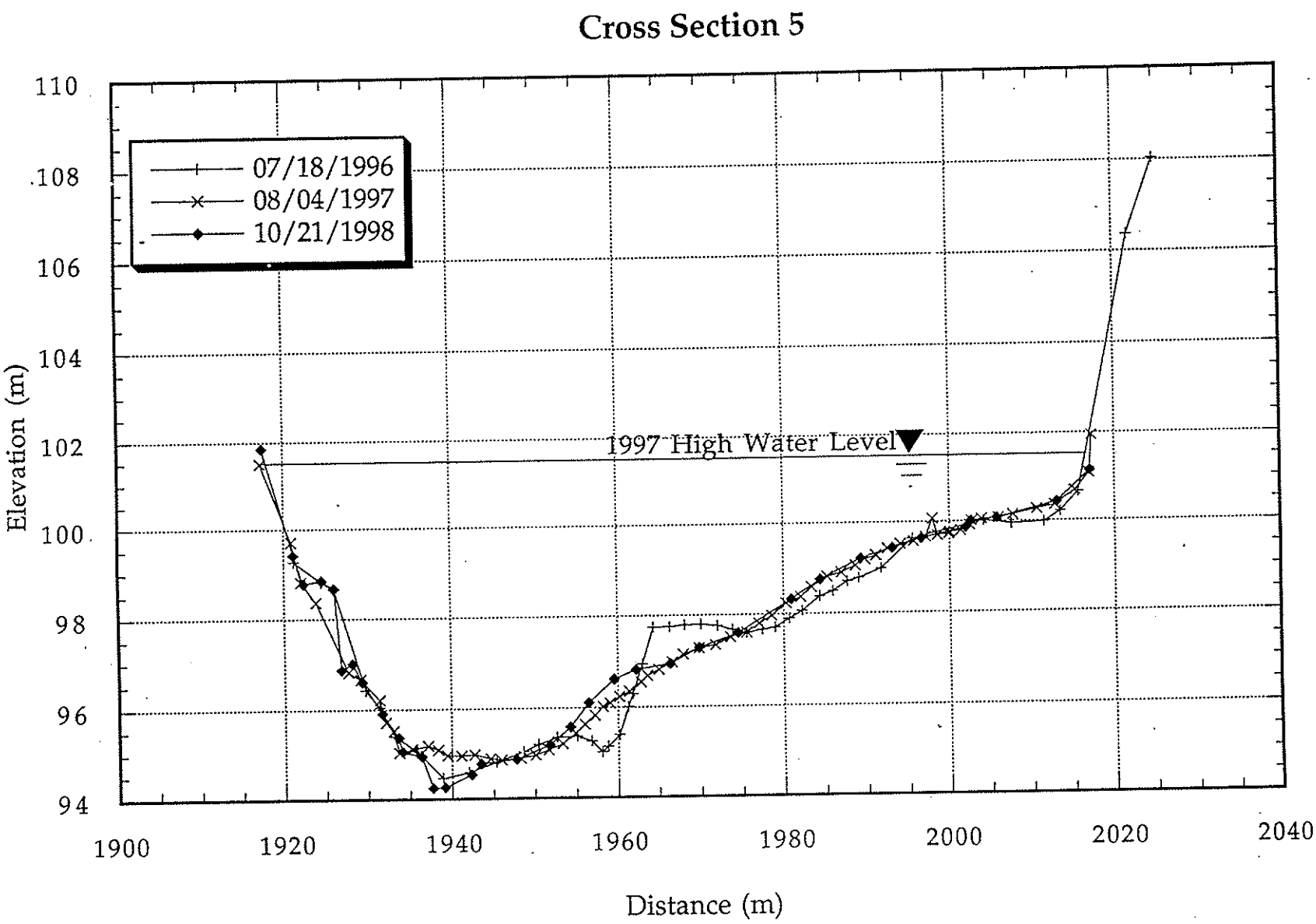
Cross Section 5
07/18/1996
08/04/1997
10/21/1998
1997 High Water Level
Elevation (m)
110
108
106
104
102
100
98
96
94
1900
1920
1940
1960
1980
2000
2020
2040
Distance (m)

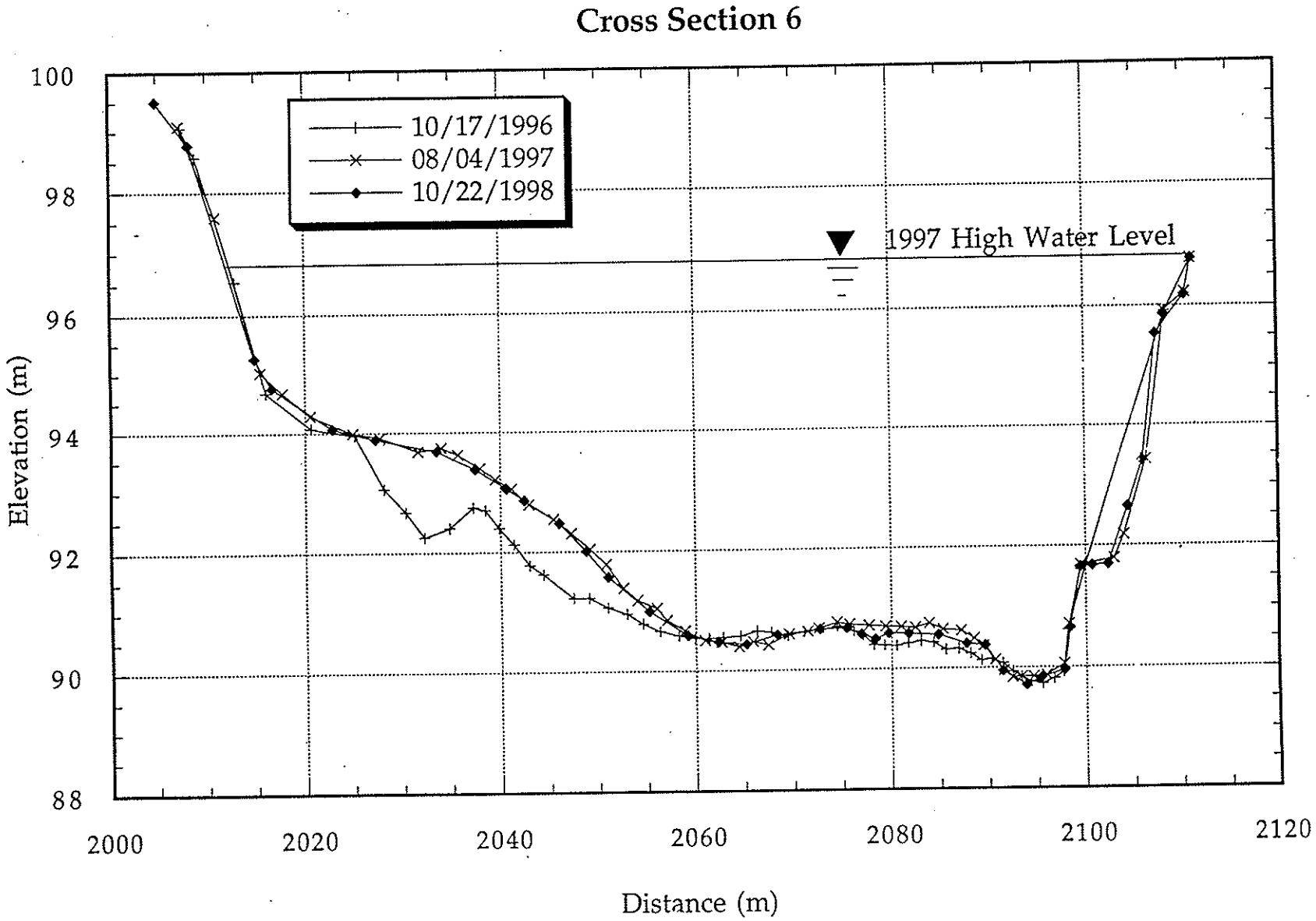
Cross Section 6
10/17/1996
08/04/1997
10/22/1998
1997 High Water Level
Elevation (m)
100
98
96
94
92
90
88
2000
2020
2040
2060
2080
2100
2120
Distance (m)

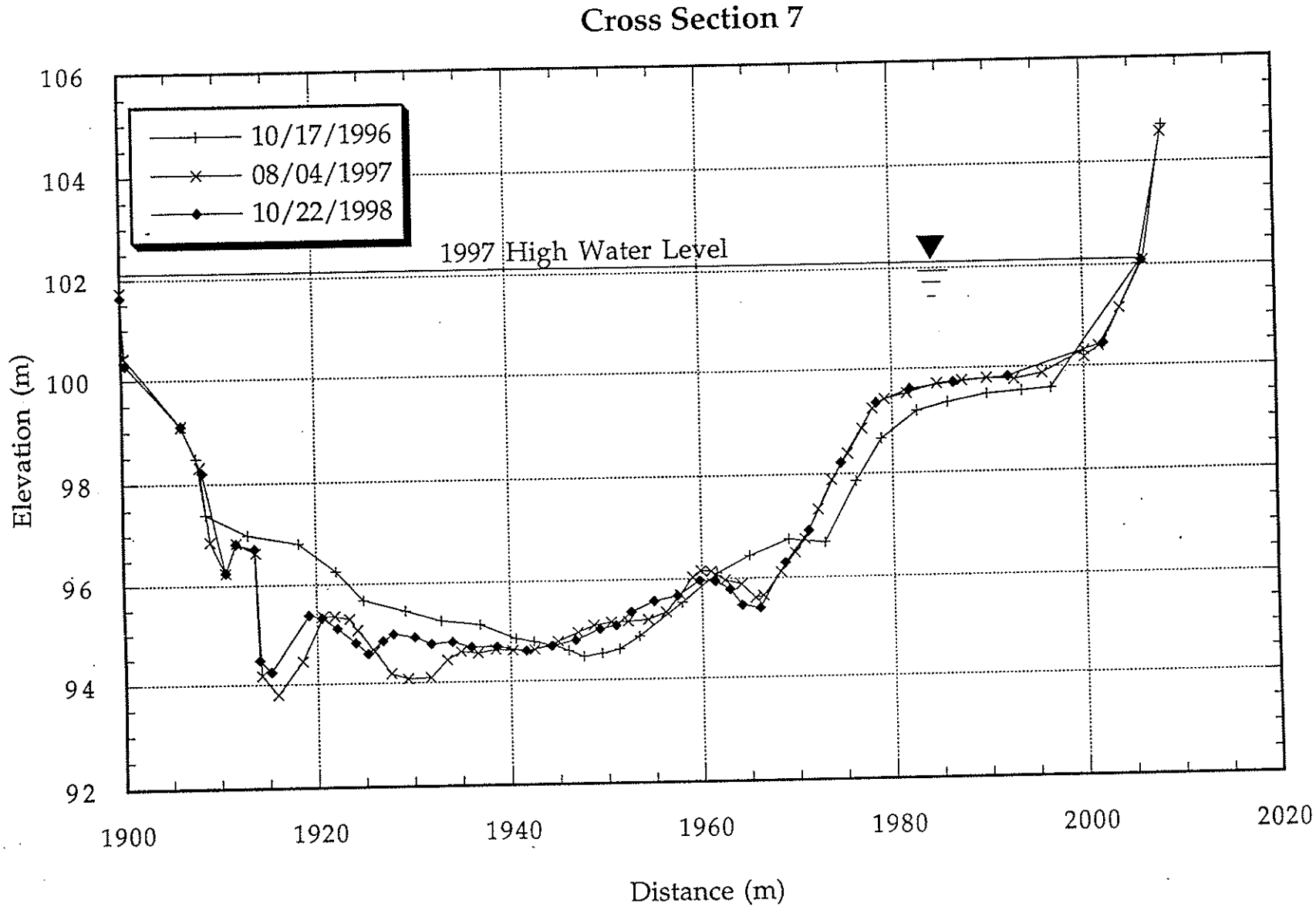
Cross Section 7
10/17/1996
08/04/1997
10/22/1998
1997 High Water Level
Elevation (m)
106
104
102
100
98
96
94
92
1900
1920
1940
1960
1980
2000
2020
Distance (m)

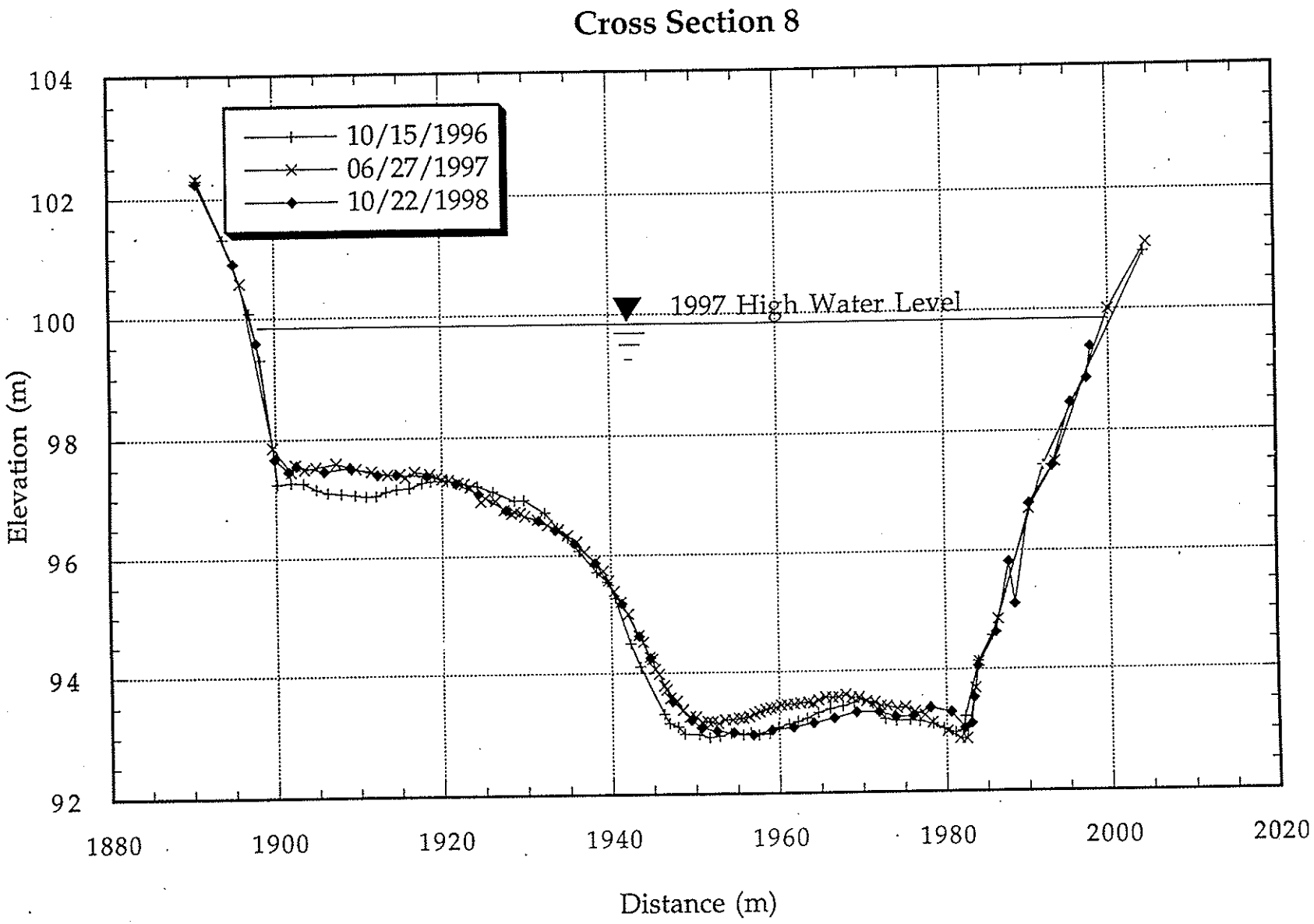
Cross Section 8
10/15/1996
06/27/1997
10/22/1998
1997 High Water Level
Elevation (m)
104
102
100
98
96
94
92
1880
1900
1920
1940
1960
1980
2000
2020
Distance (m)

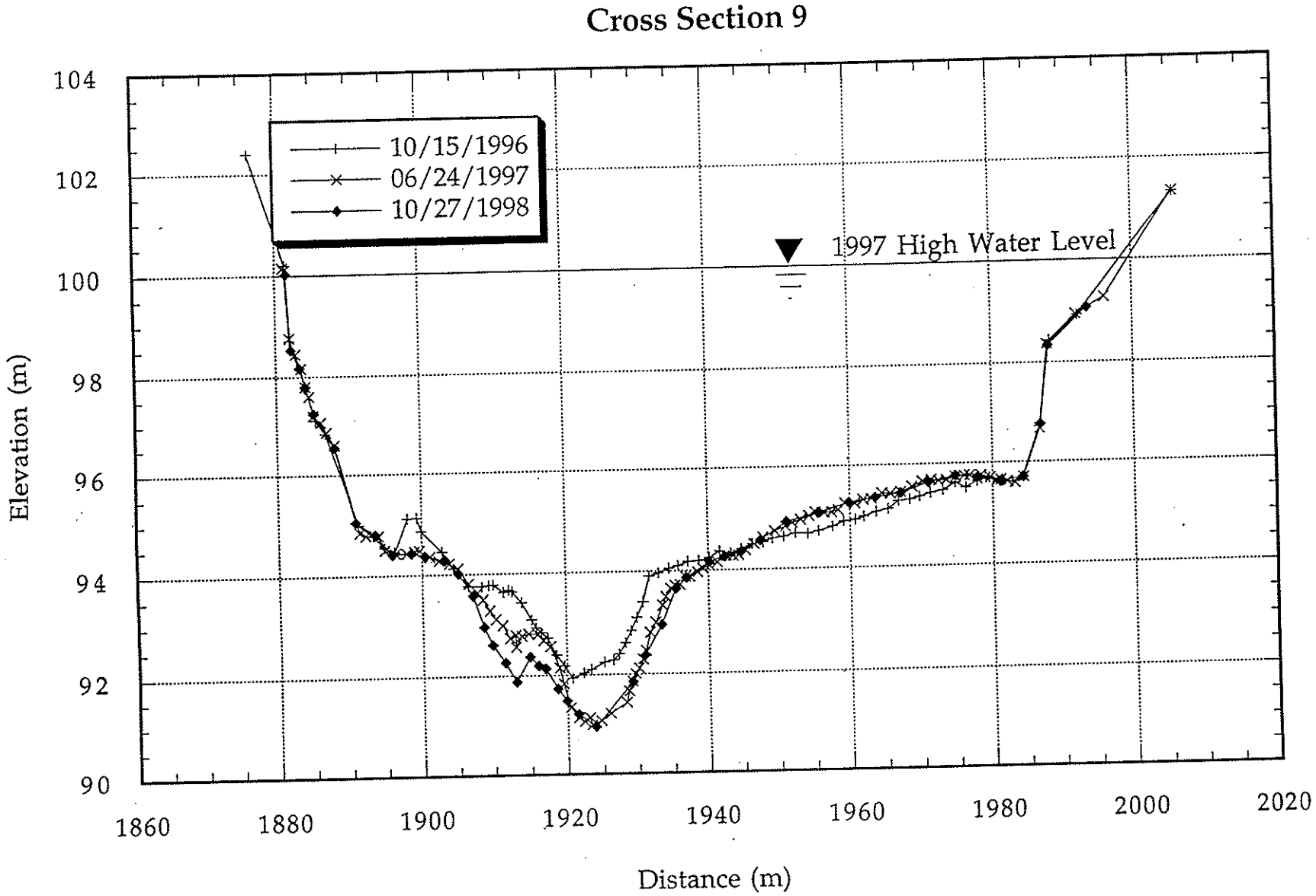
Cross Section 9
10/15/1996
06/24/1997
10/27/1998
1997 High Water Level
Elevation (m)
Distance (m)
104
102
100
98
96
94
92
90
1860
1880
1900
1920
1940
1960
1980
2000
2020

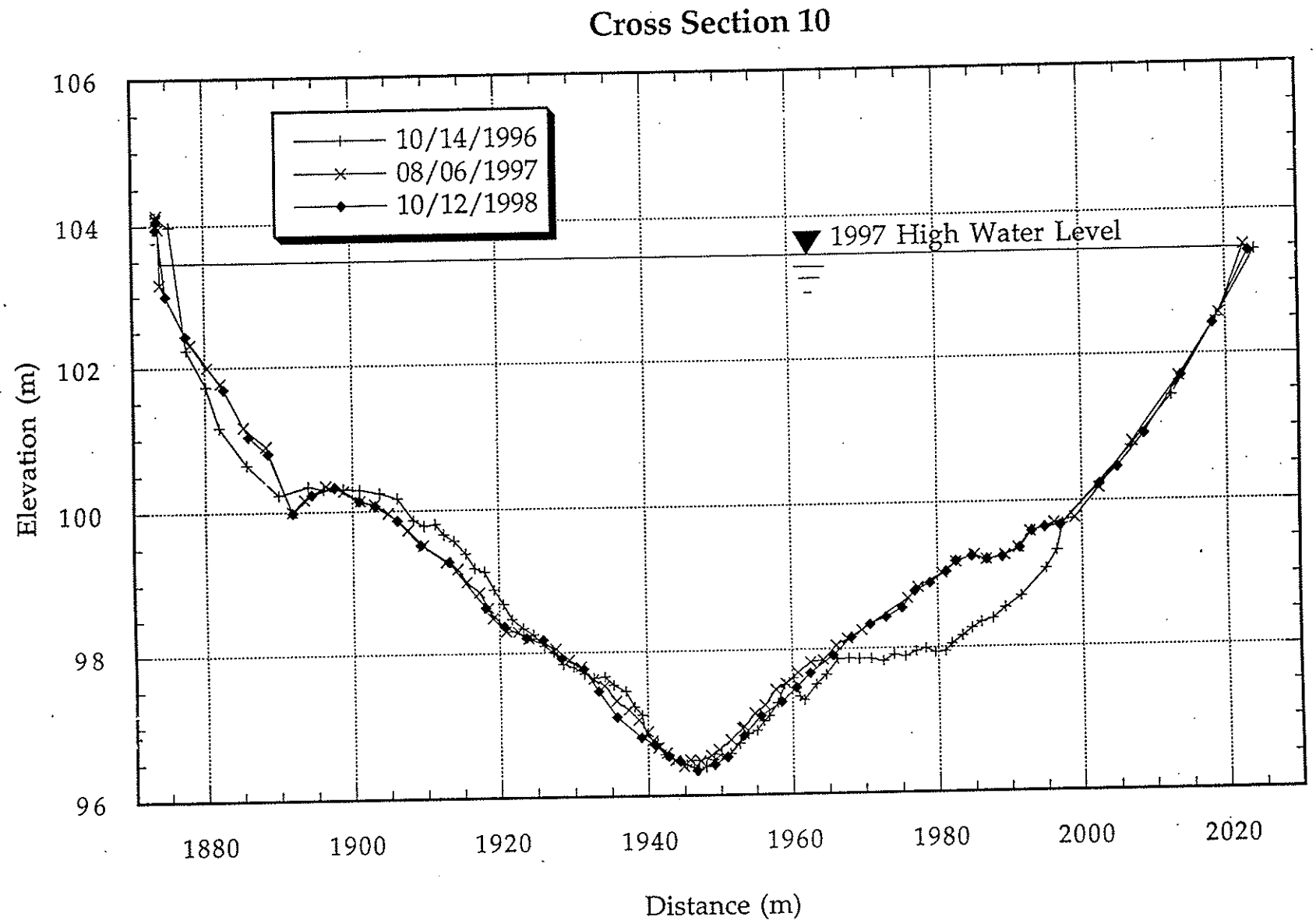
Cross Section 10
10/14/1996
08/06/1997
10/12/1998
1997 High Water Level
Elevation (m)
106
104
102
100
98
96
1880
1900
1920
1940
1960
1980
2000
2020
Distance (m)

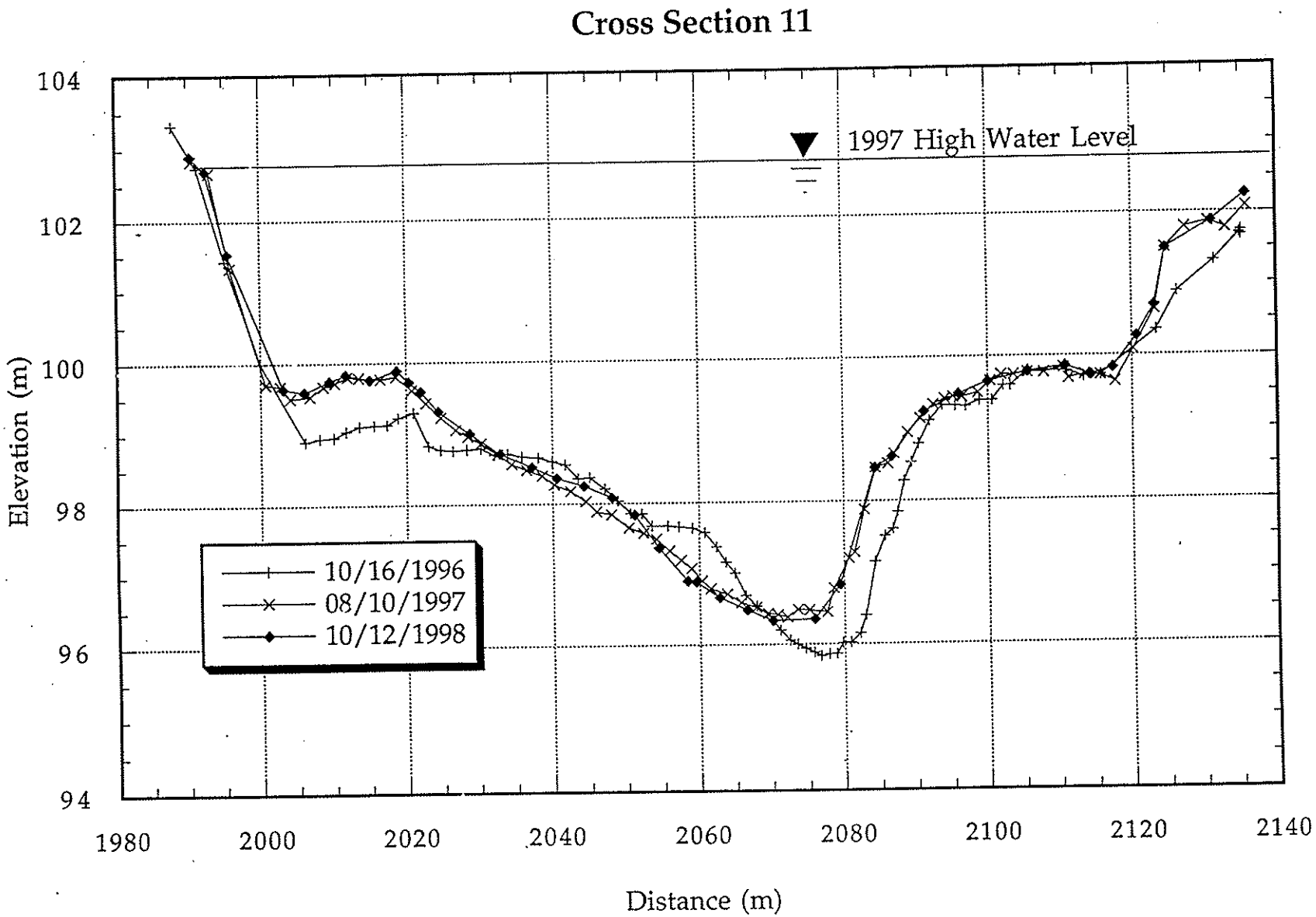
Cross Section 11
1997 High Water Level
10/16/1996
08/10/1997
10/12/1998
Elevation (m)
Distance (m)
104
102
100
98
96
94
1980
2000
2020
2040
2060
2080
2100
2120
2140

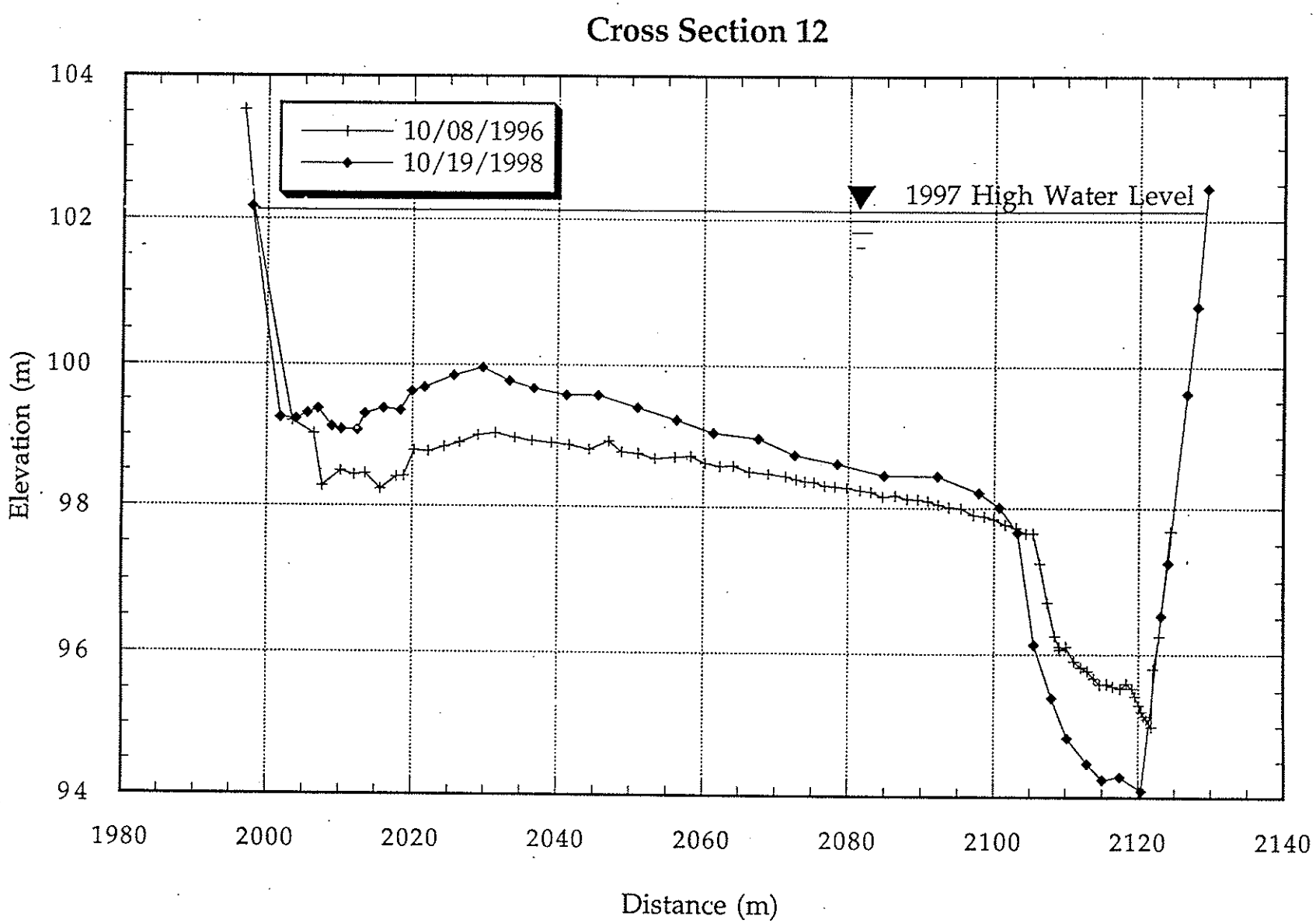
Cross Section 12
104
102
100
98
96
94
Elevation (m)
10/08/1996
10/19/1998
1997 High Water Level
1980
2000
2020
2040
2060
2080
2100
2120
2140
Distance (m)

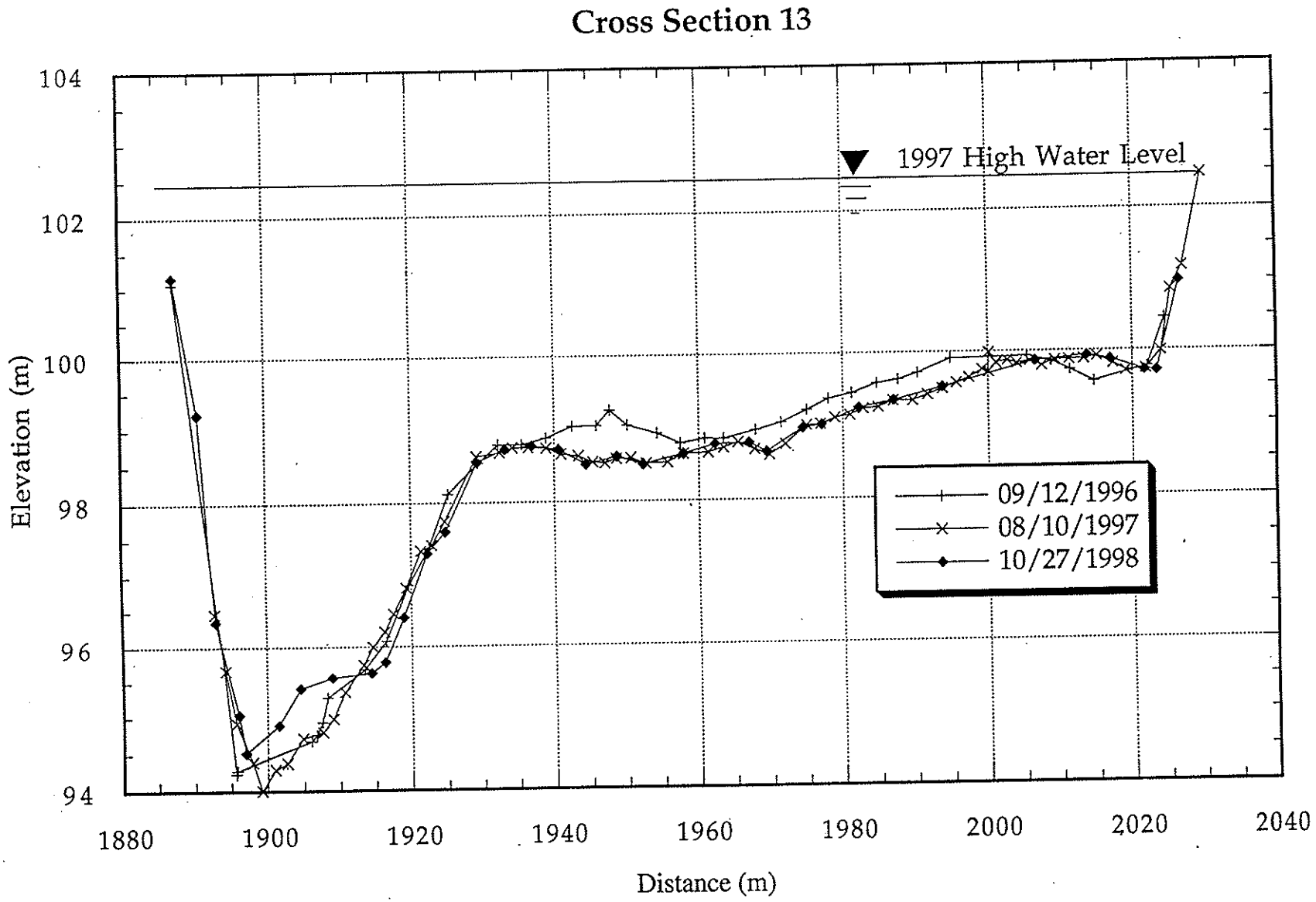
Cross Section 13
104
102
100
98
96
94
Elevation (m)
1880
1900
1920
1940
1960
1980
2000
2020
2040
Distance (m)
1997 High Water Level
09/12/1996
08/10/1997
10/27/1998

Appendix 3

Sediment Sample Data

The following tables and graphs contain grain size distribution data from 13 sediment samples performed on alternate bars in the reach. Surface and subsurface sediment samples were taken on the top of each alternate bar. All samples were performed near the geographic center of the bar, which was determined by pacing out the length and width of each bar. Surface sediment samples were taken by performing Wolman (1954) counts, in which one hundred particles were picked off the bed surface from and ten pace by ten pace grid while averting ones eyes, measured and tabulated into 1/2 ϕ (phi) sizes. Once the surface count was completed, the surface layer was removed to a depth equal to the surface D_{84}, the subsurface was mixed using a shovel and/or pick ax and the subsurface sediment was sampled on a ten by ten taped grid which had grid spacing equal to half the surface D_{100} (after Buffington, 1996 and Wohl et al., 1996). The subsurface sediment was also tabulated into 1/2 ϕ sizes. On all counts, material finer than 8 mm was lumped together.

Bar 1 (SS 1): Located on left bank, straddling cross-section 2. Left bank is Pleistocene Terrace, right bank is bedrock. The bar is 710 m long and 58 m wide at it's midpoint.

SURFACE

Particle Size (mm)	Count	Cumulative # less than	Cumulative % less than
512		96	100
360	3	93	97
256	7	86	90
180	28	58	60
128	10	48	50
90	16	32	33
64	15	17	18
45	4	13	14
32	8	5	5
23	1	4	4
16	1	3	3
11	0	3	3
8	0	3	3
<8	3		

SUBSURFACE

Particle Size (mm)	Count	Cumulative # less than	Cumulative % less than
512			
360		90	100
256	5	85	94
180	9	76	84
128	12	64	71
90	13	51	57
64	13	38	42
45	12	26	29
32	5	21	23
23	2	19	21
16	3	16	18
11	1	15	17
8	0	15	17
<8	15		

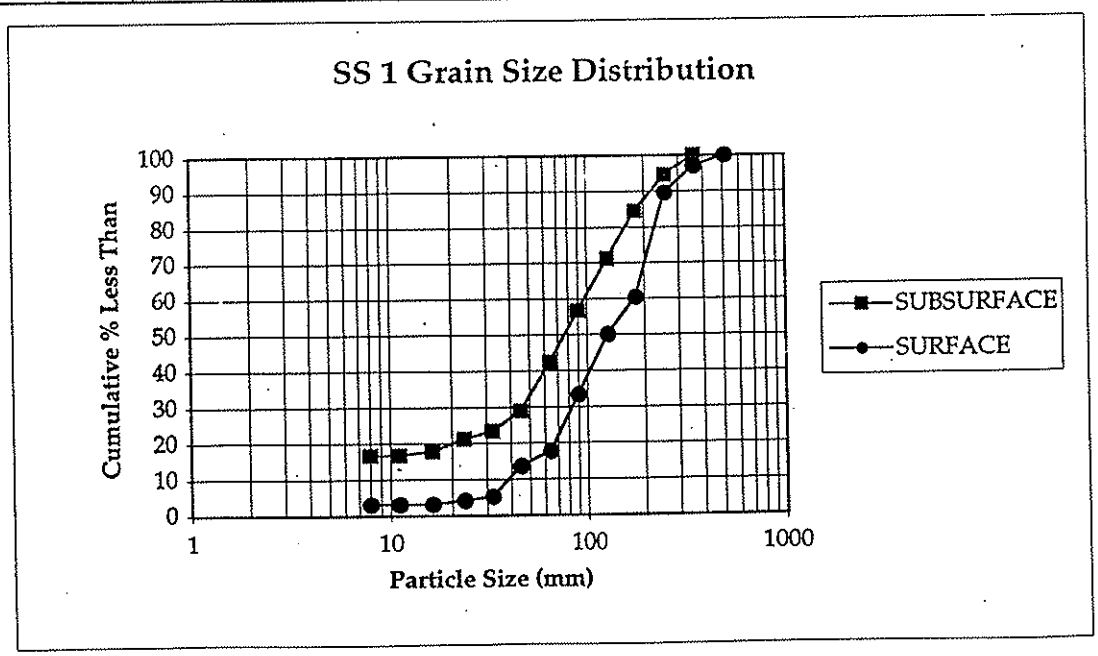

Bar 2 (SS 2): Located on right bank, straddling cross-section 3. Left bank is bedrock, right bank is Pleistocene Terrace. The bar is 267 m long and 50 m wide at it's midpoint.

SURFACE

Particle Size (mm)	Count	Cumulative # less than	Cumulative % less than
512		95	100
360	2	93	98
256	18	75	79
180	15	60	63
128	11	49	52
90	11	38	40
64	8	30	32
45	7	23	24
32	5	18	19
23	3	15	16
16	3	12	13
11	3	9	9
8	1	8	8
<8	8		

SUBSURFACE

Particle Size (mm)	Count	Cumulative # less than	Cumulative % less than
512		101	100
360	9	92	91
256	15	77	76
180	10	67	66
128	7	60	59
90	9	51	50
64	10	41	41
45	5	36	36
32	3	33	33
23	7	26	26
16	4	22	22
11	5	17	17
8	2	15	15
<8	15		

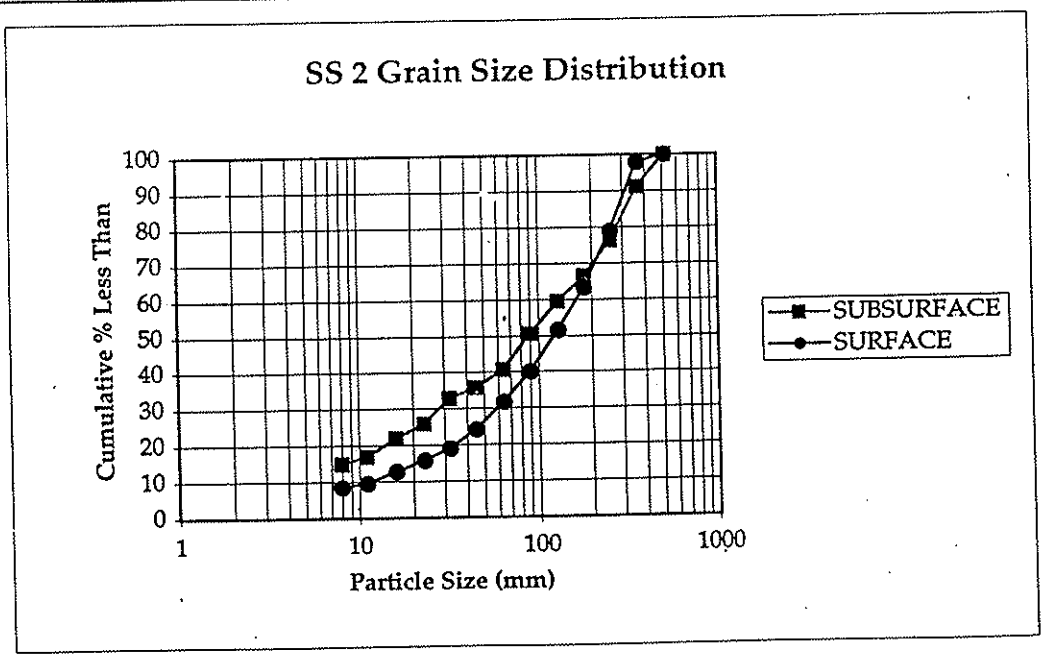

Bar 3 (SS 3): Located on left bank, straddling cross-section 4. Left bank is Pleistocene Terrace, right bank is bedrock. The bar is 334 m long and 40 m wide at it's midpoint.

SURFACE

Particle Size (mm)	Count	Cumulative # less than	Cumulative % less than
512		99	100
360	2	97	98
256	0	97	98
180	11	86	87
128	26	60	61
90	19	41	41
64	16	25	25
45	7	18	18
32	6	12	12
23	3	9	9
16	2	7	7
11	2	5	5
8	1	4	4
<8	4		

SUBSURFACE

Particle Size (mm)	Count	Cumulative # less than	Cumulative % less than
512			
360		100	100
256	5	95	95
180	8	87	87
128	6	81	81
90	14	67	67
64	13	54	54
45	14	40	40
32	9	31	31
23	7	24	24
16	11	13	13
11	4	9	9
8	1	8	8
<8	8		

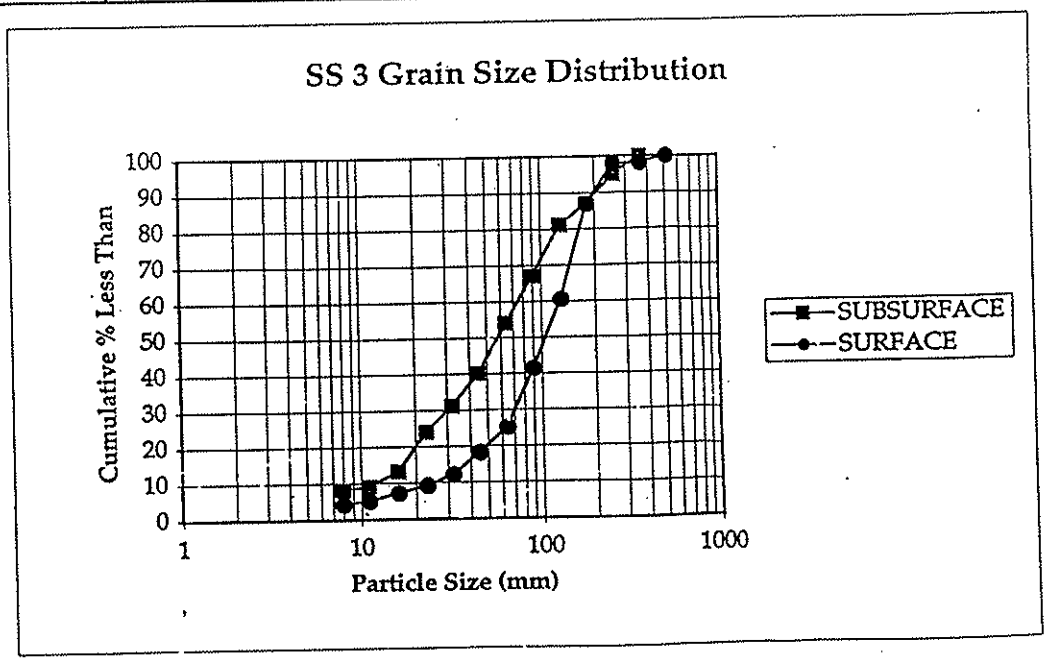

Bar 4 (SS 4): Located on right bank, straddling cross-section 5. Left bank is bedrock, right bank is Pleistocene Terrace. The bar is 300 m long and 50 m wide at it's midpoint.

SURFACE

Particle Size (mm)	Count	Cumulative # less than	Cumulative % less than
512			
360		100	100
256	4	96	96
180	10	86	86
128	13	73	73
90	15	58	58
64	10	48	48
45	9	39	39
32	16	23	23
23	7	16	16
16	4	12	12
11	2	10	10
8	1	9	9
<8	9		

SUBSURFACE

Particle Size (mm)	Count	Cumulative # less than	Cumulative % less than
512			
360			
256		100	100
180	12	88	88
128	13	75	75
90	15	60	60
64	12	48	48
45	13	35	35
32	10	25	25
23	3	22	22
16	2	20	20
11	4	16	16
8	2	14	14
<8	14		

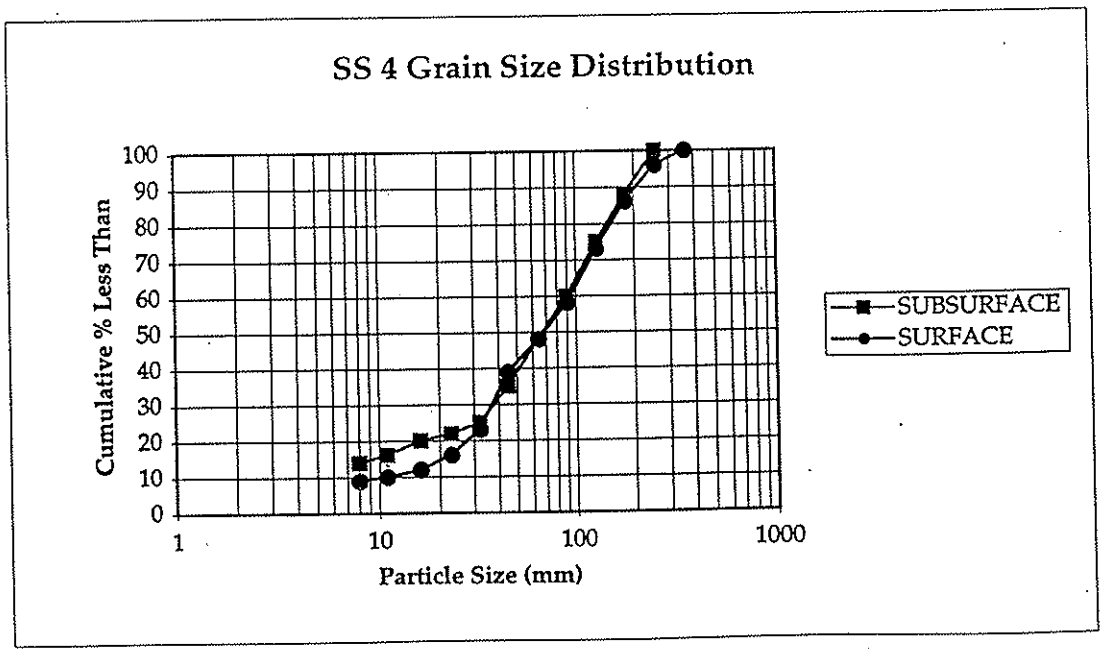

Bar 6 (SS 6): Located on right bank, straddling cross-section 7. Left bank is bedrock, right bank is Pleistocene Terrace. The bar is 167 m long and 42 m wide at it's midpoint.

SURFACE

Particle Size (mm)	Count	Cumulative # less than	Cumulative % less than
512			
360		97	100
256	8	89	92
180	18	71	73
128	11	60	62
90	14	46	47
64	12	34	35
45	9	25	26
32	8	17	18
23	4	13	13
16	5	8	8
11	1	7	7
8	1	6	6
<8	6		

SUBSURFACE

Particle Size (mm)	Count	Cumulative # less than	Cumulative % less than
512			
360			
256		101	100
180	1	100	99
128	7	93	92
90	13	80	79
64	12	68	67
45	15	53	52
32	12	41	41
23	8	33	33
16	4	29	29
11	9	20	20
8	7	13	13
<8	13		

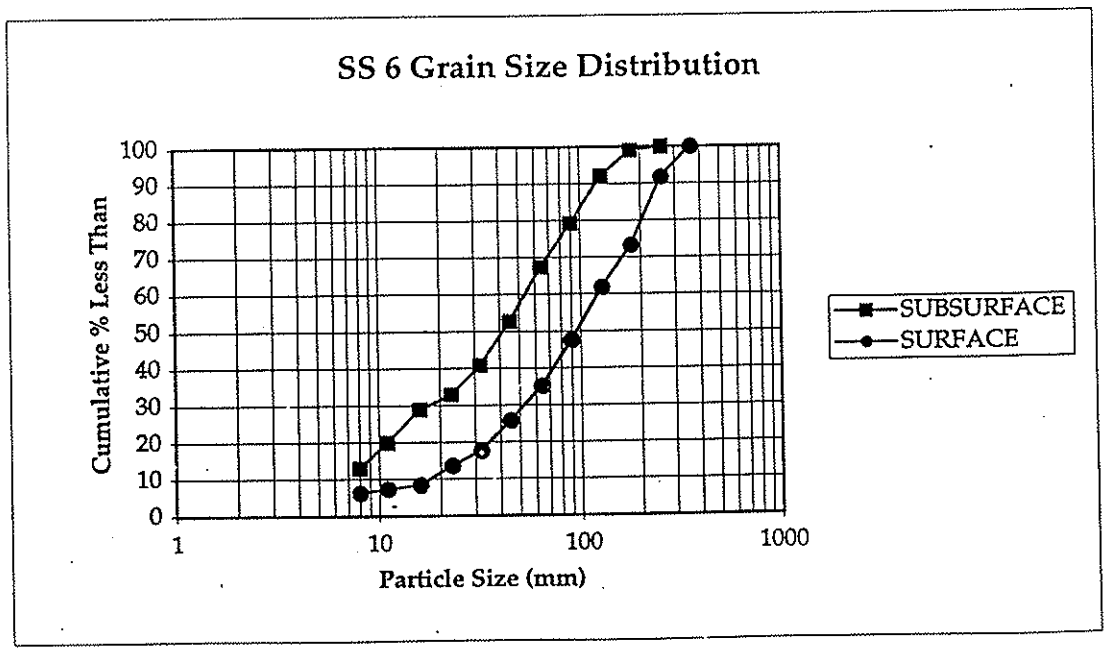

Bar 7 (SS 7): Located on left bank, straddling cross-section 8. Left bank is Pleistocene Terrace, right bank is bedrock. The bar is 460 m long and 50 m wide at it's midpoint.

SURFACE

Particle Size (mm)	Count	Cumulative # less than	Cumulative % less than
512			
360			
256			
180		101	100
128	11	90	89
90	16	74	73
64	24	50	50
45	21	29	29
32	16	13	13
23	7	6	6
16	3	3	3
11	1	2	2
8	0	2	2
<8	2		

SUBSURFACE

Particle Size (mm)	Count	Cumulative # less than	Cumulative % less than
512			
360			
256			
180		98	100
128	6	92	94
90	15	77	79
64	12	65	66
45	23	42	43
32	8	34	35
23	9	25	26
16	3	22	22
11	2	20	20
8	0	20	20
<8	20		

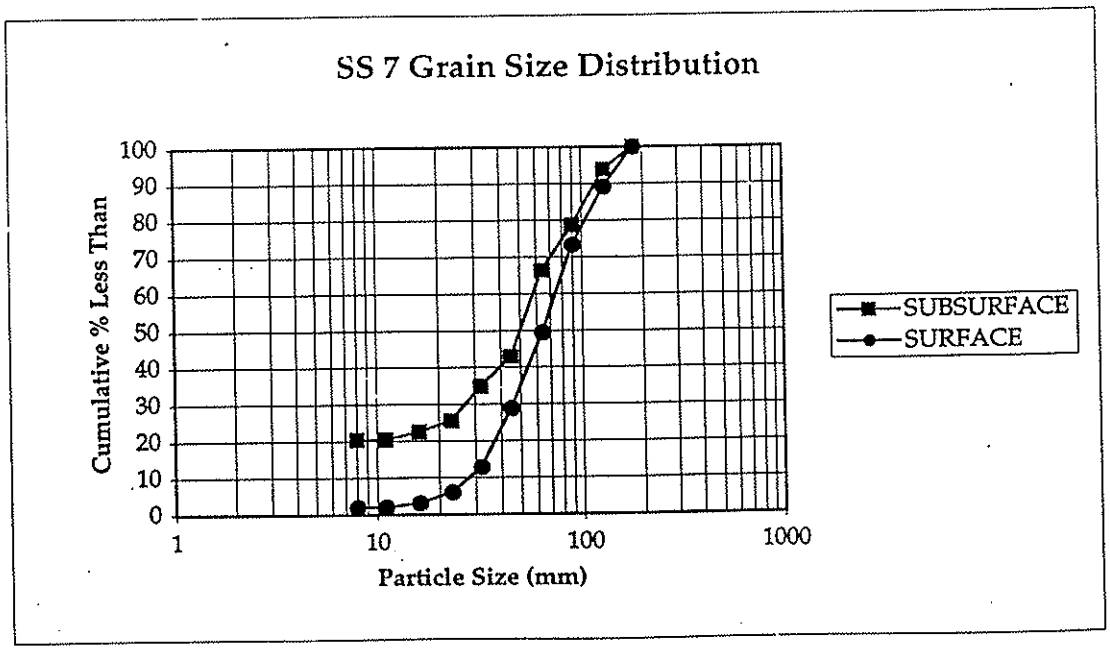

Bar 8 (SS 8): Located on right bank, straddling cross-section 9. Left bank is bedrock, right bank is Pleistocene Terrace. The bar is 184 m long and 50 m wide at it's midpoint.

SURFACE

Particle Size (mm)	Count	Cumulative # less than	Cumulative % less than
512			
360			
256		100	100
180	9	91	91
128	16	75	75
90	22	53	53
64	19	34	34
45	14	20	20
32	6	14	14
23	11	3	3
16	2	1	1
11	1	0	0
8	0	0	0
<8	0		

SUBSURFACE

Particle Size (mm)	Count	Cumulative # less than	Cumulative % less than
512			
360			
256		100	100
180	1	99	99
128	19	80	80
90	17	63	63
64	14	49	49
45	19	30	30
32	10	20	20
23	3	17	17
16	3	14	14
11	1	13	13
8	0	13	13
<8	13		

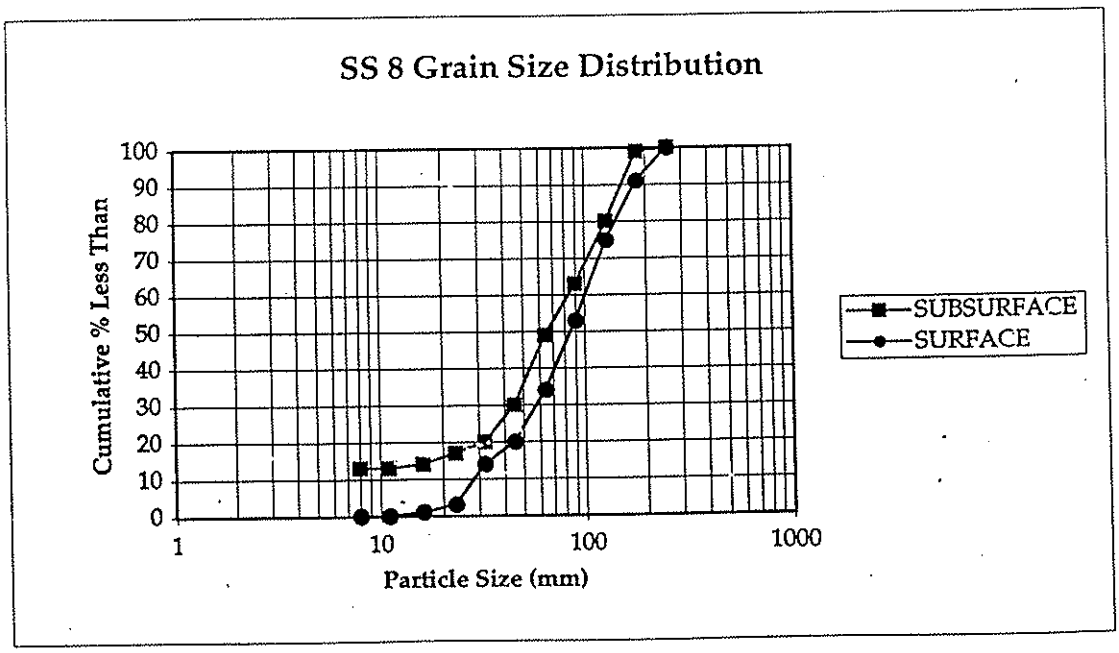

Bar 9 (SS 9): Located on left bank, straddling cross-section 10. Left bank is Pleistocene Terrace, right bank is bedrock. The bar is 501 m long and 44 m wide at it's midpoint.

SURFACE

Particle Size (mm)	Count	Cumulative # less than	Cumulative % less than
512			
360			
256		100	100
180	6	94	94
128	21	73	73
90	16	57	57
64	17	40	40
45	12	28	28
32	13	15	15
23	7	8	8
16	3	5	5
11	0	5	5
8	1	4	4
<8	4		

SUBSURFACE

Particle Size (mm)	Count	Cumulative # less than	Cumulative % less than
512			
360			
256		88	100
180	3	85	97
128	9	76	86
90	11	65	74
64	19	46	52
45	6	40	45
32	12	28	32
23	7	21	24
16	9	12	14
11	2	10	11
8	1	9	10
<8	9		

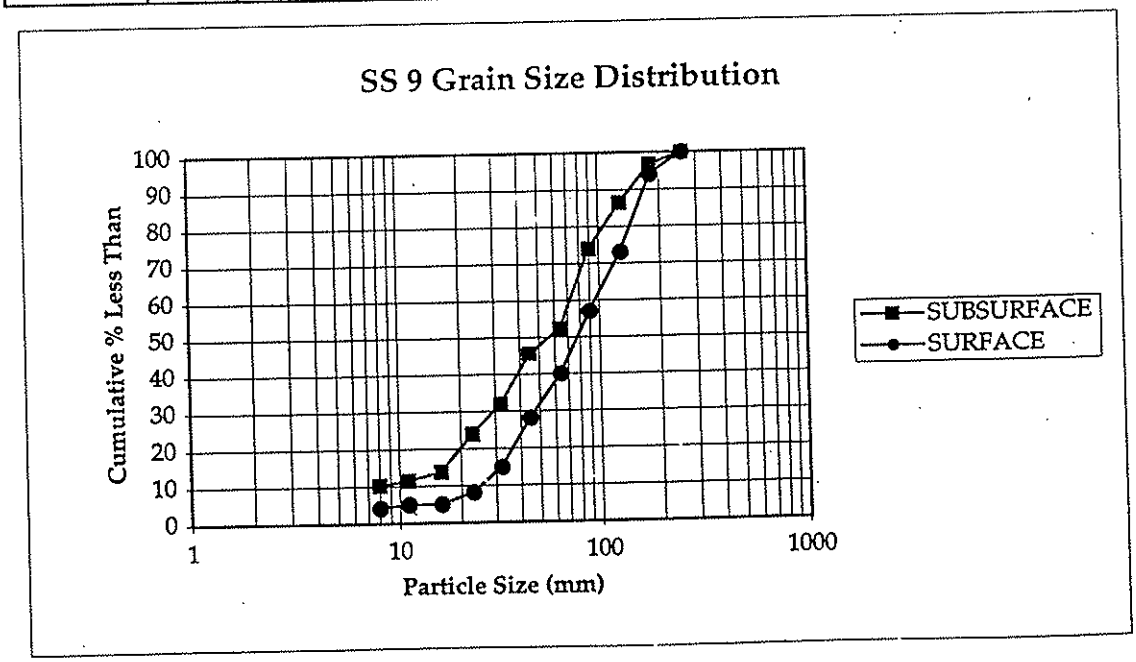

Bar 10 (SS 10): Located on right bank, straddling cross-section 10 and 11. Left bank is bedrock, right bank is Pleistocene Terrace. The bar is 417 m long and 50 m wide at it's midpoint.

SURFACE

Particle Size (mm)	Count	Cumulative # less than	Cumulative % less than
512			
360		100	100
256	2	98	98
180	13	85	85
128	23	62	62
90	28	34	34
64	19	15	15
45	9	6	6
32	2	4	4
23	3	1	1
16	0	1	1
11	0	1	1
8	0	1	1
<8	1		

SUBSURFACE

Particle Size (mm)	Count	Cumulative # less than	Cumulative % less than
512			
360			
256		102	100
180	2	100	98
128	10	90	88
90	23	67	66
64	12	55	54
45	14	41	40
32	9	32	31
23	4	28	27
16	2	26	25
11	1	25	25
8	0	25	25
<8	25		

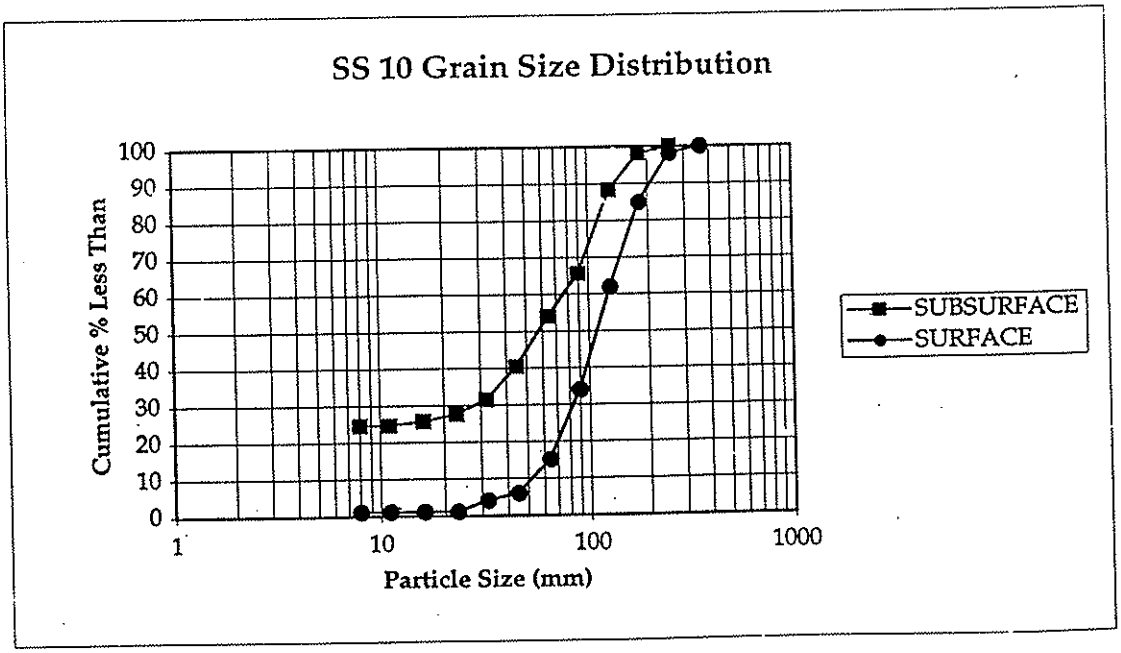

Bar 11a (SS 11a) : Located on left bank, straddling cross-section 11. Left bank and right bank are vegetated bedrock slopes. The bar is 317 m long and 67 m wide at it's midpoint.

SURFACE

Particle Size (mm)	Count	Cumulative # less than	Cumulative % less than
512			
360		100	100
256	2	98	98
180	1	97	97
128	8	89	89
90	17	72	72
64	18	54	54
45	22	32	32
32	15	17	17
23	10	7	7
16	5	2	2
11	1	1	1
8	1	0	0
<8	0		

SUBSURFACE

Particle Size (mm)	Count	Cumulative # less than	Cumulative % less than
512			
360			
256		95	100
180	3	92	97
128	2	90	95
90	10	80	84
64	15	65	68
45	14	51	54
32	8	43	45
23	8	35	37
16	4	31	33
11	5	26	27
8	5	21	22
<8	21		

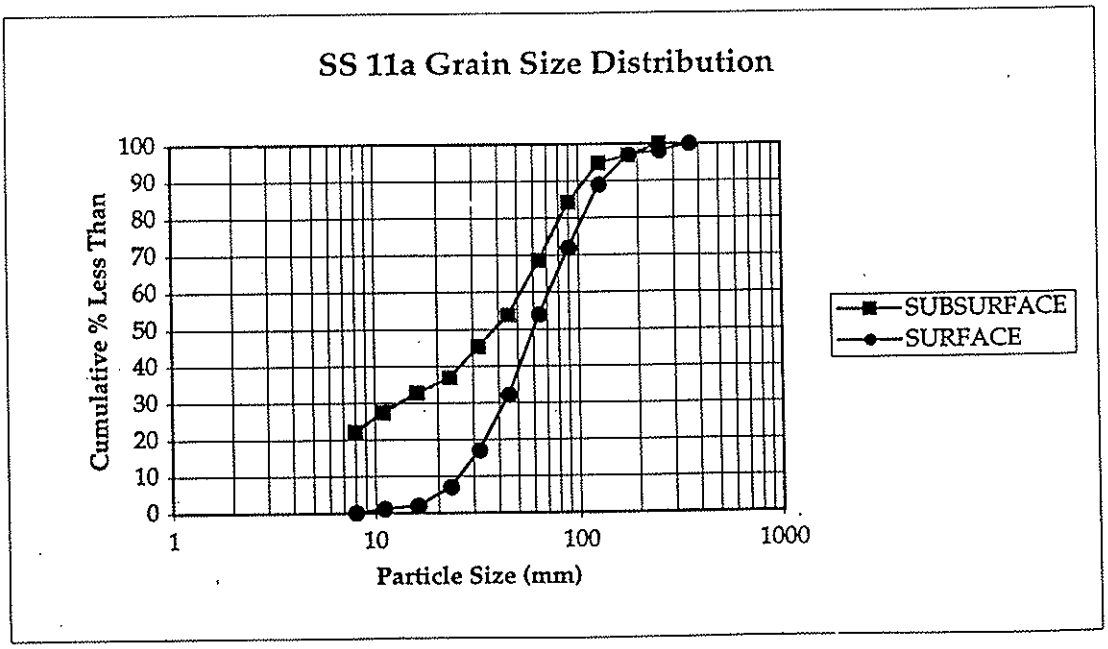

Bar 11b (SS 11b) : Located on left bank, straddling cross-section 12. Left bank and right bank are vegetated bedrock slopes. The bar is 334 m long and 58 m wide at it's midpoint.

SURFACE

Particle Size (mm)	Count	Cumulative # less than	Cumulative % less than
512			
360		102	100
256	1	101	99
180	1	100	98
128	11	89	87
90	18	71	70
64	19	52	51
45	20	32	31
32	13	19	19
23	12	7	7
16	4	3	3
11	2	1	1
8	0	1	1
<8	1		

SUBSURFACE

Particle Size (mm)	Count	Cumulative # less than	Cumulative % less than
512			
360			
256		100	100
180	2	98	98
128	3	95	95
90	17	78	78
64	17	61	61
45	11	50	50
32	7	43	43
23	12	31	31
16	9	22	22
11	3	19	19
8	2	17	17
<8	17		

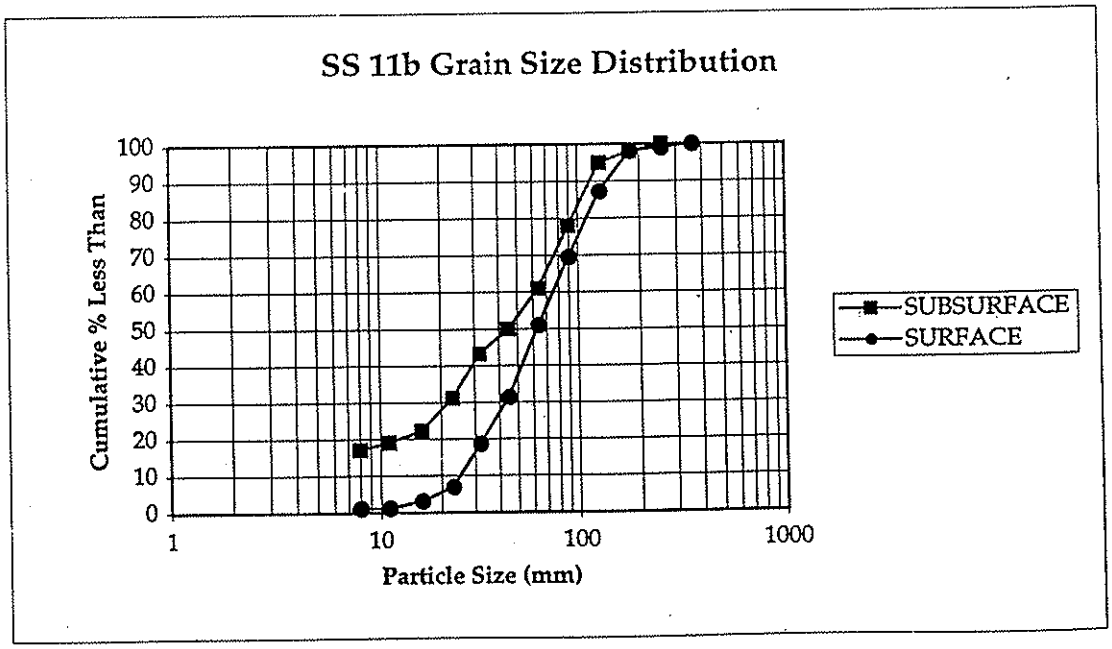

Bar 12 (SS 12): Located on right bank, straddling cross-section 13 and 14. Left bank is bedrock, right bank is bedrock. The bar is 284 m long and 58 m wide at it's midpoint.

SURFACE

Particle Size (mm)	Count	Cumulative # less than	Cumulative % less than
512			
360			
256		100	100
180	1	99	99
128	4	95	95
90	11	84	84
64	23	61	61
45	19	42	42
32	23	19	19
23	13	6	6
16	5	1	1
11	0	1	1
8	1	0	0
<8	0		

SUBSURFACE

Particle Size (mm)	Count	Cumulative # less than	Cumulative % less than
512			
360			
256		99	100
180	1	98	99
128	5	93	94
90	12	81	82
64	10	71	72
45	16	55	56
32	18	37	37
23	15	22	22
16	3	19	19
11	0	19	19
8	0	19	19
<8	19		

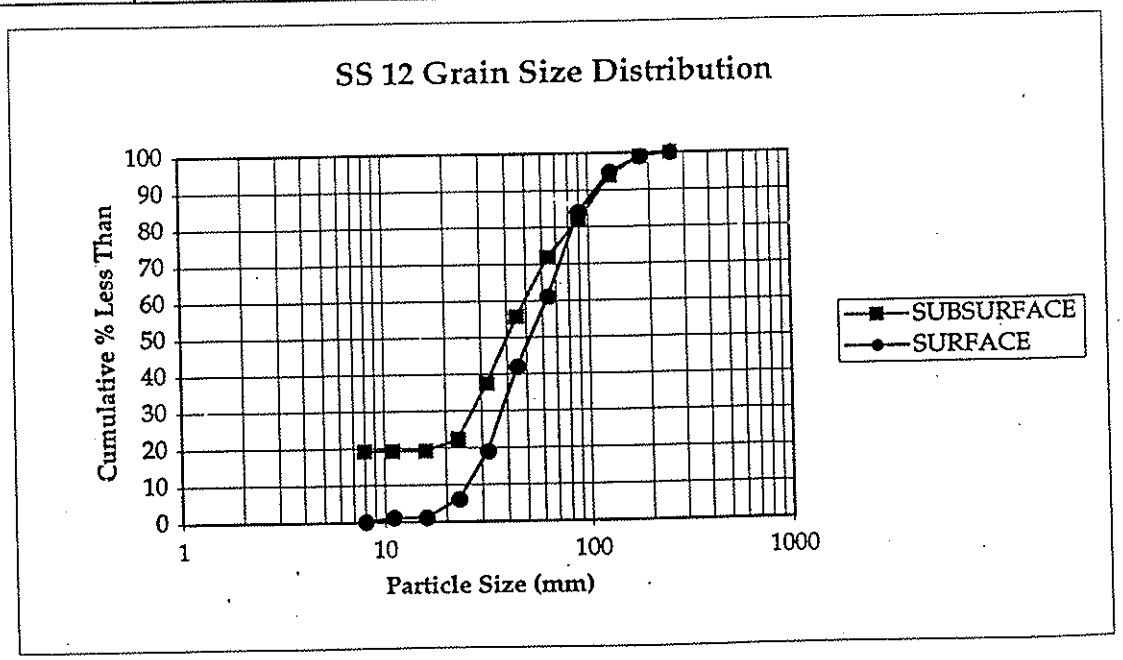

Bar 13 (SS 13): Located on left bank, straddling cross-section 14. Left bank is steep vegetated canyon wall, right bank is bedrock. The bar is 251 m long and 46 m wide at it's midpoint.

SURFACE

Particle Size (mm)	Count	Cumulative # less than	Cumulative % less than
512			
360		100	100
256	2	98	98
180	1	97	97
128	10	87	87
90	18	69	69
64	16	53	53
45	24	29	29
32	13	16	16
23	10	6	6
16	4	2	2
11	1	1	1
8	0	1	1
<8	1		

SUBSURFACE

Particle Size (mm)	Count	Cumulative # less than	Cumulative % less than
512			
360			
256			
180		100	100
128	5	95	95
90	16	79	79
64	12	67	67
45	13	54	54
32	9	45	45
23	9	36	36
16	6	30	30
11	0	30	30
8	0	30	30
<8	30		

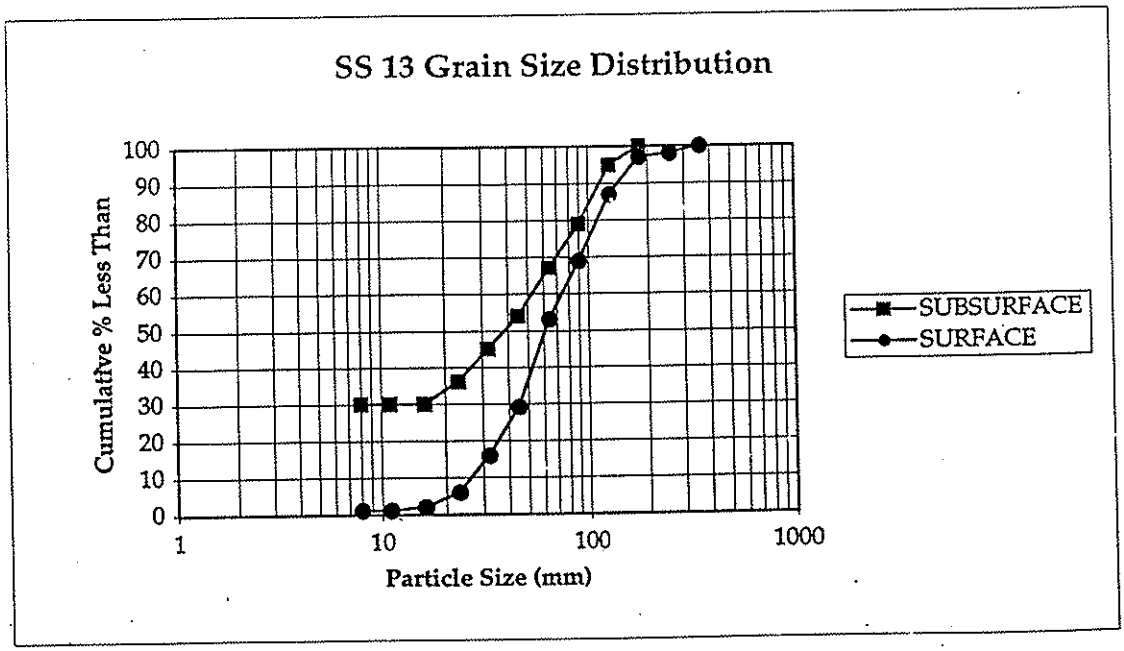

Appendix 4

Local Water Surface Profiles

The following graphs show the longitudinal profiles of the 1997 high water mark on the left bank (LB) and right bank (RB) for each of the sediment sample locations (SS1-SS13). The profiles extend for the upstream bar head to the downstream bar tail. Distance downstream of the entire reach was calculated for each bank and therefore, due to channel bends, the distance downstream on the left bank (LB) rarely coordinates with that of the right bank (RB). Local water depth on each banks was measured as the difference in elevation between the sediment sample and that of the high water mark. The slope and the local depth of water over each sediment sample site was determined by interpolation between the right and left bank profiles.

See appendix 5 for a table including the high water data used in these plots.

SS1LB

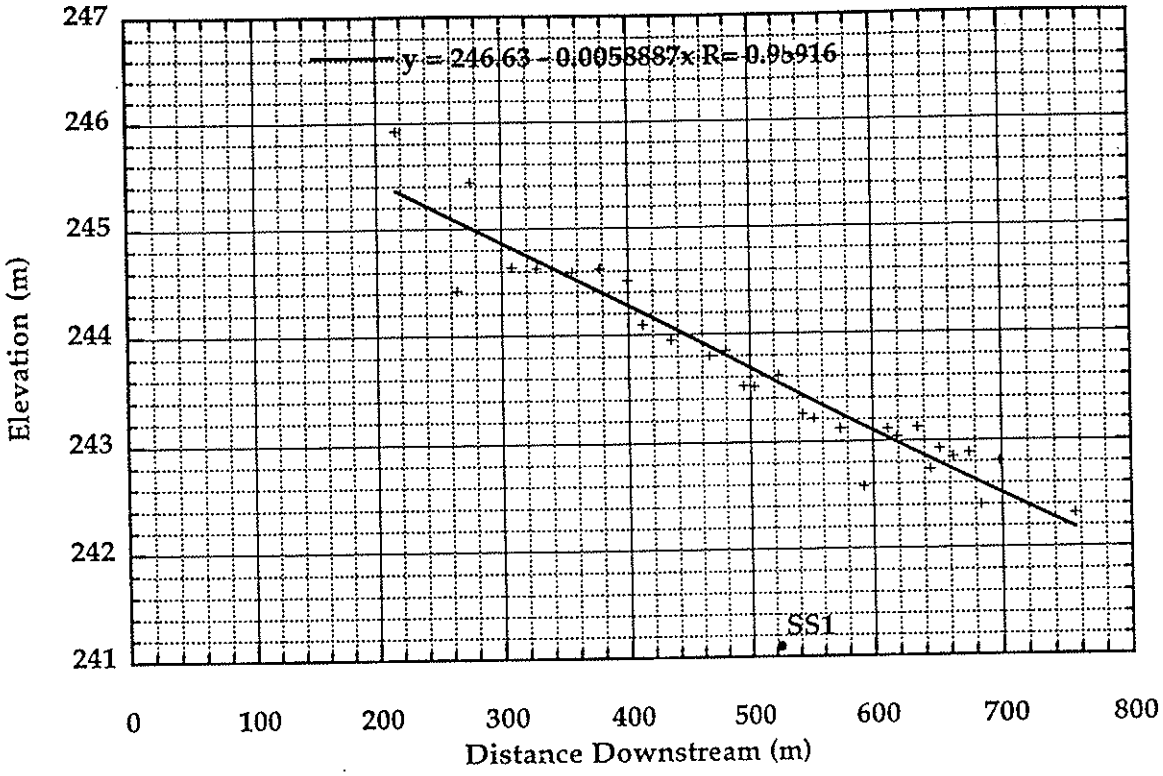
y = 246.63 - 0.0058887x R= 0.9b916
247
246
245
244
243
242
241
Elevation (m)
SS1
0
100
200
300
400
500
600
700
800
Distance Downstream (m)

SS1RB

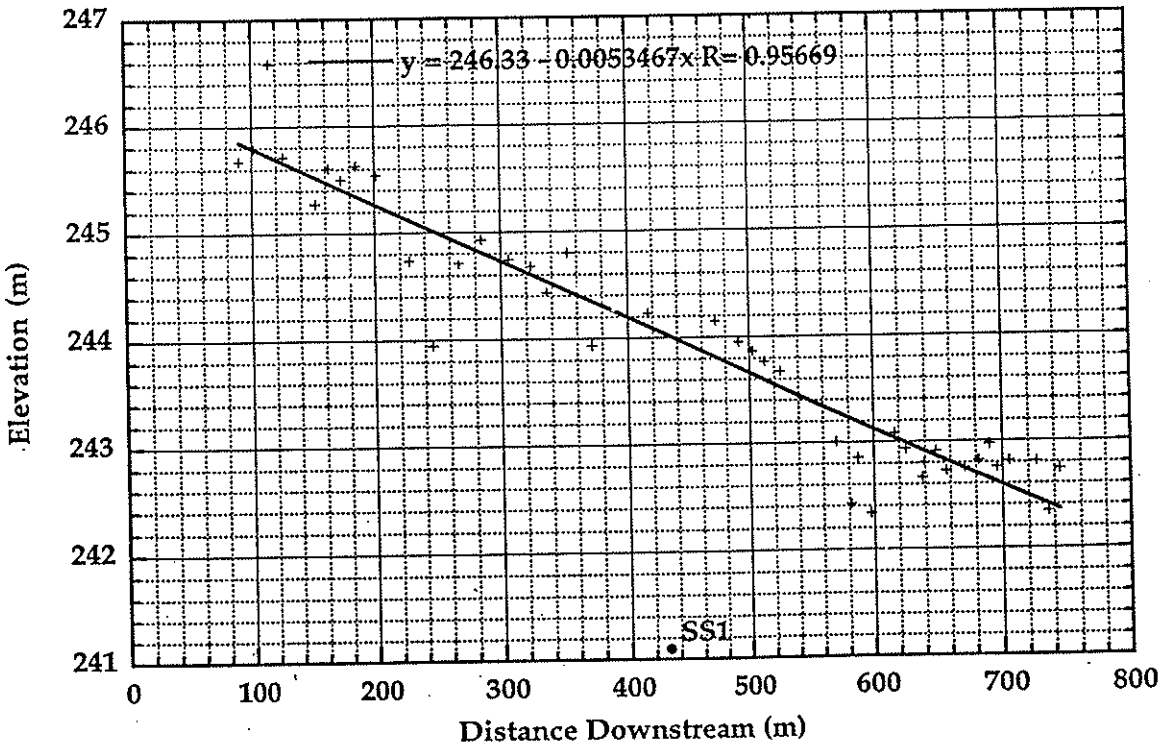
y = 246.33 - 0.0053467x R= 0.95669
247
246
245
244
243
242
241
Elevation (m)
SS1
0
100
200
300
400
500
600
700
800
Distance Downstream (m)

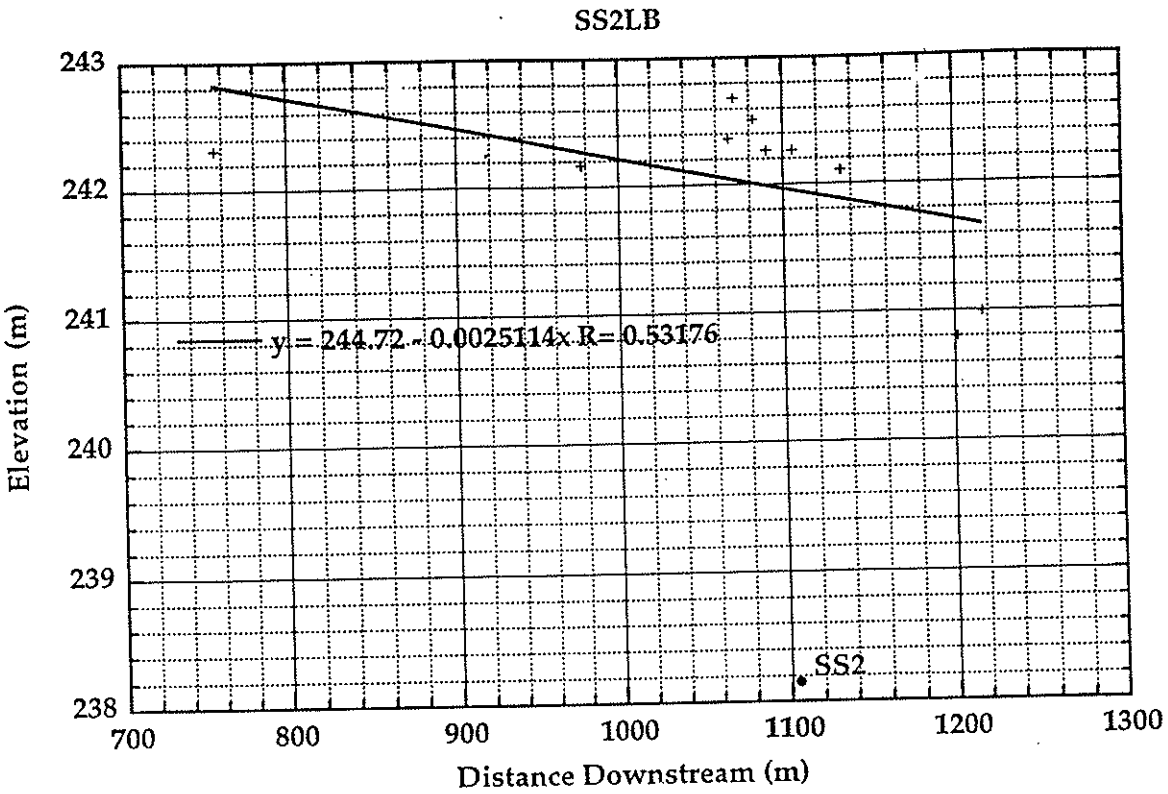
SS2LB
243
242
241
240
239
238
Elevation (m)
y = 244.72 - 0.0025114x R= 0.53176
SS2
700
800
900
1000
1100
1200
1300
Distance Downstream (m)

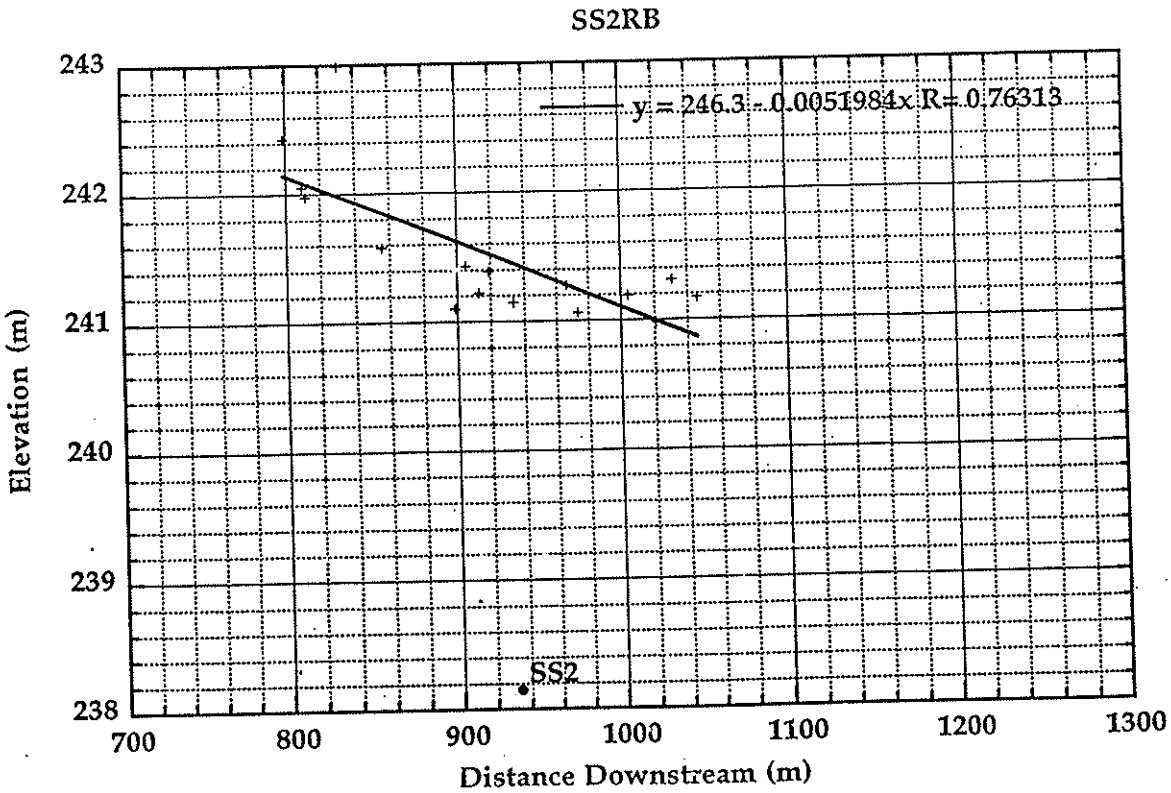
SS2RB
243
242
241
240
239
238
Elevation (m)
y = 246.3 - 0.0051984x R= 0.76313
SS2
700
800
900
1000
1100
1200
1300
Distance Downstream (m)

SS3LB

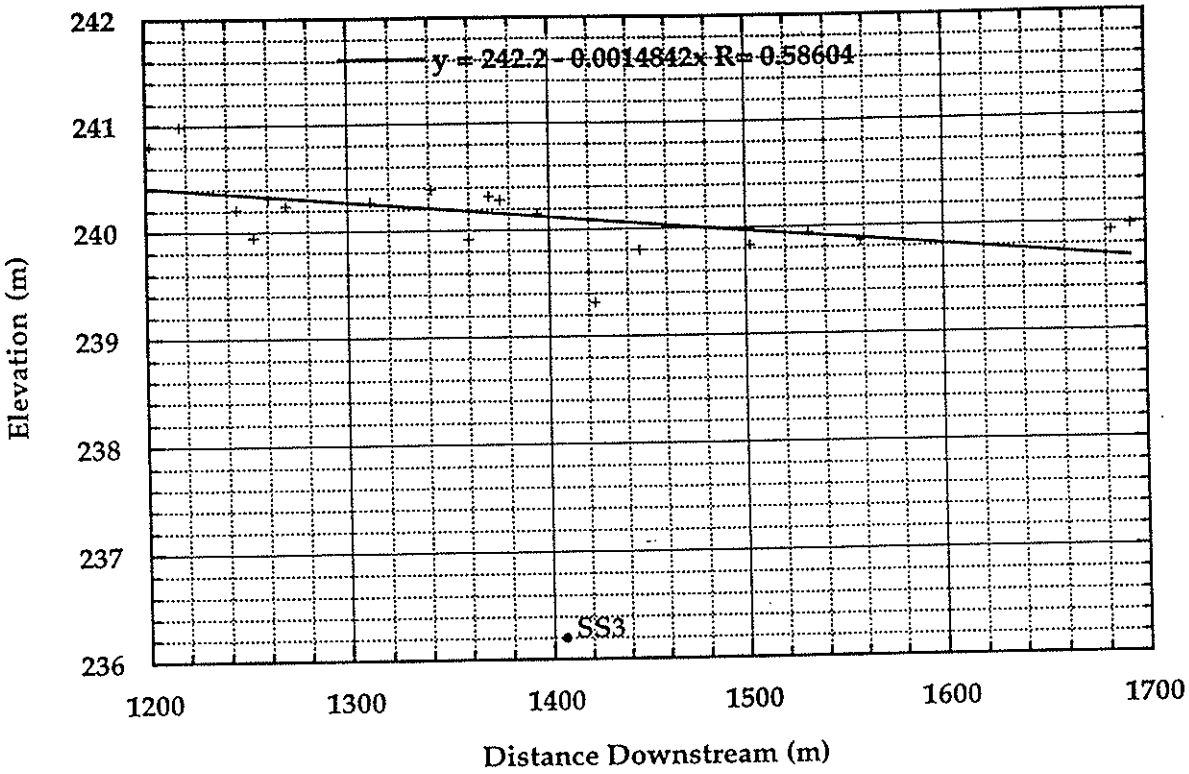
y = 242.2 - 0.0014842x R= 0.58604
242
241
240
239
238
237
236
SS3
1200
1300
1400
1500
1600
1700
Elevation (m)
Distance Downstream (m)

SS3RB

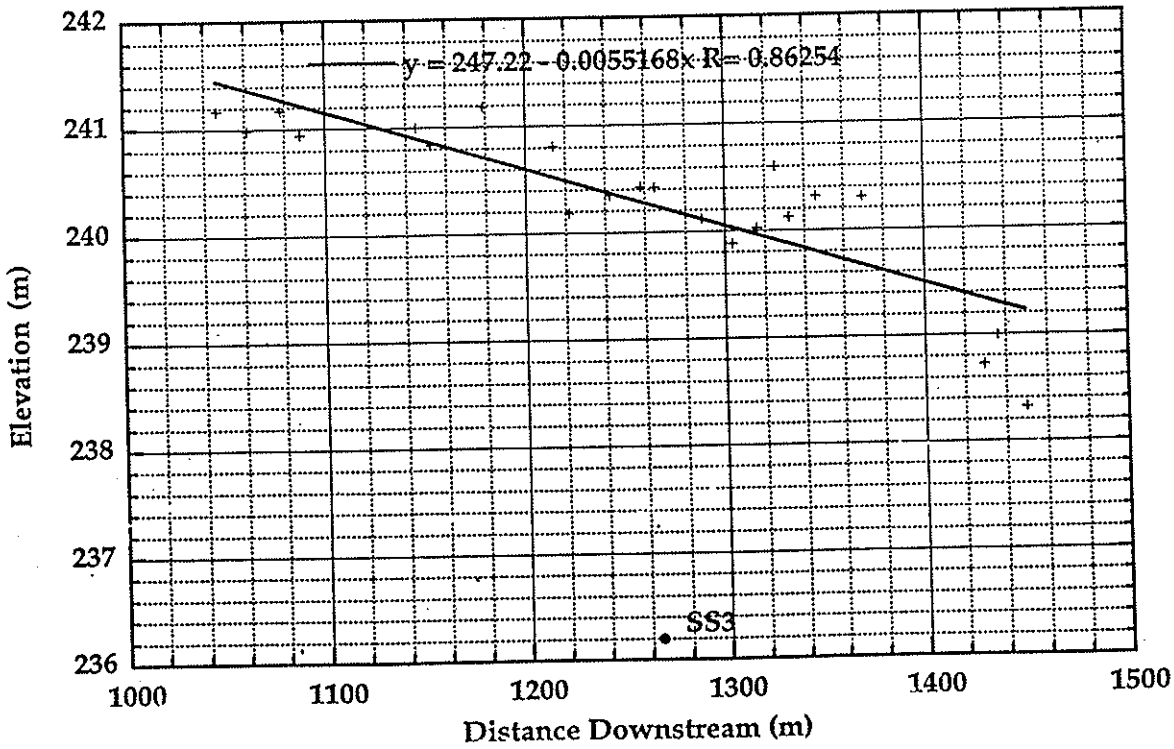
y = 247.22 - 0.0055168x R= 0.86254
242
241
240
239
238
237
236
SS3
1000
1100
1200
1300
1400
1500
Elevation (m)
Distance Downstream (m)

SS4LB

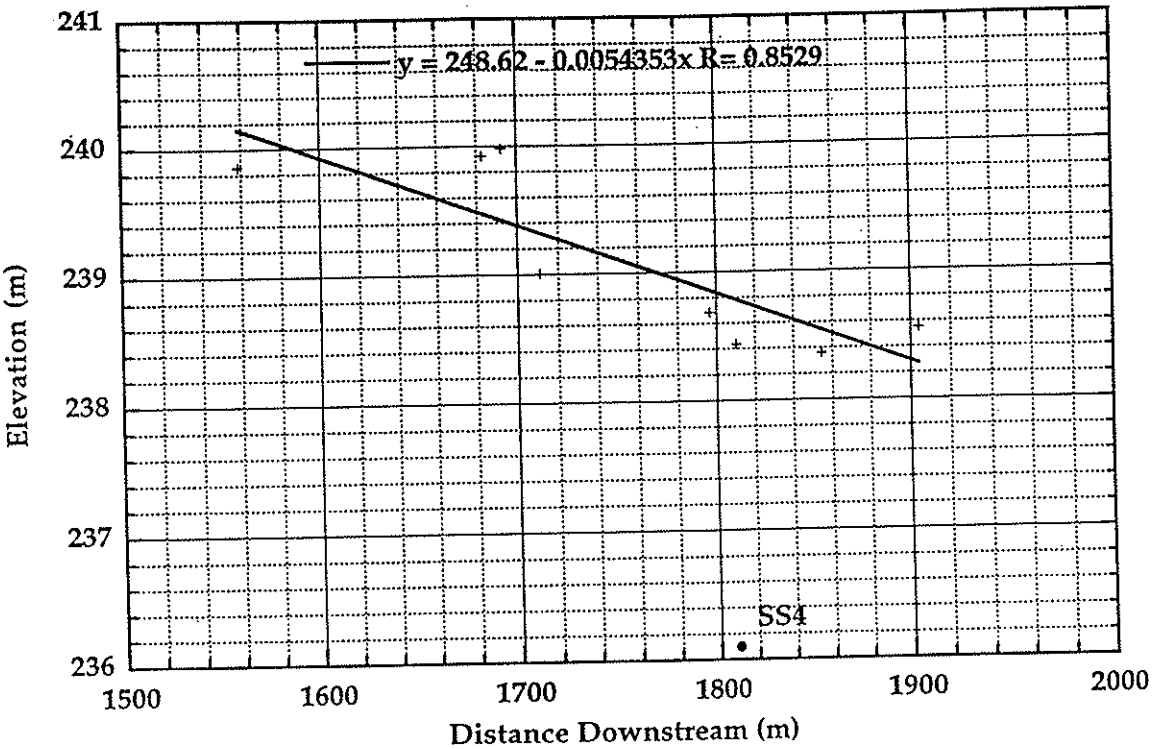
y = 248.62 - 0.0054353x R= 0.8529
241
240
239
238
237
236
Elevation (m)
SS4
1500
1600
1700
1800
1900
2000
Distance Downstream (m)

SS4RB

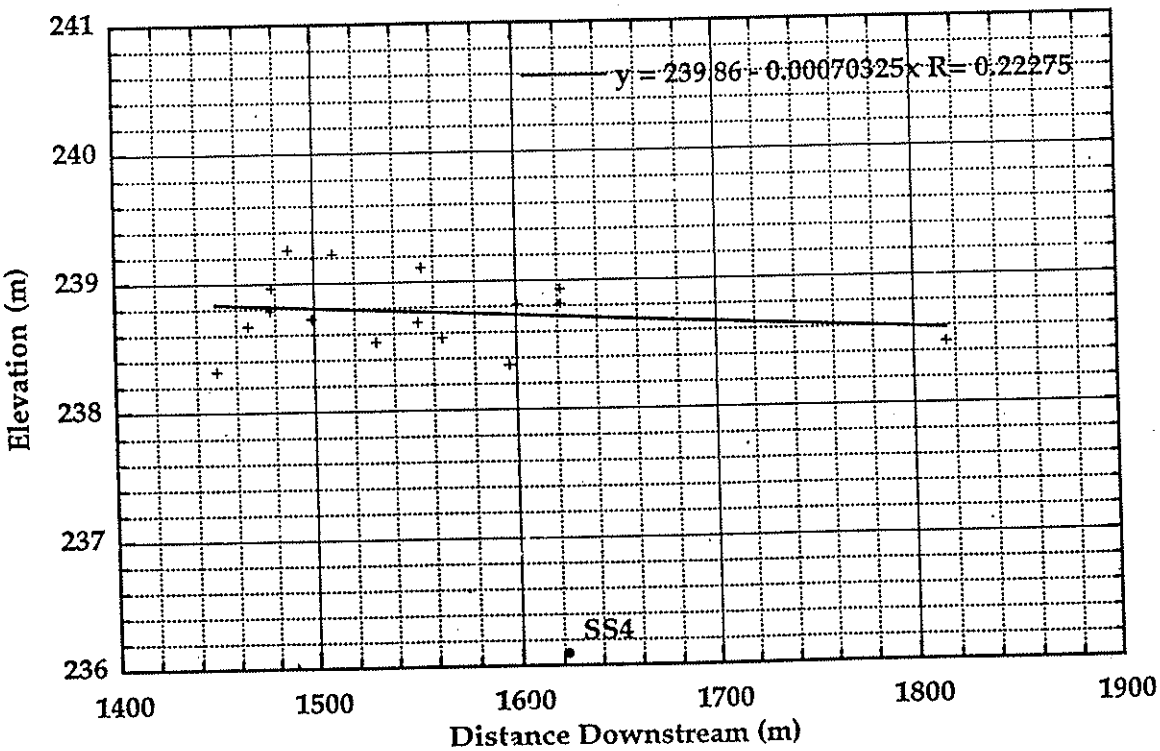
y = 239.86 - 0.00070325x R= 0.22275
241
240
239
238
237
236
Elevation (m)
SS4
1400
1500
1600
1700
1800
1900
Distance Downstream (m)

SS6LB

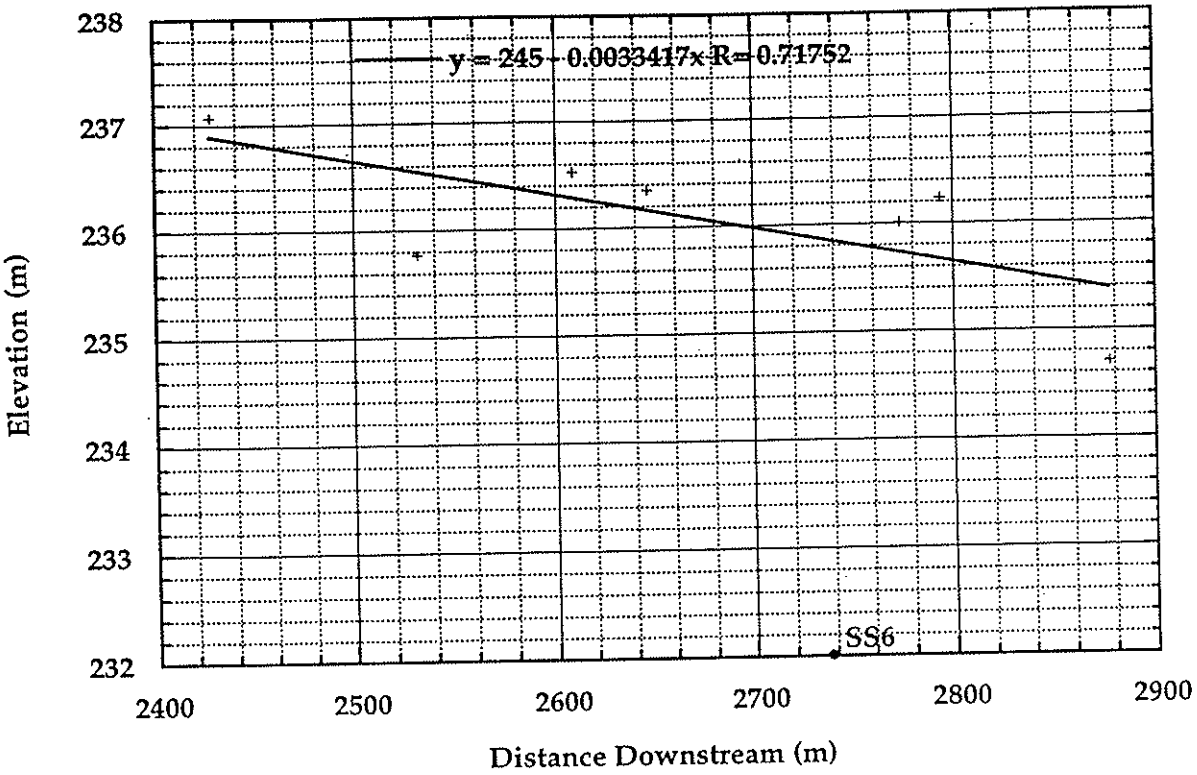
y = 245 - 0.0033417x R= 0.71752
238
237
236
235
234
233
232
Elevation (m)
SS6
2400
2500
2600
2700
2800
2900
Distance Downstream (m)

SS6RB

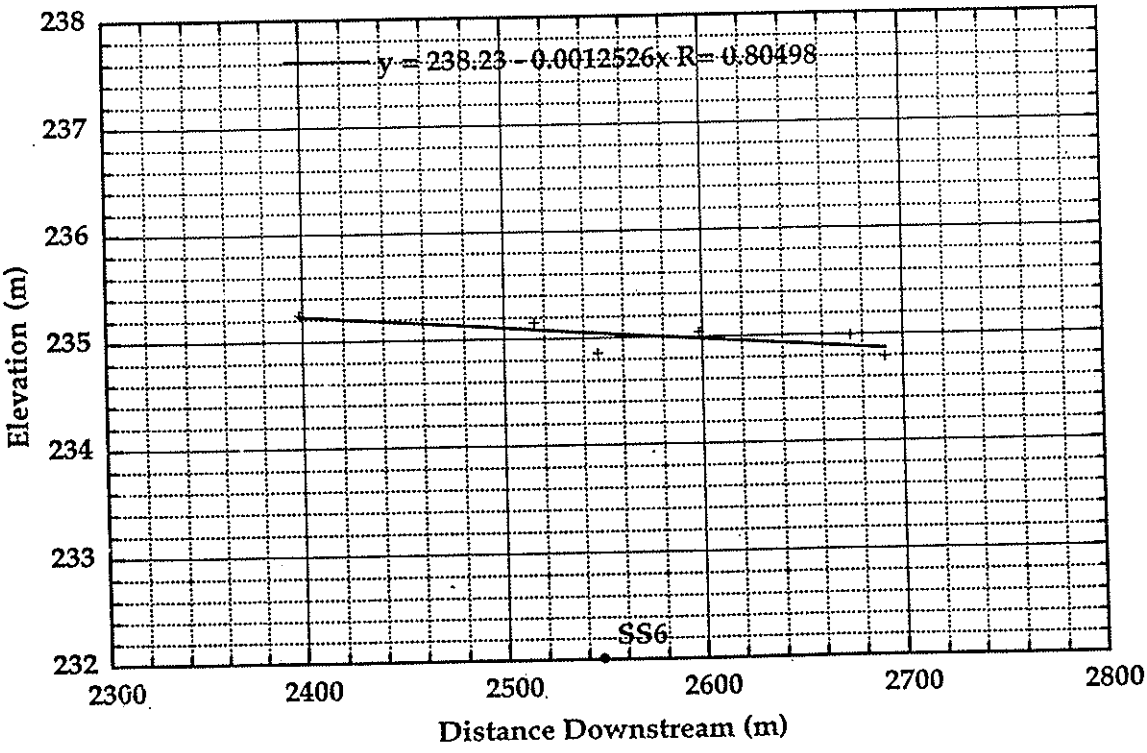
y = 238.23 - 0.0012526x R= 0.80498
238
237
236
235
234
233
232
Elevation (m)
SS6
2300
2400
2500
2600
2700
2800
Distance Downstream (m)

SS7LB

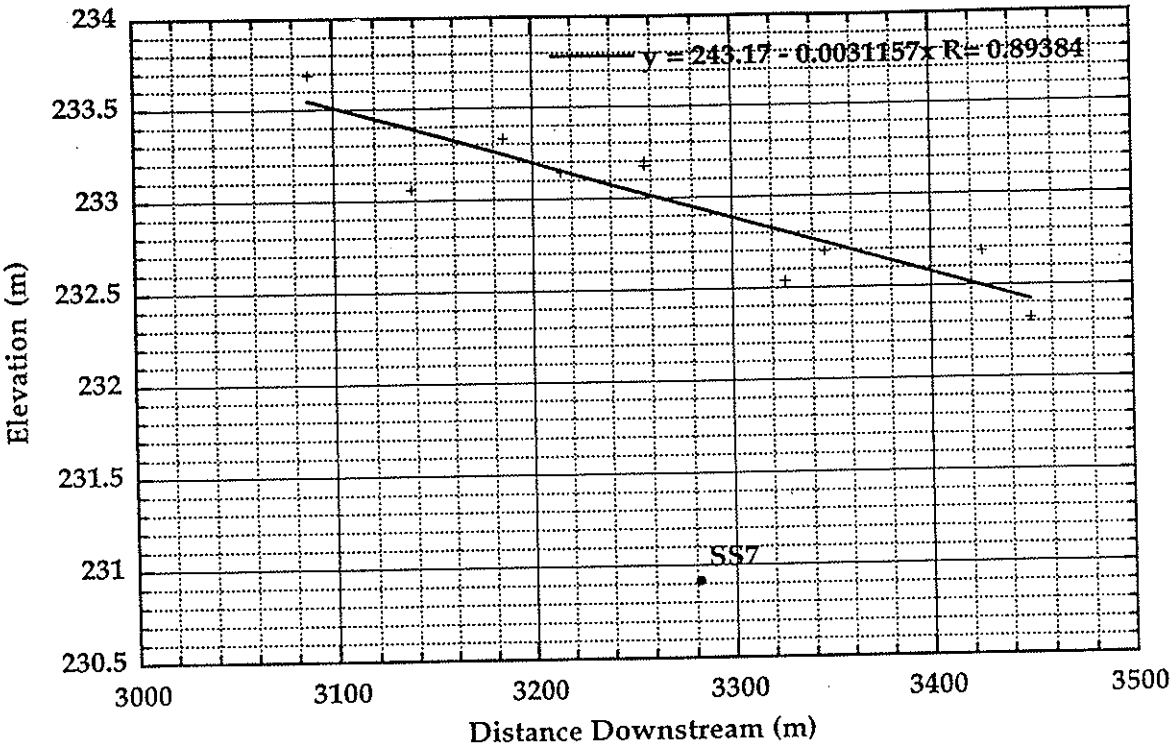
y = 243.17 - 0.0031157x R= 0.89384
SS7
234
233.5
233
232.5
232
231.5
231
230.5
3000
3100
3200
3300
3400
3500
Elevation (m)
Distance Downstream (m)

SS7RB

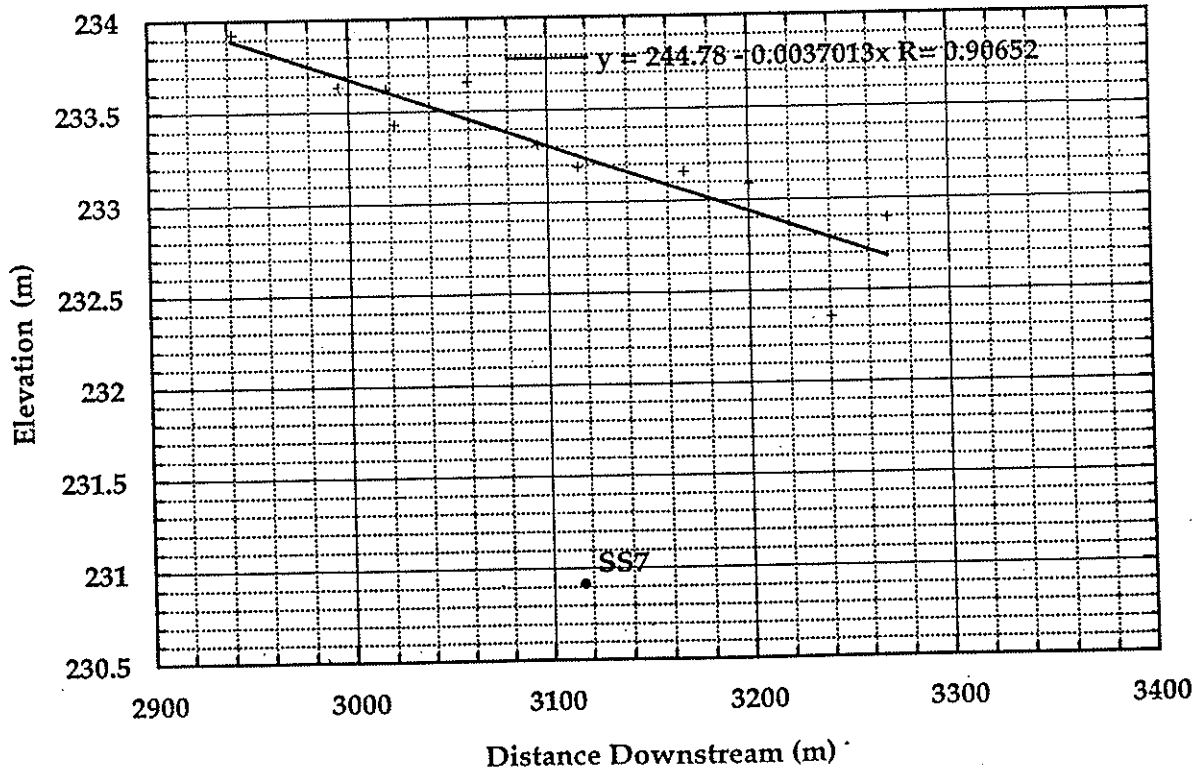
y = 244.78 - 0.0037013x R= 0.90652
SS7
234
233.5
233
232.5
232
231.5
231
230.5
2900
3000
3100
3200
3300
3400
Elevation (m)
Distance Downstream (m)

SS8LB

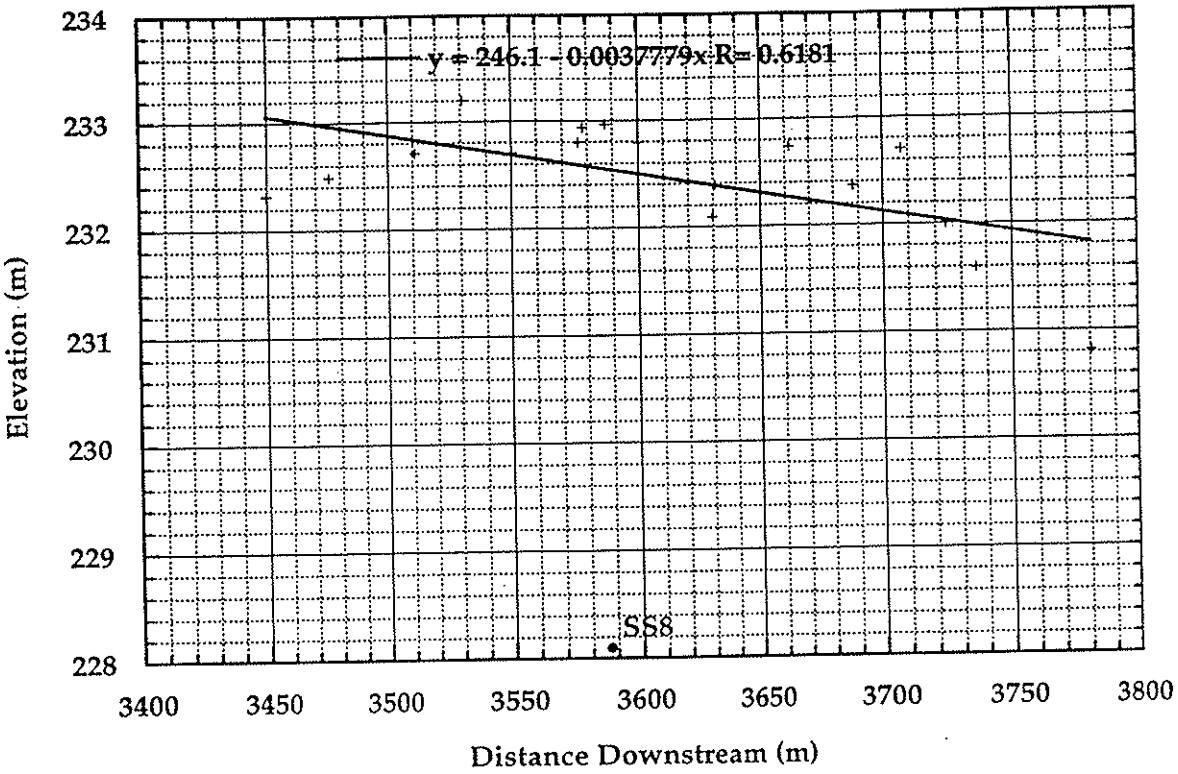
y = 246.1 - 0.0037779x R= 0.6181
SS8
Elevation (m)
234
233
232
231
230
229
228
3400
3450
3500
3550
3600
3650
3700
3750
3800
Distance Downstream (m)

SS8RB

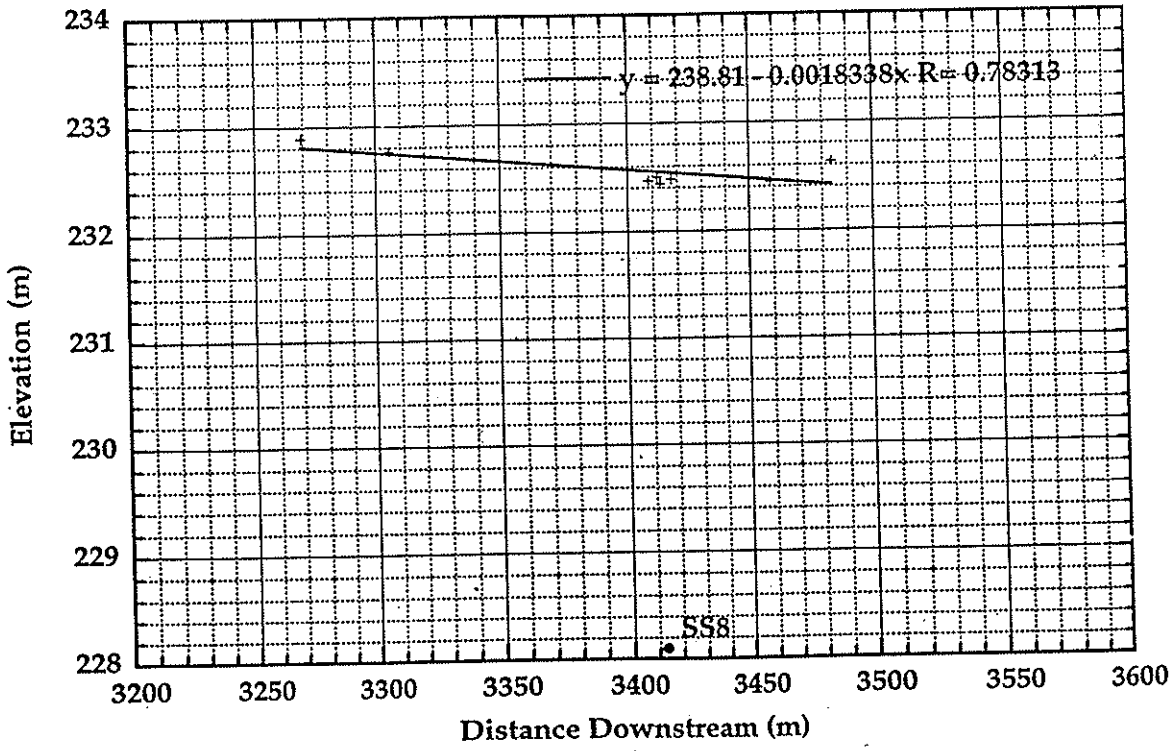
y = 238.81 - 0.0018338x R= 0.78313
SS8
Elevation (m)
234
233
232
231
230
229
228
3200
3250
3300
3350
3400
3450
3500
3550
3600
Distance Downstream (m)

SS9LB

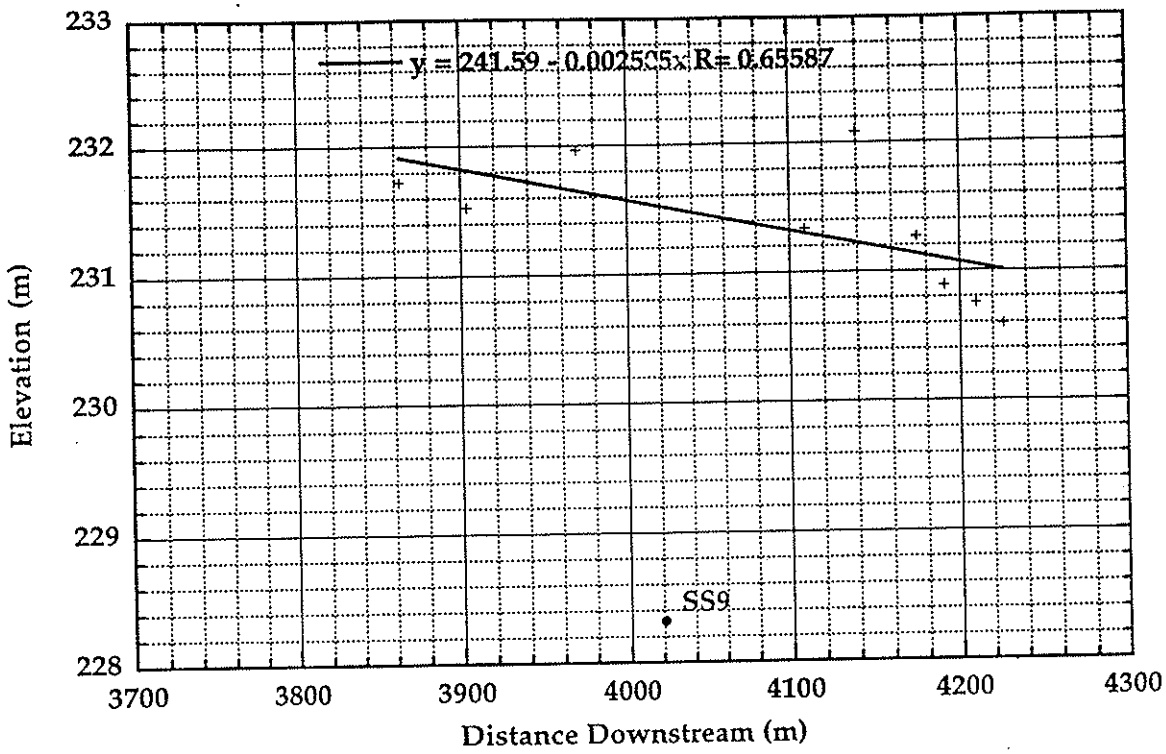
y = 241.59 - 0.002505x R= 0.65587
233
232
231
230
229
228
Elevation (m)
SS9
3700
3800
3900
4000
4100
4200
4300
Distance Downstream (m)

SS9RB

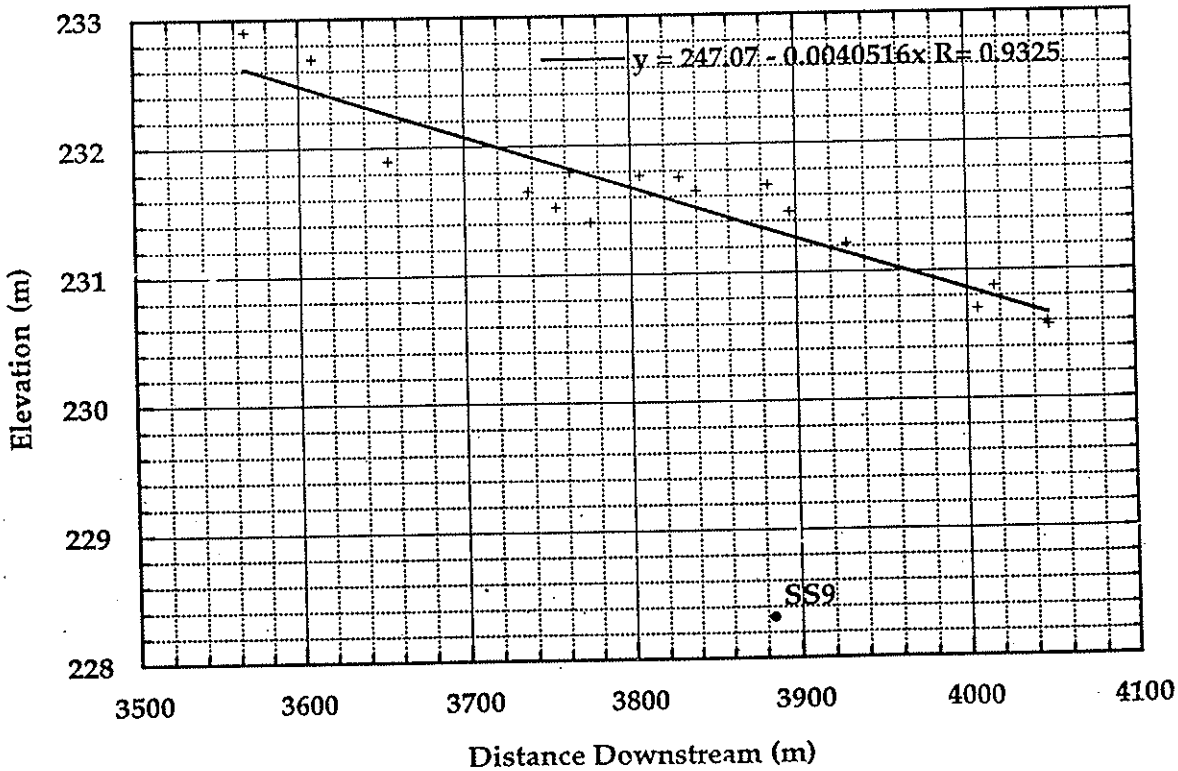
y = 247.07 - 0.0040516x R= 0.9325
233
232
231
230
229
228
Elevation (m)
SS9
3500
3600
3700
3800
3900
4000
4100
Distance Downstream (m)

SS10LB

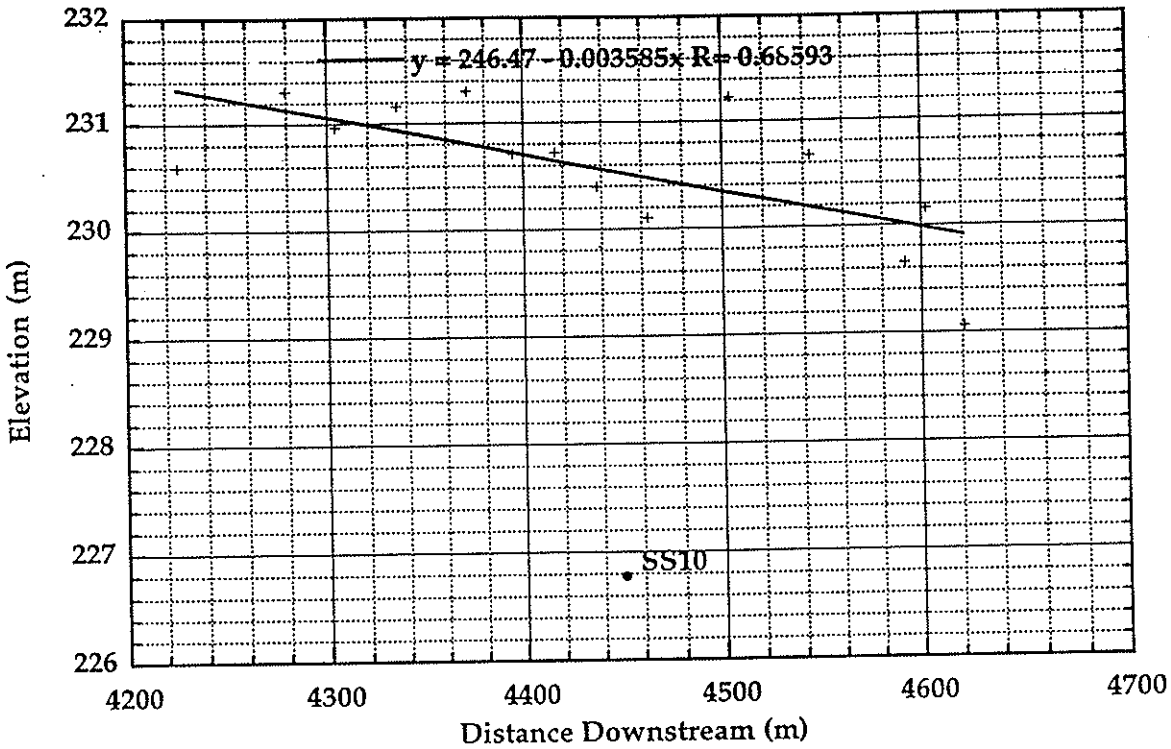

SS10RB

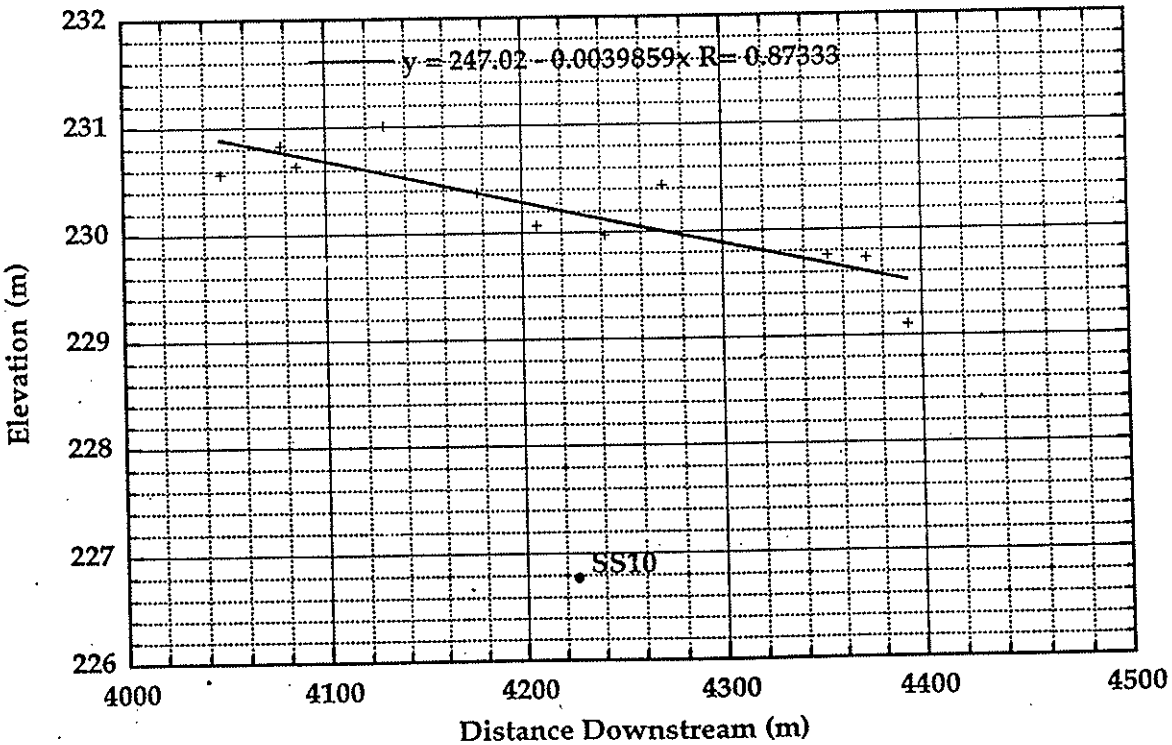

SS11aLB

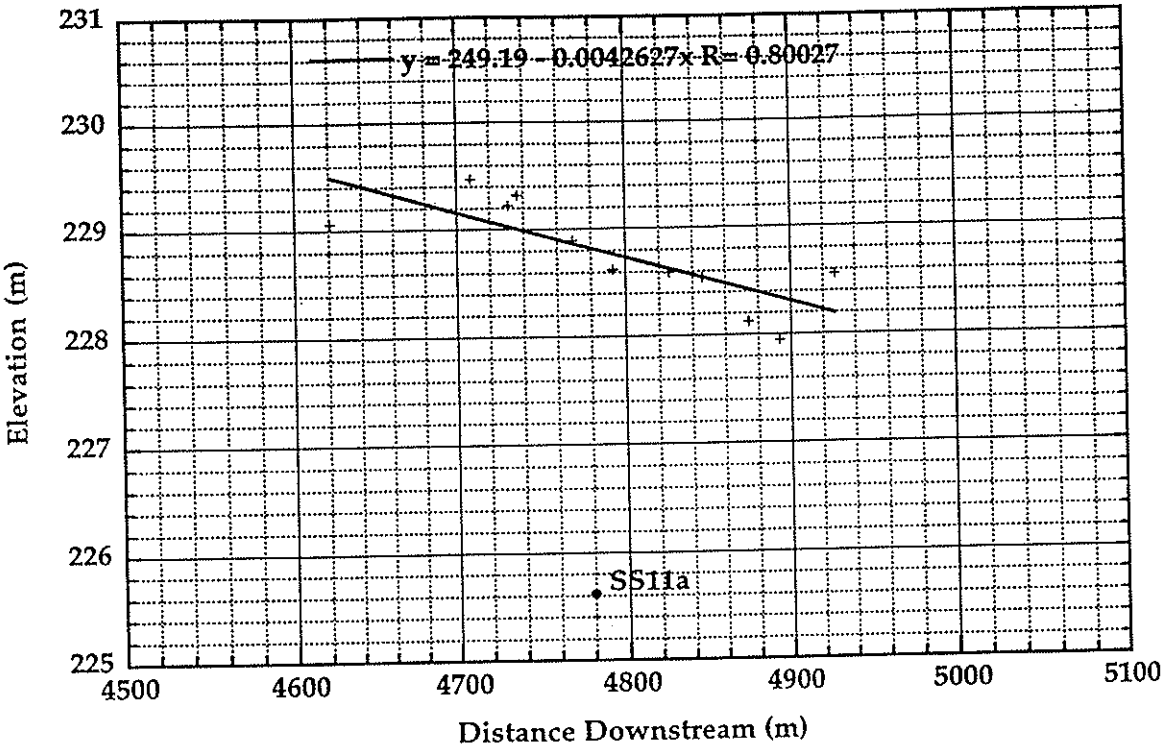

SS11aRB

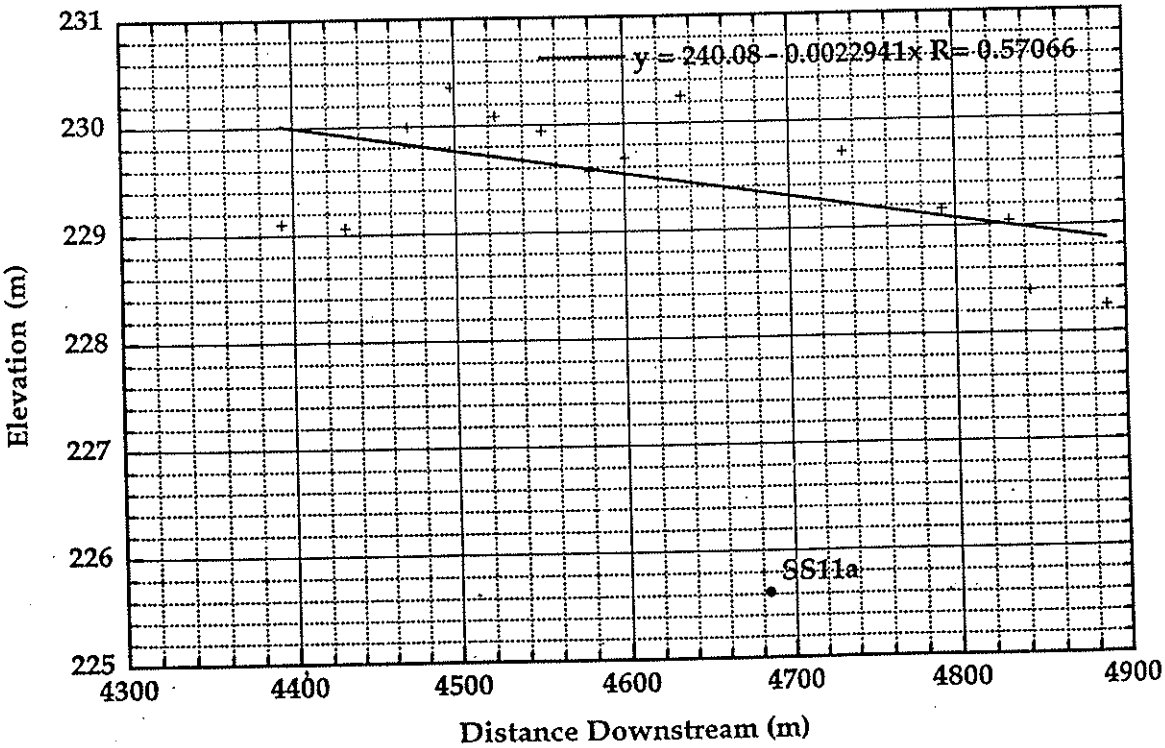

SS11bLB

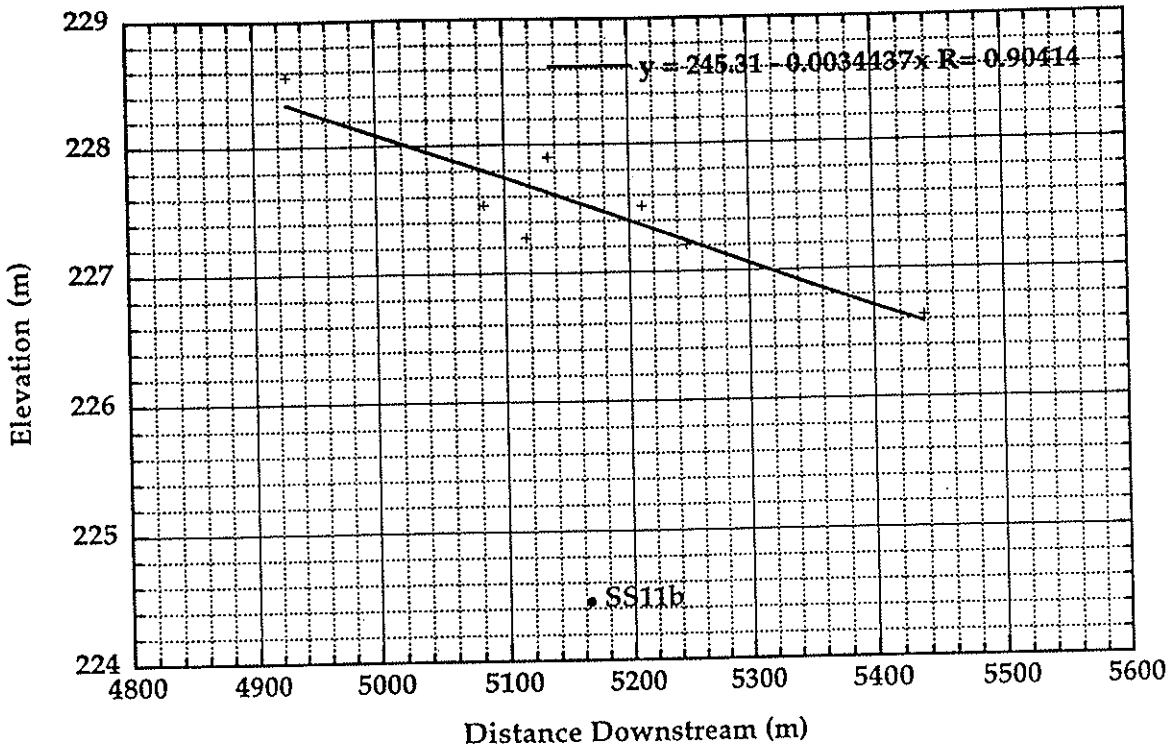

SS11bRB

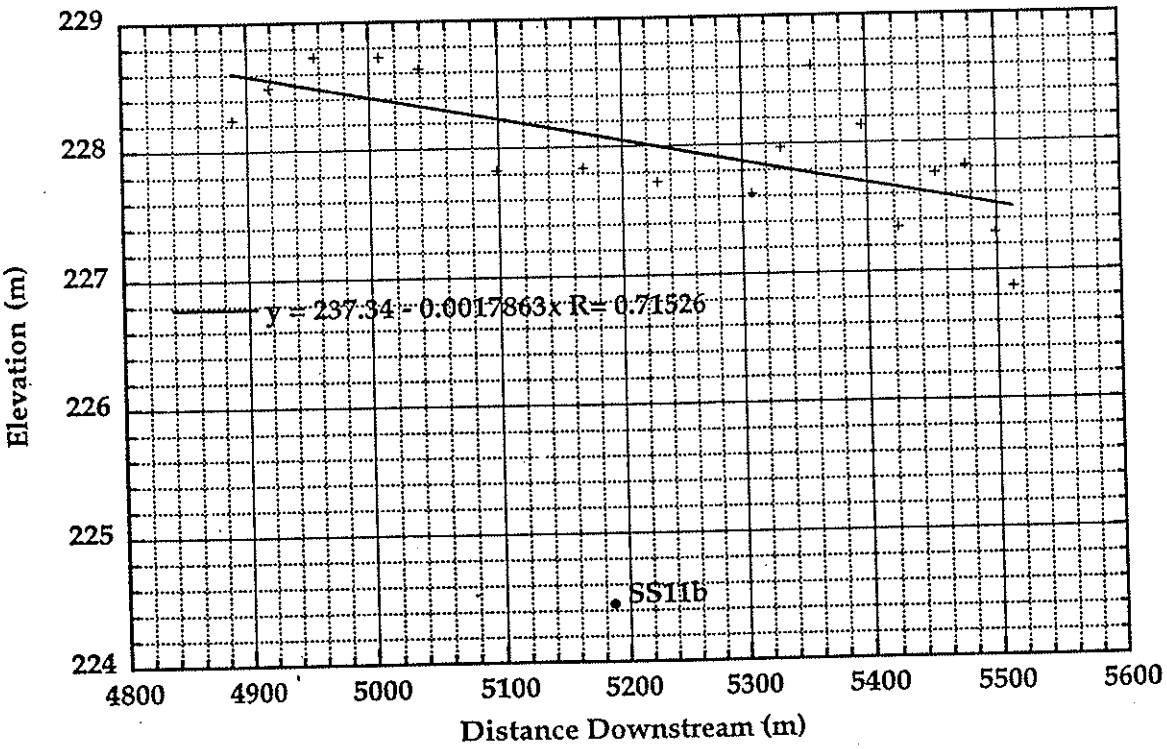

SS12LB

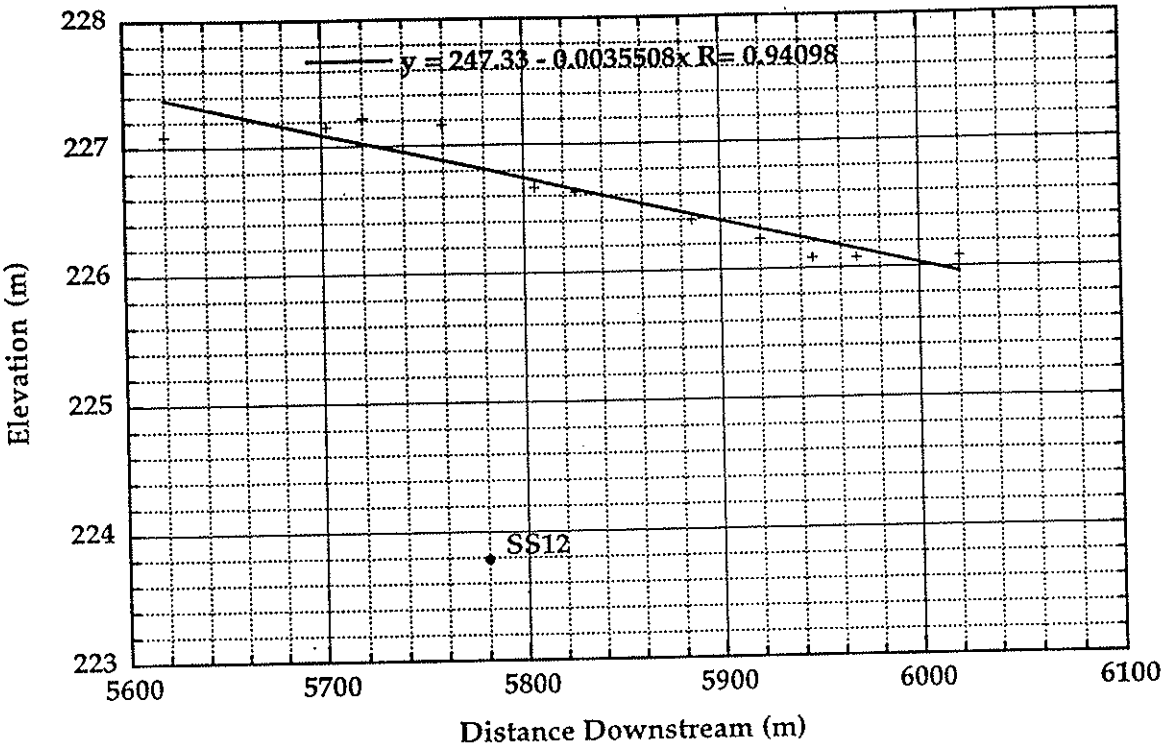

SS12RB

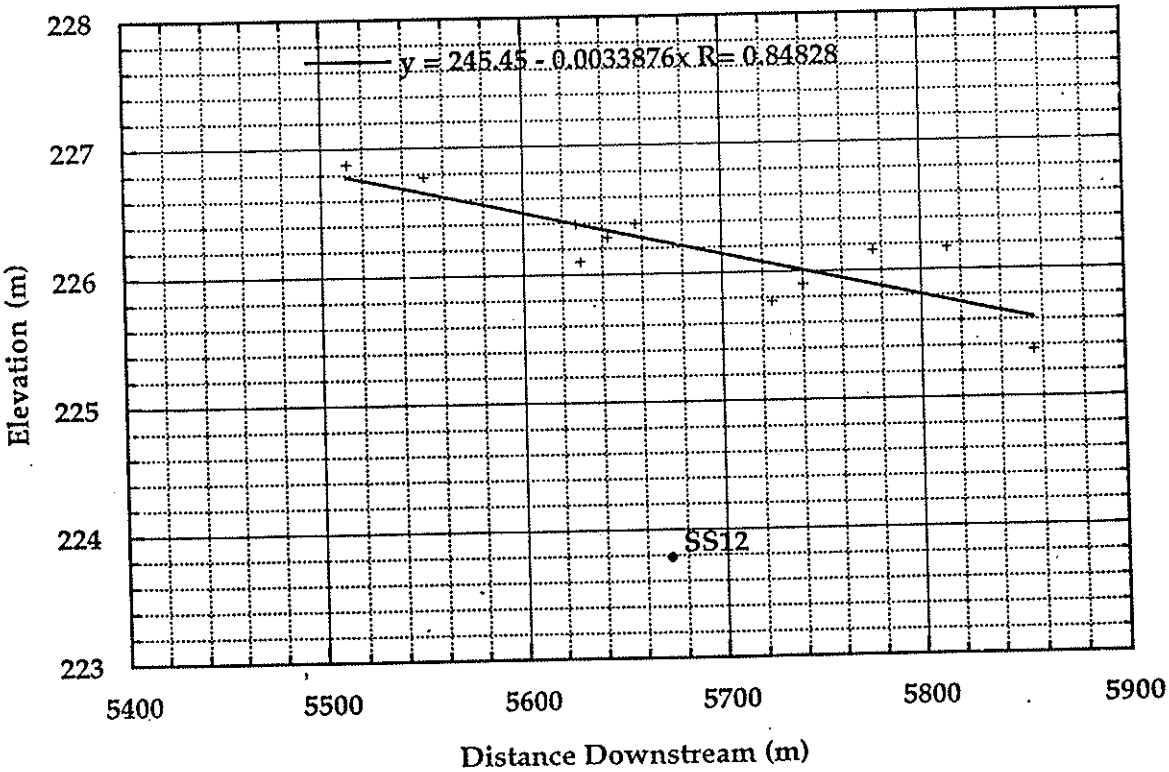

SS13LB

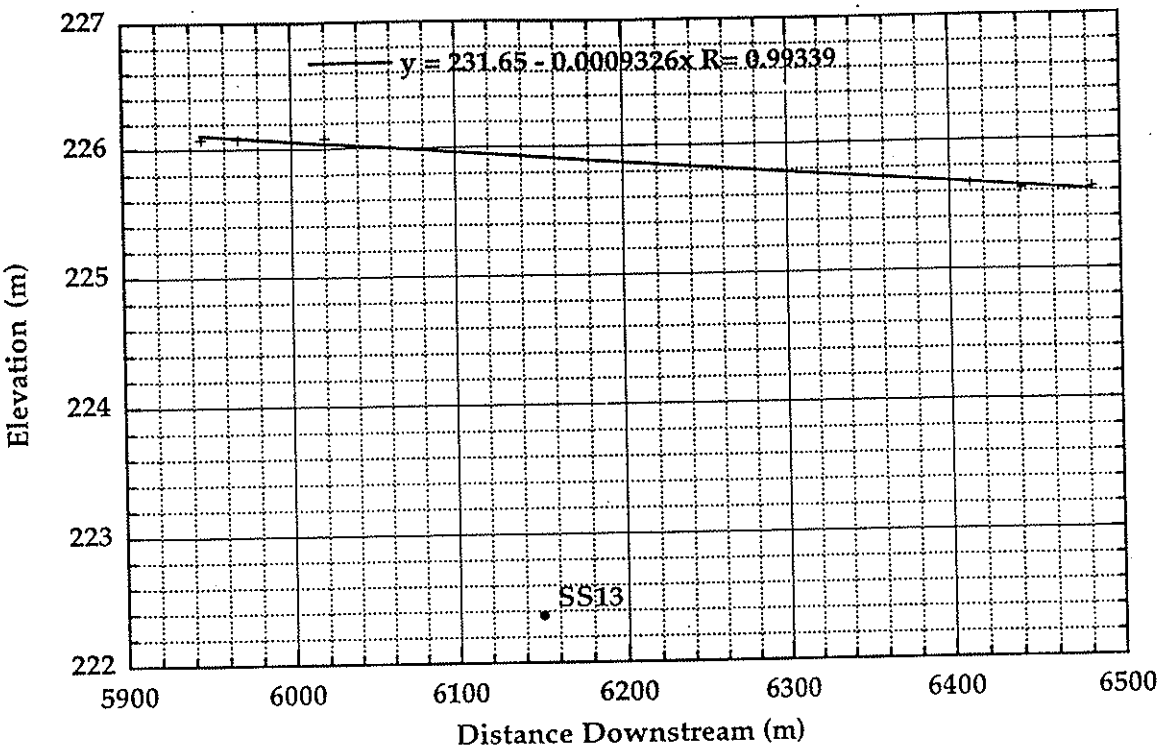

SS13RB